AFOSR-TR- 78-1010

FOR FURTHER TRAN

AD A054979

FINAL REPORT

High Gain Long Period Seismograph Station

Sponsored by
Advanced Research Projects Agency (DOD)

ARPA Order No. 3291
Monitored by AFOSR under
Contract # F44620-73-C-0060

DDC
RECEIVED
JUN 9 1978
B

APRA Order 3291
Program Code 7F10
The Regents of The University of Michigan
Term: 1973 April 01 - 1978 March 15
Cost: $165,557
Contract No. F44620-73-C-0060
James T. Wilson, Principal Investigator
(313) 764-6200
William J. Best, Program Manager
(202) 767-5011
HGLP Seismograph Station (WPM)

AD No.
DDC FILE COPY

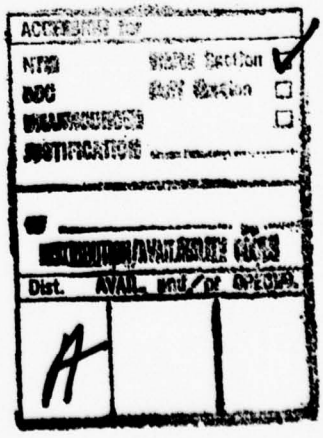
DISTRIBUTION STATEMENT A
Approved for public release;
Distribution Unlimited

The views and conclusions contained in this document are those of the authors and should not be interpreted as necessarily representing the official policies, either expressed or implied, of the Defense Advanced Research Projects Agency or the U. S. Government.

AIR FORCE OFFICE OF SCIENTIFIC RESEARCH (AFSC)
NOTICE OF TRANSMITTAL TO DDC
This technical report has been reviewed and is
approved for public release IAW AFR 190-12 (7b).
Distribution is unlimited.
A. D. BLOSE
Technical Information Officer

TABLE OF CONTENTS

	Page
Acknowledgments	i
Abstract	ii
Introduction	1
Associated Research	2
Development of the HGLP Station WPM	3
Appendix I Routine M_o Calculations from an AR Parameter Method for WWSSN Instruments	
Appendix II A Tectonic-Based Rayleigh Wave Group Velocity Model for Prediction of Dispersion Character through Ocean Basins	
Appendix III Various abstracts of papers presented at scientific meetings	
Appendix IV Catalog of Events for the White Pine High Gain Long Period Seismograph Station, July 1974 - April 1975	



ACKNOWLEDGMENTS

This report has been prepared by the principal investigator; however, the semiannual Technical Reports that are excerpted were written, for the most part, by Frederick J. Mauk. Dr. Mauk was the principal worker in establishment of the White Pine station. He was assisted ably at White Pine and Ann Arbor by various graduate students but primarily and extensively by Mr. Stephen G. Henry. Dr. Barbara R. Williams worked primarily on long period data.

The project could not have been carried forward without the cooperation of the White Pine Copper Mine and a number of the mine staff. Their efforts, and in particular the continued enthusiastic cooperation of Dr. Walter Finlay who headed the mine's research group, made the project possible.

The Albuquerque Seismological Center of the U. S. Geological Survey was of great aid in furnishing and assembling equipment, giving technical advice, and aiding in the actual installation of some of the instrumentation. Special thanks to Don Rock and Jack Dorenden for their help and expertise.

The Seismic Data Center in Alexandria, Virginia was most helpful in furnishing long period data and advice on data manipulation to Dr. Williams.

Finally, the skillful project monitoring by Mr. William Best of the Air Force Office of Scientific Research is appreciated.

ABSTRACT

This final report on Contract No. F44620-73-C-0060, April 1, 1973 - March 15, 1978, describes the work carried out under the terms of the contract.

A High Gain Long Period (HGLP) seismograph station was installed in the White Pine Copper Mine in Ontonagan County, Michigan. The station went through a series of stages starting with a long period vertical recording through a phototube amplifier on a strip chart and ending as an essentially standard HGLP station. Because of the difficulties of servicing and recording without telemetry, the station was closed at the end of 1976.

Much useful information regarding the engineering and installation of HGLP stations in mines was obtained. The station produced many months of useful long period data.

Concurrently with the station installation two extensive research efforts in long period seismology were carried on. One developed a Rayleigh wave velocity model for ocean basins and the other applied long period P wave spectra to the determination of seismic moments.

INTRODUCTION

This project, lasting nearly five years from April 1, 1973 to March 15, 1978, involved the installation of a High Gain Long Period (HGLP) seismograph station in the White Pine Copper Mine located at White Pine, Michigan in Ontonagan County. The station was developed in a series of planned steps. It was initiated in 1973 with a vertical component using a phototube amplifier and recording on a strip chart. The station was ultimately expanded to three components and by the time it was shut down in 1976, it was in essence a standard HGLP station.

Various innovations were made in the installation. Perhaps the most significant was the manner in which the horizontals were installed. The standard large steel pressure containers used to shield the horizontal seismometers from barometric effects were modified by removing their bottoms and cementing the rim directly to the sandstone of the mine floor. This permitted the installation of the seismometer directly on the rock rather than on the strained bottom plate of the container. There was still some barometric shielding but as the horizontals have only modest sensitivity to barometric effects, the gain in stability, particularly on initial set up or at times of adjustment, was marked.

The history of the station, the engineering developments, and the various details of the installation are all to be

found in the semiannual Technical Reports. Selected sections of them are given again in this final report.

Concurrently, with the development of the station an extensive research effort was carried on using data from the HGLP stations and from long period seismograms from the WWSSN stations.

ASSOCIATED RESEARCH

The research in long period seismology led to two Ph.D. theses. One by Barbara R. Williams, "Source Parameters for Large Earthquakes from High Gain Long Period Body Wave Spectra", and one by Frederick J. Mauk, "A Tectonic-Based Rayleigh Wave Group Velocity Model for Prediction of Dispersion Character through Ocean Basins".

The first deals with the use of long period spectra of P and PP to determine the moment of large earthquakes. A large number of spectra were calculated using both Fast Fourier Transform (FFT) and Maximum Entropy Spectra Analysis (MESA) methods. It became evident that while an estimate of the moment could be obtained, the noise (probably both instrumental and earth) above 100 seconds was too large to make this a completely satisfactory method. The corner frequency could not be determined reliably but the determinations were consistent with moments derived from field observations and aftershock distribution. An extensive elaboration of Brune's AR method was made and the method further adapted to WWSSN records and oceanic paths. Moments calculated by the AR

method were also used for moment comparison.

The second thesis developed a new model to predict Rayleigh wave group velocity dispersion (periods 30 through 100 seconds) through ocean basins. It is based on a 5° x 5° integration of weighted Rayleigh group velocities for the 2592 geographic grid elements constituting the earth's surface.

Both theses are available from University Microfilms, Ann Arbor, Michigan. Appendix I is a draft manuscript from Dr. Williams' thesis and Appendix II is a manuscript submitted to JGR from Dr. Mauk's thesis. Appendix III includes various abstracts presented at scientific meetings.

A detailed log of all events recorded at the White Pine station (WPM) has been made and is on file at the Seismological Observatory, Department of Geology and Mineralogy, University of Michigan. Appendix IV is a Catalog of Events for the period July 1, 1974 through April 30, 1975.

DEVELOPMENT OF THE HGLP STATION WPM

The location of the station was chosen because of the availability of a suitable site in the White Pine Copper Mine in Ontonagan County, Michigan at a geographic location such that relatively uncomplicated paths were thought to exist (and indeed do) across the arctic from Eurasia.

The location was 89 meters below the surface at an elevation of 193.5 meters in the Parting Shale member of the

Nonesuch formation of preCambrian age. The geographic coordinates of the vault are 45° 45' 05."5 N, 89° 33' 17."8 W. The location is in drift S13, W4 of section 31-A of the mine. A stratigraphic section and map of the vault are shown in Appendix IV, pages 5 and 6.

This portion of the mine is a room and pillar operation which leaves about half of the rock to support the overlying strata. In both the initial area for the vertical (vault 1) and the expanded area (vault 2) to accommodate the horizontals, supporting pillars were used as part of the enclosure and the open areas closed with plywood sealed with six inches of polyurethane foam.

Within the enclosed area containing the seismometers, the temperature of the mine fluctuated only a few degrees from 55°F. The pressure tanks were filled with spun glass insulation to reduce thermal effects. During the summer months, the humidity was high (95%) but was considerably lower in the winter.

The following, referring to the initial installation of the vertical, is excerpted from the Technical Report for the period 1 April - 30 September 1973.

> Before the seismometer pressure tank could be installed, the floor was cleaned and all loose debris removed. Most of the floor was found to be unsuitable for the installation of the one meter tank, either because of extensive cross jointing or more often because normal production blasting highly fractures the floor.

To reduce the problems of tilting normally associated with the curing of concrete, the tank was installed directly on bedrock with a minimal amount of cement to seal the tank bottom to the floor. Four-threaded cadmium-plated rods were cemented 38 centimeters into bedrock with epoxy resin to secure the tank bottom. Before mounting the tank, the bottom was prestressed into a dome with maximum displacement of 2 centimeters at the center. The tank was then set on a slurry of sand and cement and bolted to the floor. The prestressing tension was then gradually released over the next twenty-four hours.

In addition to the AC electrical system provided by the mine, data and control cabling had to be installed. To minimize pressure leakage into the seismometer tank, all cables entering the tank were stripped of insulation, sealed with General Electric Glyptal 1201 and potted in 3-M Scotchcast resin plugs. These resin plugs were then seated in Marsh-Marine fittings to insure pressure integrity of the sealed system. Control cabling consisted of Belden 6-pair shielded instrument cable. All other wiring was done with individual shielded-pair cable to reduce cross-talk between pairs and maintain integrity of the data lines.

The seismometer used at station WPM is a Geotech model S-11 which has been modified to accommodate a Sprengnether model VCT-210 displacement transducer. The natural frequency of the instrument has been set at 0.003 Hertz (T_o=30 seconds).

A preliminary investigation employing a Geotech model 5240A phototube amplifier was run from 23 August to 25 September to determine the feasibility of a permanent installation. In mid-October the phototube amplification system will be replaced with a Geotech model AS-650 low noise amplifier incorporating telemetry capabilities.

The output of the phototube amplifier was recorded at two gain settings on Esterline Angus model S601-S six-inch strip chart recorders. Output from the displacement transducer system was recorded on an Esterline Angus model E1101-S ten-inch strip chart recorder.

Time marks are provided by a Sprengnether S-100 chronometer which was determined to have a constant drift rate of -4000 milliseconds per day. All power for amplifiers and recorders is controlled by a Sorensen ACR-3000 power regulator which reduces the problems of power fluctuations at the station. The most severe power fluctuations occur when a mine compressor in the area is turned on. This causes a momentary 10 volt power dip followed by a transient surge. The power regulator reduces the 10 volt dip to 2 volts and eliminates the associated surge.

Continuous seismic recordings were run from this preliminary installation through the period August 23 to September 25, 1973. Two gain levels (40K at 45 seconds and 400K at 45 seconds) were used. Figure 1 shows the response curve at 400K together with those for other high gain stations. Figure 2 shows the seismogram for a magnitude 5.3 event from the north Atlantic followed by a smaller event of unknown location.

More details and illustrations of the initial installation can be found in the first Technical Report.

The preliminary installation was shut down from September 25, 1973 to March 2, 1974, while awaiting equipment to telemeter the signals from the mine to the surface. Minimal recentering was required to return to operation. A permanent

Figure 1

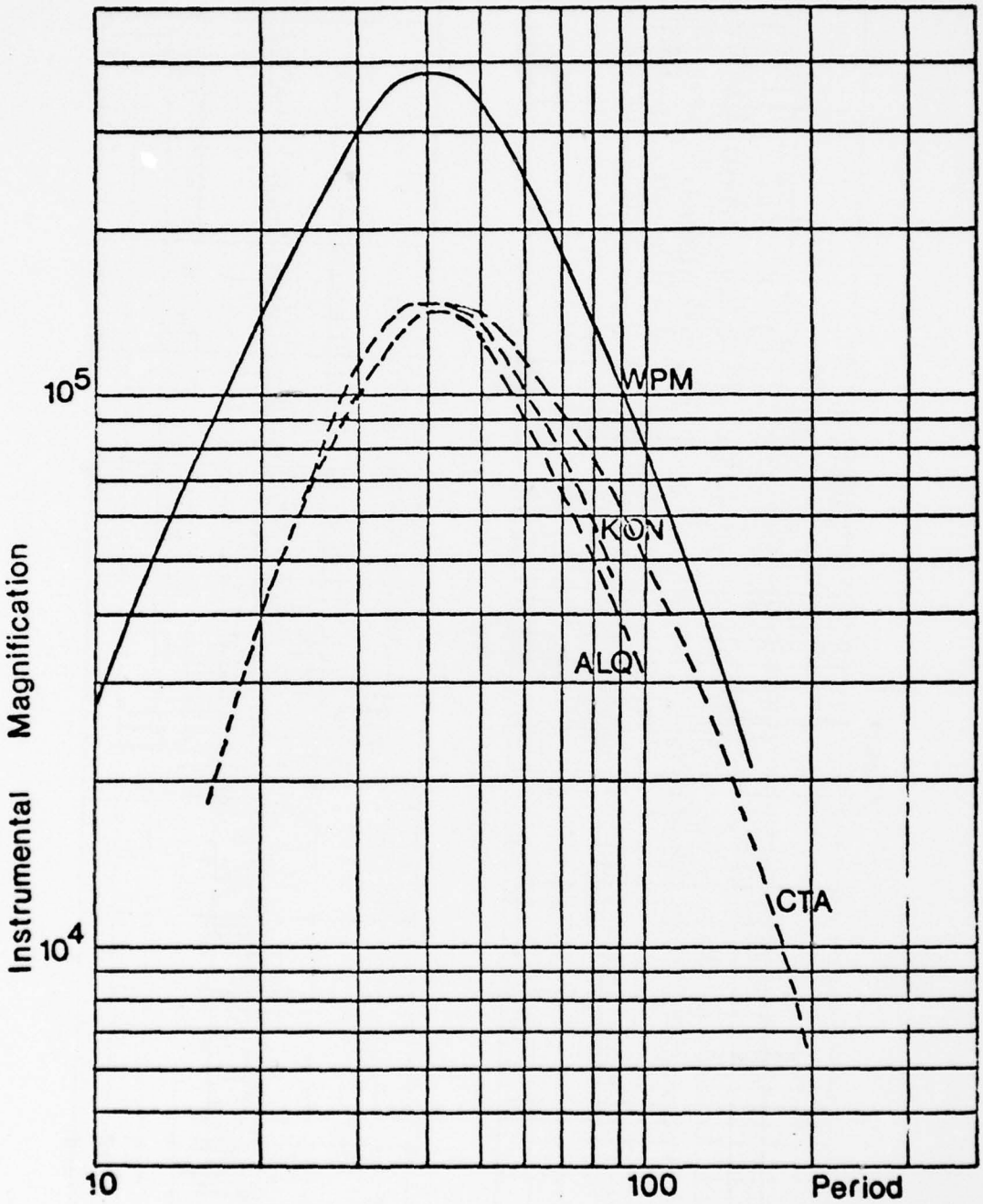
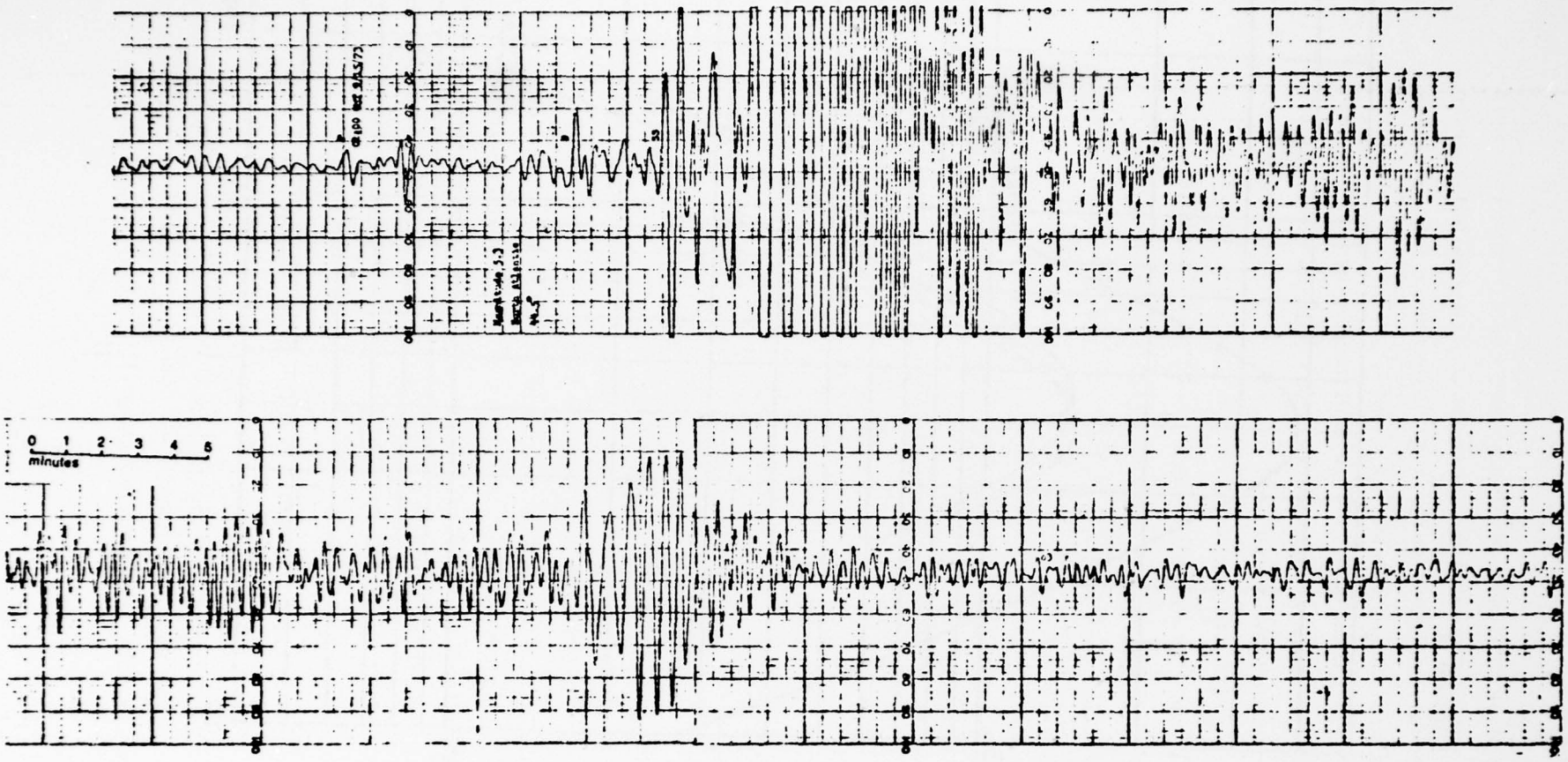

Instrumental Magnification
10^5
10^4
WPM
KON
ALQ
CTA
10
100
Period

Figure 2



hard wire telemetry link was installed at this time to permit recording at one of the mine research buildings on the surface.

In the summer of 1974, two long period horizontals were installed. (See Technical Report 1 April - 30 September, 1974). A second vault had to be constructed. The following is from the Technical Report.

> All loose floor debris was removed before wall construction was begun. This substantially reduced the difficulty of selecting tank installation sites since the entire vault 2 floor was exposed. Although production blasting had reduced the usable floor space, as in vault 1, two unfractured, unjointed sections of the Copper Harbor Conglomerate were deemed suitable for tank placement. These sections of floor were meticulously cleaned and any loose fragments removed. This resulted in relatively smooth, impermeable tank foundations.
>
> Unlike other HGLP installations, where prestressing of the tank bottom was necessary to insure proper bonding of the metal to concrete beneath it, we chose to minimize tank tilt effects on the horizontal seismometers by decoupling the two components. Before installation, the tank bottoms were cut out leaving only a rim four inches wide for bonding. Four cadmium-plated threaded rods for each tank were then cemented 38 centimeters into bedrock using an epoxy resin. The use of epoxy bolts rather than mechanical bolts was suggested by mine personnel. Both resin and mechanical bolting are widely employed in the White Pine Mine, and resin bolting has been shown to be more effective than mechanical bolting. Since it was unnecessary to insure a bottom contact with concrete, prestressing of the tank was unnecessary. The tank was then set onto a slurry of sand and cement and bolted securely to the bedrock. By wobbling the tank before

final bolting, it was possible to reduce the average thickness of the cement to less than 5 millimeters. The cement was then permitted to cure for three days undisturbed. Following the curing period, the inside of the tanks, bedrock and concrete junctions were triple-sealed with epoxy. The concrete outside the tank was also sealed. Each epoxy coat was permitted to harden thoroughly before the next was applied. Finally, the interior and exterior of each tank was coated with zinc chromate to inhibit rust formation.

All but two ports entering the tanks were sealed with teflon-coated plugs which were tightened and then coated internally and externally with General Electric Glyptal 1201. The remaining two ports were fitted with Marsh-Marine connectors which clamped onto molded wire plugs.

To minimize pressure leakage into the seismometer tanks, all cables entering the tanks were stripped of insulation, sealed with General Electric Glyptal 1201, and potted in 3-M Scotchcast resin plugs. The resin plugs were then seated in the Marsh-Marine connectors to insure pressure integrity of the sealed system. Several different castings of the plugs were necessary before usable plugs could be obtained. It was found that the 3-M Scotchcast resin became brittle and shattered upon removal from the molds if permitted to harden in the ambient mine conditions. Good plugs could be obtained only when the molds were continuously warmed with heat lamps during the hardening process. Control cabling consisted of Belden 6-pair shielded instrument cable. All other wiring was done with individual-shielded pair cable to reduce cross-talk between pairs and maintain integrity of the data lines.

The horizontal seismometers employed at station WPM are Geotech model 8700C's which have been modified to accommodate Sprengnether model VCT-210 displacement transducers. The natural frequency of each instrument has been set at 0.033 Hertz (T_o=30 sec). Following calibration, each seismometer

with its associated displacement transducer electronics was thoroughly insulated with spun glass and then sealed in its tank. With no physical connection between the tank and seismometer, C-clamps could be tightened until the seismometers "quieted down". There was a direct connection between the output noise and effectiveness of the tank seal, and the noise level would dramatically decrease when a good seal was effected. Since there was no direct connection between tank and seismometer, stresses induced in the tanks during clamping were not transmitted as tilts to the seismometers. Hence, it was possible to tighten or loosen clamps or add additional clamps, as necessary, without affecting the seismometers. Throughout the clamping procedure neither seismometer needed recentering.

In addition to the seismometers, a subsurface control area has been installed in the northeast corner of vault 1. Three phototube amplifiers have been made operational as well as a Geotech AS-650 solid state amplifier. Recording of horizontal seismograms was done on two Esterline Angus model S601-S six-inch strip chart recorders in the subsurface control area throughout the summer of 1974. Instrumentation in the subsurface control rack consists of a boom position monitor and reposition motor drive panel, a calibration panel, a waveform generator, a Sprengnether S-100 chronometer, and power regulation and distribution devices. All boom monitoring and repositioning for both vertical and horizontal seismometers, as well as calibration, must be effected from this rack. No calibration or repositioning capability exists, or is likely to exist, at the surface recording site. The telemetry link to the surface recording site for frequency modulated signals is also accessible at a panel in the subsurface control area.

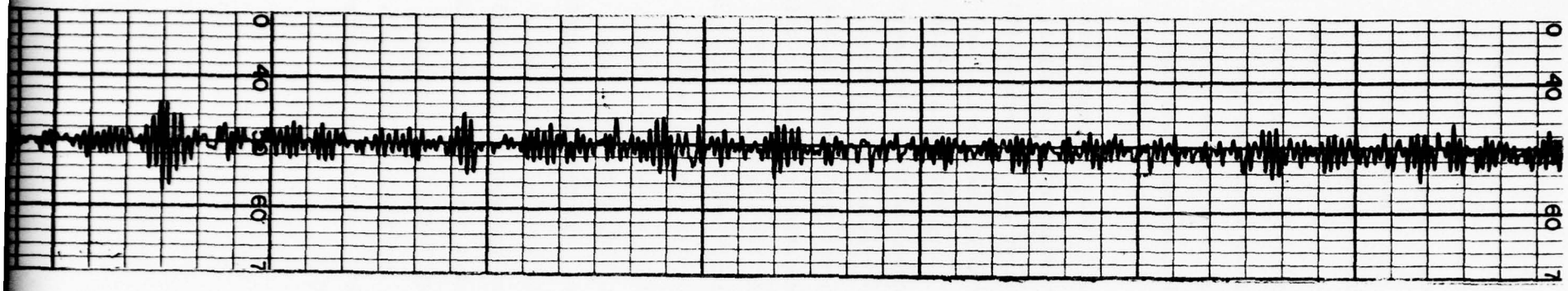
As of October, 1974, the installation of a preliminary station had been completed and it was possible to make an

assessment of what had been learned and to feel assured that White Pine was a more than suitable site. The following lengthy excerpt from the Technical Report 1 April 1974 - 30 September 1974, summarizes this information. It will be noted that reference is made to a short period vertical which was operated intermittently as a test of the site.

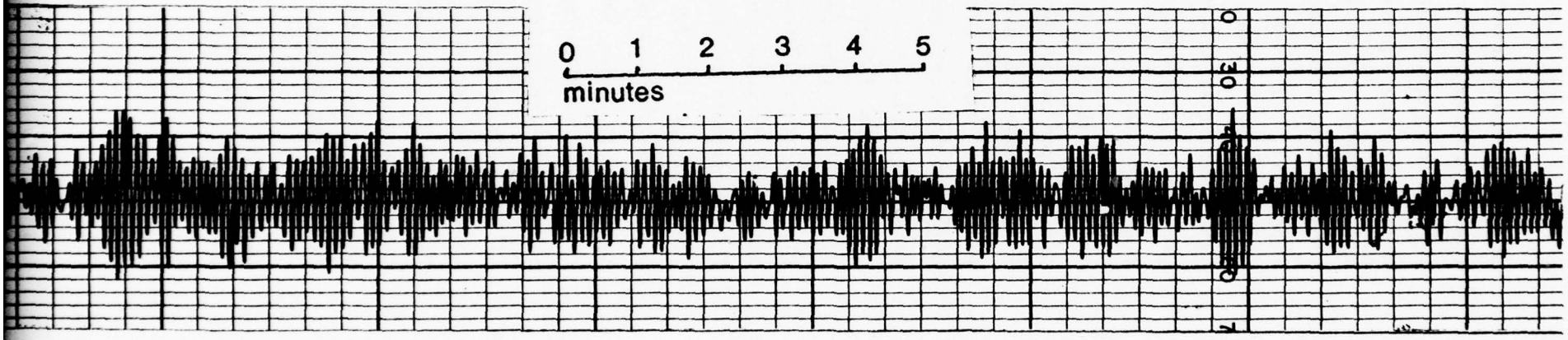
a) Comparison of Geotech AS-650 solid state amplifier and phototube amplifier - In June, 1974, the long period vertical instrument was switched from phototube amplifier to a Geotech AS-650 solid state amplifier. This permitted recording of long period vertical (in addition to short period vertical) seismic signals on the surface since the output of the AS-650 was multiplexed to a 1020 Hertz carrier. The successful recording of the short period vertical signal on the surface has been discussed previously (see Technical Report 1 October 1973 - 31 March 1974). No interference or direct coupling between the long period and short period systems was observable on nearly continuous records from June to September, 1974. Further discussion of the short period system is given in part b) of this section.

The Geotech AS-650 amplifier, unlike the phototube amplifier, does not have a 0.167 Hertz notch filter incorporated. This resulted in high six-second microseismic noise, especially during "storm" periods. This noise proved to be the principal gain limiting factor for the WPM long period vertical system. The vertical magnification ranged from 88K during periods of intense microseismic activity to 100K during quiet "noise" periods. The bottom trace of Figure 3 illustrates the signal appearance during an intense noise period. To reduce this effect, a galvanometric preconditioning scheme was employed (see Pomeroy et. al.; B.S.S.A., Vol. 50, pp 135-151, 1960). A Leeds and Northrop critically damped 0.167 Hertz

Figure 3



Vertical seismogram Station WPM T_o=30 sec. Geotech AS-650 amplifier
Gain 88,000 employing Leeds & Northrup bandpass filter galvanometer
T_g=7.0 sec. (Pomeroy, 1960: P2F configuration)



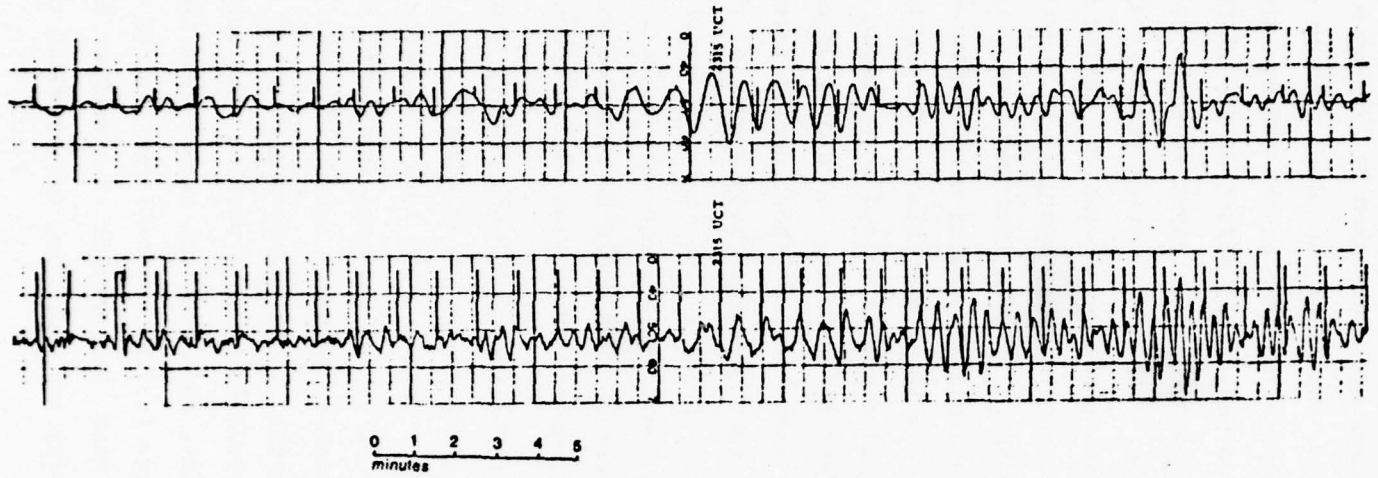
Vertical seismogram Station WPM T_o=30 sec. Geotech AS-650 amplifier
Gain 88,000 without filter galvanometer

galvanometer was inserted in series between the seismometer and the AS-650 amplifier (Pomeroy P2F configuration). The galvanometer in this mode acted as a band rejection filter, preconditioning the signal before amplification. This resulted in a six-second microseismic noise reduction by a factor of two (upper trace, Figure 3). The use of the galvanometric band rejection filter scheme, therefore, is being employed with the AS-650 amplifier at WPM on HGLP vertical signals. Two gain levels, 10K and 100K, are being recorded for the HGLP vertical.

During the period 1 through 4 August 1974, a comparative test was run using the vertical seismometer. The signal from one data coil was amplified using the Geotech AS-650 solid state amplifier. Simultaneously, the signal from the other data coil was amplified using the Geotech 5240-A phototube amplifier. The AS-650 employed the galvanometric band rejection filtering technique previously described while the phototube amplifier employed the Geotech 6824-15 special filter. Three of the seismograms recorded in this manner are included in this report (see Figures 7-9).* This comparison revealed several important facts: most of the longer period (20 to 100 seconds) noise was being generated within the phototube system since it did not appear to be higher for periods in the 50 to 60-second range from the phototube amplifiers, substantial distortion of 10 to 20-second periods exists; usually body phase arrivals are substantially more recognizable on the AS-650 records. We believe, therefore, that the seismograms from the AS-650 are more useful to seismologists than those from the Geotech 5240-A phototube amplifiers. Hopefully, the Ithaco replacements will exhibit more of the characteristics of the AS-650 than the 5240-A.

*Figure 7 is shown as Figure 4 in this report.

Figure 4



Comparison of phototube amplifier (top) and AS-650 amplifier (bottom) signals from HGLP vertical seismometer. Event from Kurile Islands, 46.2 N, 153.2 E, depth 42 km, on July 30, 1974 at 223944.5 UCT, Mb-5.0, Ms-8.7

4

b) Suitability of the White Pine Mine for a complete HGLP installation - The White Pine Copper Company experienced a strike shutdown during the latter two weeks of August. During this period, only routine maintenance of underground and surface facilities was undertaken by limited mine personnel. This was, therefore, an ideal time to see what affect the mining operations had on the seismic signals at WPM. There was no noticeable affect on any of the three HGLP instruments; that is, there appeared to be no reduction of long period noise. The short period vertical system underwent substantial signal enhancement. During active mining periods, the short period vertical is operable at a maximum gain of 25K. The gain limiting factor is a persistent 4 Hertz resonance associated with mining activities and possibly surface milling operations. During the shutdown period, the gain could be raised by at least a factor of 4 and possibly greater. It is, therefore, apparent that to run a high gain vertical short period instrument, it must be remote from the active mining area of the White Pine Copper Company. Prior to the installation of the HGLP vertical instrument in 1973, a micro-earthquake survey was run. Gains in excess of 100K could be obtained at a distance of 10 miles from the White Pine mining operations.

The environmental stability of the WPM seismic vaults has been discussed in previous technical reports (see TR 1 April - 30 September 1973; TR 1 October 1973 - 31 March 1974). At that time the long period vertical instrument had been successfully operated at gains in excess of 400K. The horizontal instruments, installed during June and July, 1974, also have proved to be very stable. The horizontal instruments, in fact, have been far more stable than the vertical. They require less frequent recentering than the vertical and have gone for periods of a week or more, immediately following installation, during which there was

no apparent drift at all. Presumably this stability is a reflection of the decoupling of the seismometer from its pressure tank. The stability of the horizontals is disrupted, however, when personnel enter vault 2 (possibly a thermal agitation affect or actual vault tilt), and so entrance is restricted to major maintenance only. Figure 5b* illustrates the response curves of the three WPM HGLP instruments. Five selected events recorded at WPM are illustrated in Figures 10-14.**

Difficulties with the installation during this report period are as follows:

1) Stability of the power supplied by the White Pine Copper Company both on the surface and underground has become suspect. During this report period, the underground installation has experienced no less than four major power outages, the surface installation more than ten. Damage of the AS-650 amplifier occurred due to surging when power was resumed. To prevent recurrence of this, an adequate power isolation system is required both above and underground.

2) Recording of horizontal seismograms was accomplished in vault 1 of the underground faciltiy. To complete the installation, these signals must be telemetered to the surface. This includes displacement transducer signals as well as velocity transducer signals.

3) Many problems exist with the Astrodata data logger system, which must be corrected with the assistance of the Albuquerque Seismological Center personnel.

Following the completion and testing of the "experimental" station described above, it was decided to bring the station

*Figure 5 in this report

**Figures 10 and 13 are shown as Figures 6 and 7 in this report.

Figure 5
Long period instrumental
response curves for WPM

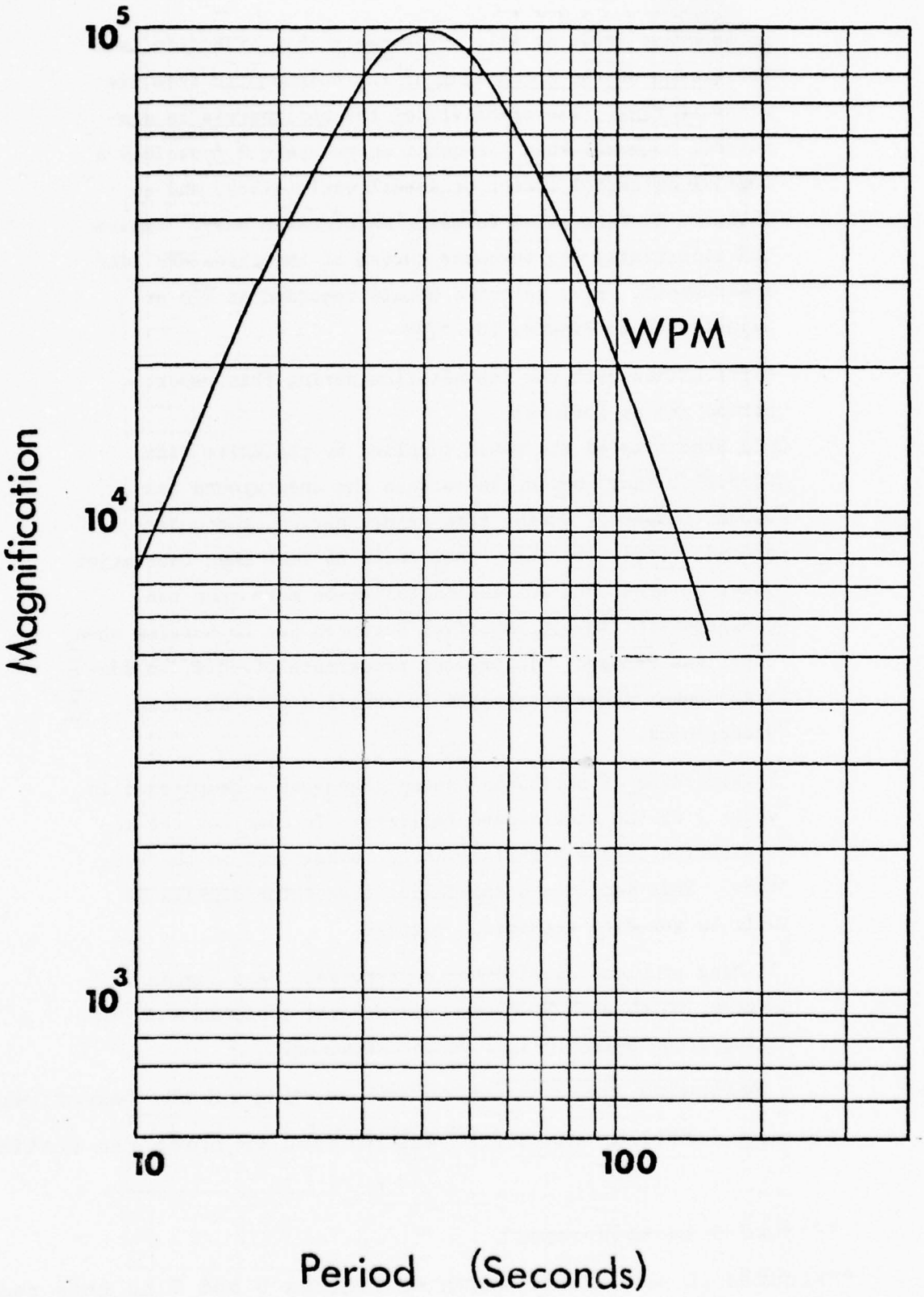
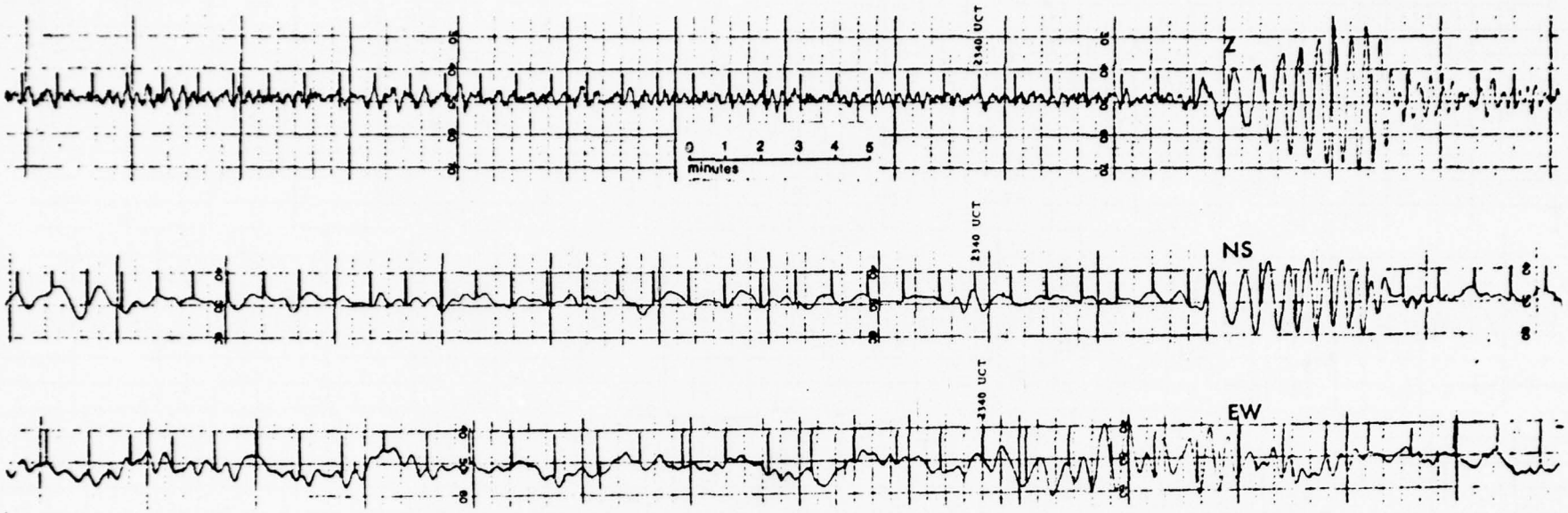


Figure 6



Vertical, North-South, and East-West HGLP records for an event in the Greenland Sea, 73.4 N, 6.5 E, normal depth on August 8, 1974 at 232442.4 UCT, Mb=4.2, Ms=4.5. For HGLP East-West records, advance rate is 15 mm per minute rather than 12.5.

Figure 7



Vertical (high and low gain), North-South, and East-West HGLP records. Event at Tadyhik-Sinkiang Border Region, 39.4 N, 73.9 E, normal depth on August 11, 1974 at 070208.5 UCT, Mb-5.2, Ms-5.4. For HGLP East-West records, advance rate is 15 mm per minute instead of 12.5.

into a mode as nearly like the standard HGLP stations as feasible. During the period covered by the Technical Report 1 October 1974 - 31 March 1975, planning and engineering went on and the timing system was upgraded. Work was initiated with the Albuquerque Seismological Center of the U. S. Geological Survey through which a new telemetry system, Sprengnether VCT-210 seismometer systems, and Ithaco amplifiers - all standard for HGLP stations - were readied for installation. An uninterruptible power system was also readied by Albuquerque to avoid the unreliability and voltage irregularity of the commercial power at White Pine.

In early December of 1974, the LPZ velocity signal was transferred from strip chart to rectilinear helicorder recording which improved the continuity of recording.

During the summer of 1975, much of the work to convert the station was completed. The following excerpts from the Technical Report 1 April - 30 September 1975, give the main details.

> Subsurface instrumentation - During this report period the following alterations of the White Pine subsurface installation have been effected: (1) complete rewiring of the vaults with shielded solid two-conductor cable replacing stranded and shielded multiconductor cables; (2) installation of an uninterruptible power system; (3) replacement of the phototube and AS-650 amplifiers with Ithaco solid state amplifiers; (4) installation of a six-component VCO system for multiplexing both velocity and displacement data.

Rewiring of the White Pine subsurface vaults was accomplished in July at the suggestion of Albuquerque Center personnel. Difficulty in locating the source of high frequency noise induced in the signals prompted this decision. All shielded stranded two-conductor and shielded multiconductor cables connecting the HGLP tanks were replaced with shielded solid two-conductor. Although this did not result in a significant noise reduction, it considerably improved the ease of subsurface trouble shooting.

A WWSSN-type uninterruptible power system consisting of a LaMarche charger and Nicad batteries was provided by the Albuquerque Center in June. Prior to this time, the vault power was supplied directly by available circuits in the mine.

Replacement of the Phototube amplifiers and the AS-650 amplifier with Ithaco HGLP amplifiers was effected in July. With this alteration, the White Pine frequency response of the velocity outputs will match all other HGLP observatories.

A six-component VCO system with active mixers was added to the subsurface instrumentation in June. Initial testing of the multiplexing-demultiplexing portion of the circuit revealed excessive high-frequency noise which would severely limit the gain of the analog records. Although inexperience with telemetry equipment led to a random logical approach to the noise reduction, eventually all major sources of interference were located and minimized. Three major sources of interference, all associated with the telemetry circuits, were responsible for approximately 95% of the noise. Over-driving the telephone line with voltages too high for six center frequencies was found to be the most significant noise source. When the individual output levels were adjusted so that the combined line input was at the 0 db level, the noise reduced by an order of magnitude. The second noise source was attributable

to an unfortunate choice of center frequencies. Algebraic addition of several carrier frequency pairs was found to yield resultants which interfere with a third channel. Avoiding this difficulty using constant bandwidth telemetry is extremely difficult and cannot be completely eliminated but only minimized. At White Pine this noise reduction was accomplished by splitting the six components into two mixed three-component line drivers and telemetering the signals on two separate telemetry lines. In addition, the center frequencies were adjusted to minimize interchannel interference. The third noise source was found to be the telemetry line itself. The communication line provided by the White Pine Copper Company was of minimal quality and had AC voltages as large as 50 volts induced on it. In addition, the transmission of higher frequencies was severely impaired. This difficulty was overcome by installing a new data line of Spiral-4, provided by the Albuquerque Center, from the subsurface vaults to the surface recording facility.

Surface installation. During this report period, the following alterations of the White Pine surface installation have been effected: (1) installation of the uninterruptible power system, (2) transferral to the TG-120 timing system and RV 301 helicorders, (3) initiating operation of the Astrodata data logger.

The Astrodata data logger has been put into operation with the assistance of Albuquerque personnel. Several integrated circuit cards were faulty and had to be replaced.

Several unavoidable problems arose, all of which were eventually surmounted but which are mentioned in the following extract from the Technical Report 1 April - 30 September 1975. Station installers should never be discouraged.

Difficulties encountered. A major mine collapse occurred on August 11, 1975, one thousand feet to the southeast of the HGLP vaults. The initial collapse was 300 feet by 300 feet and ran to the surface. At approximately the same time, the east-west instrument began having significantly large transients which have decreased in number and amplitude with time but still persist. The north-south instrument has displayed the same characteristic but to a much lesser degree. Since the initial collapse, the cave-in has increased in size to 300 feet by 600 feet so the instability persists. Whether the instability of the east-west instrument is due to the collapse or an actual instrumental problem is not known at this time. If the instability continues when the vault area returns to ambient conditions, the east-west instrument will have to be replaced. The collapse poses no direct threat to the HGLP vaults.

On August 14, 1975, a crane operator drove through the new Spiral-4 data line. A splice in the line had to be effected at a pole midway between the vaults and recording area.

Finally, on August 20, 1975, the WPM observatory was shut down by high voltage from a strike or near strike by lightning. The extent of the damage is not yet completely rectified. Three discriminators suffered extensive damage and are currently being repaired by Geotech. The mixer card for the VCO's, was also severely damaged and had to be replaced.

As of the fall of 1975, the station was recording the velocity signals on helicorders at a gain of approximately 16K and at full gain on an Astrodata data logger.

During the period October, 1975 through March, 1976, the station was intermittently operational. The vertical

was operational only about 65% of the time in the analog mode and the horizontal about 85%. Much of the downtime was due to the lightning strike discussed earlier. The Astrodata data logger was down more frequently. Considerable trouble was encountered with large random transients on the horizontals.

In the summer of 1976, the station was recalibrated and put into routine operation. With assistance from the Albuquerque Seismological Center, difficulties with the Astrodata recorder and backup power systems were corrected. In addition, the source of the transients on the horizontals, which appeared with the installation of the Seismological Center instruments, was located and corrected. Insulating breaker bars of pressed phenolic fiber had absorbed enough moisture to cause a periodic short across one or more of the coils of both horizontal instruments. The breaker blocks were dried and desiccant added to the tanks before resealing. A series of calibration response curves were also run until the response curves for all three components matched the designated HGLP response curve to within 5% for the period range 10 to 300 seconds. It was found necessary to replace the Ithaco amplifier to match the response curve for the vertical instrument. At the end of July, all instruments were in full operation. The gains on the helicorders were set at 30K.

In October of 1976, it was decided to close the station pending decisions as to the feasibility of telemetering

the signals to Ann Arbor. It was clear at this time that the station was in an excellent location. Long period noise was low and the geographic location with respect to interesting wave paths was excellent; however, the remoteness of the location made servicing difficult and it was necessary to depend on local help for record and tape changing.

The surface recording facility was removed at this time and moved to Ann Arbor. The seismometers and associated equipment underground were left until the spring of 1978 when it was clear that telemetry was not feasible in the immediate future.

The White Pine area is clearly a prime location for a high-quality station but routine operation will be possible only with a station engineered for minimum maintenance and with the data telemetered.

A considerable amount of useful information regarding HGLP installation problems and their solutions was obtained in the course of the project. Much of this material is to be found in the technical reports and has been shared with the Albuquerque Seismic Center. It is hoped that eventually there will be a high-quality long period station in the Great Lakes region.

APPENDIX I

Draft

ROUTINE M_o CALCULATIONS FROM AN AR PARAMETER METHOD FOR WWSSN INSTRUMENTS

by

*Barbara Radovich Williams
Department of Geology and Mineralogy
University of Michigan
Ann Arbor, Michigan 48109

* Now at Exxon Production Research, P. O. Box 2189, Houston, Texas 77001

ABSTRACT

Determinations of seismic moment have been made for 12 events occurring in 1974-1975 using an expanded version of the AR parameter method applicable to the WWSSN instruments. This method sums the energy in the entire surface wave train from events of magnitude $4.0<M_s<8.0$, recorded over predominantly oceanic paths of up to 17,000 km epicentral distance on WWSSN long period three-component instruments. The AR values are calibrated directly to M. The moment values calculated include, the Utah-Idaho March 28, 1975 event, M_s + 6.0, with new moment 1.2×10^{25} dyne-cm; the Leeward Is. October 8, 1974 event, $M_s = 7.5$, with moment 1.0×10^{27} dyne-cm; the Peru October 3, 1974 event, $M_s = 7.8$, with moment 1.2×10^{28} dyne-cm; the Panama July 13, 1974 event, $M_s = 7.3$, with moment 6.0×10^{26} dyne-cm; the Kermadec July 2, 1974 event, $M_s = 7.2$, with moment 1.6×10^{27} dyne-cm; and Solomon Is. February 1, 1974 event, $M_s = 7.1$, with moment 1.4×10^{27} dyne-cm. The method is shown to give a factor of two error for continental crustal events, and a factor of three error for oceanic crustal events. The method typically requires a much smaller set of stations than in spectral amplitude or time domain fitting moment estimates. Only an approximate knowledge of the recording instrument response, path type, and depth are needed for application of the method.

INTRODUCTION

Since the wide acceptance of the seismic moment (M_o) as a way to characterize the strength of an earthquake source, many studies have been conducted to calculate M_o values for events all over the world (Tsai and Aki, 1969; Kanamori, 1971; Hanks and Wyss, 1972; Mikumo, 1973; Langston, 1976; Burdick and Mellman, 1976). These studies have employed a variety of methods but most have in common the need for digitized seismograms from many stations for each event and expensive computer fitting routines to determine the radiation pattern.

The AR parameter method was introduced by Brune, Espinosa, and Oliver (1963), and they defined the AR parameter as the sum of the area under the envelope of the surface wave amplitudes recorded on long period, three-component Press-Ewing instruments. In Wyss and Brune (1968, 1971) the AR value was related directly to spectral density,

$$AR \sim \lim_{\omega \to 0} \int_{-\infty}^{\infty} f(t)\, e^{-i\omega t}\, dt$$

They assumed that the M_o is proportional to the spectral level at low frequencies as predicted by seismic source theory, which in turn relates the M_o to the AR parameter. One Press-Ewing long period instrument was calibrated by measuring AR for a set of events in the Southern California region that had M_o values determined by other methods. Then the calibration curve was used to calculate M_o for other events in that same locality. These workers found a direct

proportionality of M_o and the AR value for a set of small events recorded over short epicentral distances. They claimed that accurate moments could be found without applying radiation pattern corrections since adding the Love and Rayleigh surface wave trains would smooth the radiation pattern effect.

Several recent investigations have also shown the method to give sufficiently accurate results for large collections of small to medium magnitude events when calibrated to a given instrument and events in the San Andreas transform fault zone (Hanks, Hileman, and Thatcher, 1975) and in the New Zealand Rift zone (Gibowicz and Hatherton, 1975).

In light of the potential of the AR parameter method to calculate M_o more easily and routinely than other methods, this paper develops a single AR parameter versus M_o calibration curve for 20 long period WWSSN stations of similar tectonic settings, recording surface waves over predominantly oceanic paths, epicentral distances up to 17,000 km and magnitudes $4.0<M_s<8.0$. The calibration curve is derived from a well studied set of events with known M_o and radiation patterns and is applied to 12 unknown events occurring in 1974 and 1975. The effects of radiation pattern on the AR value are investigated in detail using the Love and Rayleigh wave spectral density formulations of Harkrider (1970). A theoretical AR vs M_o curve is derived using the average spectral theory of Geller (1976).

DATA

The calibration earthquakes are listed in Table 1 and are from a compilation of sources by Kanamori and Anderson (1975) and from calculations of Gibowicz and Hatherton (1975). The table contains several moment estimates for some of the events and the method used. The unknown data set for earthquakes occurring in 1974-1975 is in Table 2.

Stations were chosen for measurement that had three components of the long period WWSSN instruments recorded, with T_0 = 15 sec and T_g = 100 sec. Each event has AR values from several stations; the widest range of epicentral distances, from 422 to 17,000 km, and widest azimuthal coverage possible. These stations are listed in Table 4 for each event. The paths to each station are restricted to predominantly ocean paths to simplify attenuation corrections later. Gains range from 3000 to 375 and paper speeds from 15 mm/min and 30 mm/min. The AR values are normalized to a gain of 750 and paper speed of 30 mm/min on a standard size WWSSN seismogram.

The envelope of the surface waves was drawn on Itek seismogram reproductions, and converted to AR in cm^2. This will be called AR (Δ). The larger than original size seismographs facilitated the separation of successive traces on the record, which could be a significant source of error in the measurement technique for the large earthquakes in this study. With care, even for $M_s \sim 8.0$, the surface wave envelope may be measured with errors of less than 10%.

In the next sections, the measurement errors will be minor compared to the radiation pattern variations.

Figure 1 shows several AR envelopes drawn in this study and some of the techniques used for handling special problems. These procedures, some derived from Brune et al. (1963), are described in detail in Williams (1977), and tended to reduce errors and time.

The effect of aftershocks or events occurring in the wave train of the main event is a major problem when measuring the AR value for larger events. If there are several significant aftershcoks within 2 magnitude units of the main shock, an attempt is made to identify by inspection the arrival of these events within the wave train, measure the area under the envelope to the 20 s wave arrival time, and subtract this area to form a minimum and maximum AR value.

The resulting AR(Δ) values in cm^2 for the calibration and unknown data sets are plotted vs epicentral distance in Fig. 2. These will serve as the basis for deriving corrections for AR(Δ) with distance. We will show that it is not necessary to restrict the measurements to one station and calibrate it separately to find a station correction as Brune et al. (1963), Wyss and Brune (1968), Gibowicz and Hatherton (1975) and Hanks, Hileman, and Thatcher (1975) have done. Only one station gave consistently high AR values, the South Pole station SPA. This factor of about 1.7 remained fairly constant along the magnitude range. In Fig. 2, the station SPA data has been reduced to and plotted with the other stations.

Change of AR(Δ) with Epicentral Distance

The success of the AR method depends on how accurate a correction of AR(Δ) with epicentral distance one can make. Brune et al. (1963) simplified this procedure by making the following assumption at each distance: one can characterize the decay or growth of the AR envelope by one period, and as the AR is measured at larger distances this representative period increases because the higher frequencies become attenuated.

In Fig. 3, Brune's five step model is shown for the representative period at various distances. Since we have a wide range of magnitude curves A,B, and C have been adopted as the models for small, medium, and large events, assuming in general that larger magnitude events will show longer period contributions to the surface wave train than the next smaller group. Curve A is below Brune's model because the Press-Ewing long period instruments (T_0 = 30 s, T_g = 100 s) he used have a slightly larger period response peak than the present setting of the long period WWSSN instruments (T_0 = 15 s, T_g = 100 s). Several models have been tried in this analysis and those that best fit the measured AR(Δ) data in Fig. 3 are shown as models A, B, C.

Four main corrections will be applied to the AR(Δ) that depend on period or epicentral distance; geometric spreading, instrument response, attenuation, and spreading due to dispersion of the wave train. No corrections for crustal response or source spectral shape will be applied to the AR(Δ) at this time.

The geometric spreading used is that adopted by Brune et al. (1963), a factor of $1/\sqrt{\sin\Delta^\circ}$ applied to the AR(Δ). The instrument response is based on the magnification curve for a WWSSN long period instrument at 750 gain. The attenuation corrections for the Pacific Ocean paths are based on Mitchell et al. (1976). These coefficients are used to correct for Atlantic and Indian Ocean paths as well. The Love and Rayleigh coefficients are averaged for each period. The coefficients are applied via the relation $\exp-(\gamma_L + \gamma_R/2)\Delta$, where γ_L and γ_R are the Love and Rayleigh attenuation coefficients for the period predominant at the distance Δ of the station, according to the period model A, B, or C.

After Brune, the change in the AR(Δ) due to spreading of the train is a factor of $T^{1/2}$ where T is the duration of the wave train. Brune assumed that for his set of small earthquakes, the range of group velocities was constant, therefore the duration grew linearly with distance. But in this study, oceanic paths are used and the range of group velocities will differ between curves A, B, and C. The upper limit of the goup velocity is set at 4.4 km/sec which is the Love wave oceanic group velocity for the periods of interest in this study. The group velocity lower limit, U_{min}, though will change rapidly with period due to the steep Rayleigh wave oceanic dispersion curve and the dispersion factor will depend on how fast the lower velocities become neglected.

This factor is $D(\Delta) = [\Delta\ (1/U_{min} - 1/4.4)]^{1/2}$ and Fig. 4 shows the change in duration, D(Δ) of the wave train due to the effect of group velocity dispersion, versus distance, Δ.

The curve corresponding to the A model shows a steeper slope than Brune's as the velocity range is increased through the Airy phase, then flattens as the low group velocities become neglected. B' shows an intermediate model where the Airy phase velocities are neglected at about 7000 km. The curve corresponding to model B neglects these low velocities more gradually than B', starting at about 2000 km. The C curve has a nearly constant velocity range.

If we generate decay curves of AR(Δ) with distance at this point and correct the measured data sets to a standard distance, the small, medium, and large groups of events will be offset from each other because the starting points of the three models A, B, and C are different in period and group velocity range. Several standards must be chosen which will make the AR(Δ) corrected to a given distance consistent between various magnitudes and kinds of events.

The standards are as follows:

1. All AR(Δ) will be corrected to the value at 3.8^{o}, the distance at which dispersion is completely developed for oceanic paths (Gibowicz and Hatherton, 1975).

2. Attenuation and instrument response characteristics will be normalized to those at 20 s.

3. All durations of dispersed wave trains will be scaled to the standard duration from a wave train with group velocities of .5-4.5 km/sec.

4. A fourth standard is implied by the use of predominantly shallow continental crust events in the calibration data set.

The oceanic crustal response is generally lower than the continental crustal response for a large range of periods of interest in this study and a variety of shallow source mechanisms (Harkrider, 1970). Thus, for events occurring in ocean crust settings, another scale factor calculated from Harkrider's formulations, is applied to raise the crustal response to the standard; shallow events occurring in continental crust. The Gutenberg-Bullen earth model is the continental crustal model, and the Harkrider oceanic crust model is chosen to represent the oceanic tectonic settings.

No corrections for depth are made in this study. All earthquakes are assumed to be 40 km or shallower. If depth corrections are desired, they would be applied to the combined standard scale factors.

The final three curves based on representative period models A, B, and C of AR(Δ) decay with epicentral distance are presented in Fig. 5 along with the combined standard scale factors for each model and crustal type. The theoretical decay curves in Fig. 5 show three different slopes in the 2000-10,000 km range which can be used to distinguish the three groups of events; the A model curve has the steepest slope, B an intermediate, and C the smallest slope. Fig. 2 shows that these slope changes do exist in the data by comparing the group of numbered earthquakes 68/76, 68/146, and 67/426 to the Turkey '67 and Iran

events. As predicted, there is a definite decrease in slope as the AR values become larger. The first break point seems to come at $M_s \sim 6.0$, and the second break point at $M_s \sim 7.0$. This will serve as a general guideline. Events with $M_s < 6.0$ should fit closely to the A model decay curve, events with $6.0 < M_s < 7.0$ the B model decay curve, and for $M_s > 7.0$ the C model curve. Regions on Fig. 2 outline the AR(Δ) values to be applied to each curve.

There are some exceptions to the division. The Borrego Mountain event with $M_s = 6.7$ definitely has the characteristics of the A decay curve. But this event has an exceptionally large number of aftershocks which show up on the closer stations. These will attenuate quite fast as the epicentral distance is increased, so the data points will give an apparently steep slope. The Borrego Mountain event will be fit to the B curve using the minimum AR(Δ) values.

The Solomon Islands, Leeward Islands, Kermadec 1, and India events show large kinks in their AR(Δ) values. These deviations will be shown in the next section to be due to the radiation pattern effect for these events.

Figures 6a, b, and c show the observed AR(Δ) values fit to the proper theroetical decay curve. The earthquakes chosen to fit each decay curve are labeled on the plot.

Azimuthal Variation of the $AR_{3.8}o$ Parameter

To study the azimuthal variation of the $AR_{3.8}o$ parameter, plots of the theoretical surface wave radiation pattern for the calibration set of events and for four events of 1974 will be generated. Focal mechanism solutions have been determined by previous investigators and are listed in Table 3. The $AR_{3.8}o$ values are drawn on the plots in their azimuthal position to gauge the extent of the radiation pattern and path difference effects.

Since the radiation pattern of surface waves changes with period, several periods were chosen for illustration based upon the A, B, or C representative period models. For the events fit to the A curve in the reduction of the $AR(\Delta)$ to $AR_{3.8}o$, the 20 s radiation pattern is compared to the $AR_{3.8}o$ values, for the B curve events, a 30 s pattern is chosen and for the C curve events, a 45 s pattern.

Since the $AR_{3.8}o$ parameter is related to the addition of the spectral density for each component, it will be compared to the spectral far field solutions for Love and Rayleigh waves from Harkrider (1970). The same source function used by Geller (1976) is chosen, $M(\omega)/\omega$, in which he develops average theoretical spectra for various magnitudes of events. The envelope radiation diagram will show the $E_1(\omega)$ function,

$$E_1(\omega) \equiv \left|R(\omega)\right| \exp(\gamma_L - \gamma_R)\Delta + \left|L(\omega)\right| \qquad (1)$$

where $|R(\omega)|$ is the addition of the horizontal and vertical Rayleigh wave responses and $|L(\omega)|$ is the Love wave response. These values are calculated from Harkrider's (1970) formulations and depend on crustal model, the source mechanism and spectrum. The exponential term is used to adjust the theoretical envelope for relative differences in the attenuation of Love and Rayleigh waves over oceanic paths which will affect the shape of the observed AR parameter azimuthal distribution.

The $AR_{3.8°}$ parameter must now be related to the spectral densities. The steepest descent approximation for surface waves relates the amplitudes at the phase period in the frequency domain to the group period in the time domain (Ben Menahem, 1961). The amplitudes in the time domain are modified by the slope of the dispersion curve at the group period and by the phase shifts introduced by assuming a finite earthquake source with duration time. These phase shifts have been assumed to be small except for the largest events on record (Kanamori and Anderson, 1975; and Geller, 1976) and have been neglected in this study. The final relation is from Williams (1977),

$$AR_{3.8°} = \left[R(\omega)\ e^{-\gamma_R \Delta} + L(\omega)\ e^{-\gamma_L \Delta}\right] \cdot \exp\left(\frac{\gamma_L + \gamma_R}{2}\right)\Delta \cdot M(\omega) \cdot \Omega \cdot 10^{-20}\,cm^2$$

The exponential factor is the attenuation correction adopted in the formulation of the AR decay curves with epicentral distance, an average of the Love and Rayleigh coefficients.

The scale factor Ω corrects for the standard set of parameters, i.e., 422 km distance, 750 gain, 30 mm/min paper speed, attenuation and instrument response at 20 s. This factor also scales for the fact that the $AR_{3.8°}$ value is calculated from a dispersed wave train. Developing the above equation further

$$\frac{AR_{3.8°}}{M(\omega)\ \Omega}\ e^{(\gamma_L - \gamma_R/2)\Delta} = E_1(\omega)\ \text{sec/dyne} \qquad (2)$$

Figure 7 gives the calculated and observed envelope functions from equations (1) and (2) for continental crustal events in this study that have wide azimuthal coverage. Figure 8 shows the same for oceanic crustal events. The observed envelope functions measured from $AR_{3.8°}$ values are plotted at each station's azimuth.

Stations located in predicted nodal positions rarely give $AR_{3.8°}$ values as low as predicted, but Brune's assumption that adding the Love and Rayleigh waves smooths the radiation pattern effect can be seen to work nearly completely only for strike-slip events in continental crust. The Iran and Borrego Mountain events show little observed or predicted azimuthal variation in $AR_{3.8°}$ because the Love and Rayleigh wave response is nearly equal. Even the India earthquake, more nearly a dip-slip event, shows only a factor of 2 variation. Contrast these continental crustal events to those in Figure 8, where the dip-slip events in oceanic crust produce nearly a factor of 3

variation as the Love wave response becomes much smaller than the Rayleigh wave response. Dip-slip events concentrate the Rayleigh wave energy near 90° to the strike of the fault plane. These azimuths, 45° to 135° from the strike of the fault plane, would be a favored position for a set of $AR_{3.8°}$ measurements because the maximum energy from both strike-slip and dip-slip events would be recorded.

Since the radiation pattern and aftershock activity have such a dominant effect on the AR(Δ) data fits to the theoretical curves in Figs. 6a, b, and c, the errors are best discussed in the context of certain classes of events rather than based upon the measuring procedures for each event. These procedures contribute less than 10% error to the AR(Δ) value for all magnitude ranges.

The classes of events which have the best fit to the AR(Δ) data to theoretical curve, to within a factor of two, are the continental crustal events and small oceanic events of $M_s < 6.0$, both without aftershock activity. These errors are caused by minor path variations, the presence of multipathing in the wave train, and a small radiation pattern effect. Continental crustal events with many aftershocks, and oceanic events with $M_s > 6.0$ and little aftershock activity fit the theoretical curves by a factor of three. The extra source of error for the continental events is the contamination of the wave train by interfering events, and the error in the larger oceanic earthquakes is due to the increased radiation pattern effect for all sources within

oceanic crust. A factor of four error is assigned to the last class of events, the large oceanic crustal events with much aftershock activity. The list of M_o values generated by different techniques for the calibration earthquakes in Table 1 shows that this is an acceptable kind of error for these calculations.

Calibration Curves

All the data was reduced to the standard distance to derive the $AR_{3.8°}$ value using the appropriate decay curve and standard corrections. These values are plotted for the calibration earthquakes in Fig. 9 versus the M_o accepted for these events. Error bars have been drawn for the $AR_{3.8°}$ and M_o values. In general, the $AR_{3.8°}$ parameter agrees quite well within the M_o error bars and forms a consistent calibration curve over a wide range of moment values.

The relations for the calibration curve are

$$\text{Log } M_o = \text{Log } AR_{3.8°}\text{cm}^2 + 22.0 \quad AR_{3.8°} \leq 3 \times 10^4 \text{ cm}^2$$

$$\text{Log } M_o = 1.55 \text{ Log } AR_{3.8°}\text{cm}^2 + 19.5 \quad AR_{3.8°} > 3 \times 10^4 \text{ cm}^2$$

The $AR_{3.8°}$ data from the unknown set of events in 1974-1975 are converted to M_o using the above relationships. To arrive at a final estimate, the stations are averaged. This data is in Table 4.

The strategic location of station SPA plus its low gain setting (375) makes it especially suited to record

large events in the Pacific. This station was the only one to give consistently higher $AR(\Delta)$ measurements. Now part of the calibration and unknown events can serve as a calibration for this station. This data is shown in Fig. 10. The tectonic setting of station SPA is quite different from that of the rest of the stations; SPA sits well into the continent of Antarctica while most of the other stations sit near the oceanic-continental edge. These variations in tectonic setting do not give a correction of more than a factor of two for SPA and for most of the magnitude range the factor is less. In light of this, the assumption that stations with similar paths from the epicenter could be used without calibrating each separately seems reasonable. The relations for the SPA calibration curve are

$$\text{Log } M_o = \text{Log } AR_{3.8^\circ} + 21.8 \quad AR_{3.8^\circ} \leq 3.5 \times 10^4 \text{ cm}^2$$

$$\text{Log } M_o = 1.63 \text{ Log } AR_{3.8^\circ} + 18.9 \quad AR_{3.8^\circ} > 3.5 \times 10^4 \text{ cm}^2$$

Theoretical and Observed $AR_{3.8^\circ}$ vs M_o Relations

A theoretical $AR_{3.8^\circ}$ vs M_o calibration curve can be generated for various frequencies from relation (2). Using the average $M(\omega)$ defined by Geller for a stress drop of 50 bars, and an average value for the 20 s Rayleigh-Love envelope response function, the theoretical $AR_{3.8^\circ}$ vs M_o curve with constant crustal response is presented in Fig. 11. This set of curves will move to the right for higher stress drop than 50 bars, and to the left for lower stress drop.

These curves reflect the spectral shape change with increasing M_o from source theory. Fig. 12 shows the addition of variable crustal response. The two effects of crustal response with period and spectra shape change with increasing M_o were the only two corrections left out of the $AR_{3.8°}$ and so must be applied to the theoretical curves.

Fig. 13 compares the observed calibration curve and the envelope of selected theoretical curves. This envelope increases in period with increasing M_o, which is the assumption adopted in drawing the predominant period models A, B, and C. The fit of the two curves is quite good, and the steeper slope for M_o above 3×10^{26} dyne-cm is interpreted as a source and crustal response effect. This comparison establishes the calibration curve in the $AR_{3.8°}$ parameter method to a true static M_o in the context of seismic source theory.

CONCLUSION

A single calibration curve for relating the AR parameter to M_o has been found which is applicable to 20 long period WWSSN stations recording surface waves from shallow earthquakes over predominantly oceanic paths, epicentral distances up to 17,000 km and magnitudes up to $M_s = 8.0$. The relation is

$$\text{Log } M_o = \text{Log } AR_{3.8°}\text{cm}^2 + 22.0 \quad AR_{3.8°} \leq 3 \times 10^4 \text{cm}^2$$

$$\text{Log } M_o = 1.55 \text{ Log } AR_{3.8°}\text{cm}^2 + 19.5 \quad AR_{3.8°} > 3 \times 10^4 \text{cm}^2$$

This curve relates well to that predicted by seismic source theory where M_o is interpreted as a true static M_o value.

The procedure is quick and easy, requiring only an approximate knowledge about the recording instrument response, path type, and depth. For continental events, few stations may be needed to calculate a M_o within a factor of 2 error, for the AR parameter shows little radiation pattern variation. For oceanic events, the radiation pattern effect on the AR parameter becomes more pronounced, and a set of stations azimuthally distributed are needed to calculate M_o values with factor of 3 error.

Typically, a much smaller set of stations is required for the AR parameter than in spectral amplitude or time domain estimates of moment because the AR value, being a sum of many periods, is less sensitive to path, station and source differences. Thus, M_o can be calculated more routinely than with the methods predominantly in use.

This research was supported by the Advanced Research Projects Agency of the Department of Defense and was monitored by the Air Force Office of Scientific Research under Contract No. F44620-73-C-0060.

Table 1

List of Calibration Events

Event	Type*	mb	Ms	H(Km)	M_o(dyne-cm)	Method	Source
Tokachi-Oki, 1968	CM	---	7.9	7.1	2.8×10^{28}	100 s surface waves	Kanamori (1971)
Peru, 1970	CD	6.6	7.8	43	1×10^{28}	100 s surface waves	Abe (1972)
Nemuro-Oki, 1973	CD	6.5	7.7	48	6.7×10^{27}	100 s surface waves	Shimazaki (1975)
Turkey, 1967	B	6.0	7.1	4	7.4×10^{26}	Field Data	Ambraseys & Zatopek (1969)
					9.1×10^{26}	P wave spectra	Hanks & Wyss (1972)
					8.5×10^{26}	S wave spectra	Hanks & Wyss (1972)
					1.5×10^{27}	Surface wave spectra	North (1974)
Iran, 1968	B	6.0	7.3	13	1.8×10^{27}	Field data	Ambraseys & Tchalenk (1969)
					4.8×10^{26}	P wave spectra	Hanks & Wyss (1972)
					8.6×10^{26}	S wave spectra	Hanks & Wyss (1972)
Turkey, 1970	B	6.0	7.0	20	3×10^{26}	Surface wave spectra	North (1974)
San Fernando, 1971	BD	6.2	6.6	13	1.53×10^{26}	Dislocation models	Trifunac (1974)
					6.2×10^{25}	Finite element model	Jungels & Frazier (1975)
					1.1×10^{26}	Strain and tilt data	Mikumo (1973)
					1.3×10^{26}	Field data	Wyss & Hanks (1972)

* Event type: A - small oceanic crust, B - continental crust, C - large ocean crust, D - many aftershocks contaminating wave train

Table 1 (Continued)

Event	Type*	mb	Ms	H(Km)	M_o(dyne-cm)	Method	Source
					4.7×10^{25}	P wave spectra	Wyss & Hanks (1972)
					8.8×10^{25}	S wave spectra	Wyss & Hanks (1972)
					1.64×10^{26}	Strain data	Canitez & Toksöz (1972)
Borrego Mt., 1968	BD	6.1	6.7	8	1.12×10^{26}	Body wave time domain fits	Burdick & Mellman (1976)
					3.6×10^{25}	Field data	Hanks & Wyss (1972)
					1×10^{26}	P wave spectra	Hanks & Wyss (1972)
					6.6×10^{25}	S wave spectra	Hanks & Wyss (1972)
India, 1967	B	---	6.3	10	8.2×10^{25}	Surface wave spectra	Singh et al. (1975)
					3.2×10^{25}	Body wave time domain fits	Langston (1976)
arkfield, 1966	B	5.3	6.4	4	1.4×10^{25}	Surface waves	Tsai & Aki (1969)
					1.9×10^{25}	Field data	Scholz et al. (1969)
					4.4×10^{25}	Strong motion & static data	Trifunac & Uwadia (1974)
67/426	A	6.0	---	33	4×10^{24}	AR parameter method for station WEL	Gibowicz & Hatherton (1975)
68/146	A	5.2	---	15	4.7×10^{24}	AR parameter method for station WEL	Gibowicz & Hatherton (1975)

* Event Type: A - small oceanic crust, B - continental crust, C - large ocean crust, D - many aftershocks contaminating wave train

Table 1 (Continued)

Event	Type*	mb	Ms	H(Km)	M_o(dyne-cm)	Method	Source
68/76	A	5.6	---	33	1×10^{25}	AR parameter method for station WEL	Gibowicz & Hatherton (1975)
68/58	A	4.8	---	6	1.6×10^{24}	AR parameter method for station WEL	Gibowicz & Hatherton (1975)
68/232	A	4.7	---	35	1.2×10^{24}	AR parameter method for station WEL	Gibowicz & Hatherton (1975)
68/519	A	---	---	40	4.1×10^{23}	AR parameter method for station WEL	Gibowicz & Hatherton (1975)
68/815	A	4.7	---	33	8.7×10^{23}	AR parameter method for station WEL	Gibowicz & Hatherton (1975)
66/104	A	6.1	---	27	1.8×10^{25}	AR parameter method for station WEL	Gibowicz & Hatherton (1975)
71/440	A	5.3	---	18	1.2×10^{25}	AR parameter method for station WEL	Gibowicz & Hatherton (1975)

* Event Type: A - small oceanic crust, B - continental crust, C - large ocean crust, D - many aftershocks contaminating wave train

Table 2

Events with Unknown M_o

Event	Date	Depth (Km)	m_b*	M_s**
Solomon Island	February 1, 1974	12	6.2	7.1
Szechwan Province, China	May 10, 1974	17	5.8	6.8
Mariana Island	May 11, 1974	26	6.2	5.9
Molucca Pass.	May 11, 1974	43	6.1	6.0
South India Ocean	June 25, 1974	20	6.1	6.7
Kermadec 1	July 2, 1974	33	6.5	7.2
Kermadec 2	July 3, 1974	77	6.0	6.6
Panama	July 13, 1974	12	6.4	7.3
Kurile Island	September 27, 1974	5	6.0	6.7
Peru	October 3, 1974	9	6.2	7.8+
Leeward Island	October 8, 1974	30++	6.4	7.4
Utah-Idaho	March 28, 1975	5	6.1	6.0

* ISC Bulletin
** NEIS
\+ Stewart (1978)
++ Tomblin and Aspinall (1975)

Table 3

Radiation Pattern Input Data

Event	Strike deg.	Dip deg.	Slip deg.	H km.	T sec	Crust GB or H	Source for Focal Mechanism
India	16	67	-29	12	30	GB	Langston (1976)
Borrego Mt.	315	81	178	8	30	GB	Burdick & Mellman (1976)
Iran	275	80	5	14	45	GB	Niazi (1969)
Tokachi-Oki	156	20	39	7	55	H	Kanamori (1971)
Kermadec 1	184	77	74	33	45	H	Williams (1977)
Panama	245	20	140	12	45	GB	Williams (1977)
Solomon Is.	140	61	100	12	45	H	Williams (1977)

Table 4

M_o Determined From $AR_{3.8°}$ Method

Event	Curve A,B,C	Station	$AR_{3.8°}$ x 10^3 cm^2	M_o dyne-cm x 10^{26}	Average M_o	M_o Corrected for Radiation Pattern
Kermadec 1	C	LEM	118	25	1.4×10^{27}	1.6×10^{27}
		KIP	47.4 - 52.5	6.1 - 7.2		
		MAT	48.1	6.3		
		AKU	91.4	17		
Peru '74	C	GUA	209-328	61-120	1.1×10^{28}	1.2×10^{28}
		RAR	264-359	88-140		
Panama	C	AKU	26.5 - 45.7	2.5 - 5.8	6.0×10^{26}	6.0×10^{26}
		KIP	24.2 - 48.2	2.1 - 6.3		
		RAR	48.8 - 81.4	6.4 - 14		
		WEL	48.3	6.3		
Solomon Is.	C	LEM	68.0	11	1.1×10^{27}	1.4×10^{27}
		KIP	80.9 - 108	14 - 22		
		AKU	81.6	14		
		MAT	47.1 - 50.5	6.1 - 6.8		
		LPB	49.4	6.5		
Leewards	C	AKU	36.6 - 50.5	4.1 - 6.8	1.0×10^{27}	---
		KIP	56.9 - 63.8	8.1 - 9.7		
		PDA	84.3 - 93.6	15 - 18		
S. India Ocean	B	LEM	9.32 - 10.9	.93 - 1.1	1.4×10^{26}	---
		CHG	17.7	1.8		
Szechwan Province China	B	KIP	7.28	.73	7.0×10^{25}	---
		GUA	6.63	.66		
Kermadec 2	B	KIP	7.5 - 9.64	.75 - .96	2.0×10^{26}	---
		BKS	36.4	4.1		
		LPB	11.0	1.1		
Marianas	B	COL	5.81	.58	6.2×10^{25}	---
		KIP	5.77	.58		
		BKS	6.94	.69		
Moluccas	B	KIP	4.00 - 4.87	.40 - .49	4.0×10^{25}	---
		GUA	3.28 - 3.74	.33 - .37		
Kuriles	B	GUA	26.1 - 27.8	2.6 - 2.8	3.2×10^{26}	---
		KIP	35.2	3.5		
		LPB	31.2	3.2		
Utah-Idaho	A	GUA	1.42	.14	1.2×10^{25}	---
		MAT	.972	.097		
		KIP	1.08	.11		

REFERENCES

Abe, K. (1972). Mechanisms and tectonic implications of the 1966 and 1970 Peru earthquakes, Phys. Earth Planet. Interiors 5, 367-370.

Ambraseys, N. N., and J. S. Tchalenko (1969). The Dasht-e-Bayaz (Iran) earthquake of August 31, 1968. A field report, Bull. Seism. Soc. Am. 59, 1751-1792.

Ambraseys, N. N., and A. Zatopek (1969). The Mudurnu Valley, West Anatolia, Turkey earthquake of July 22, 1967, Bull. Seism. Soc. Am. 59, 521-589.

Brune, J., A. Espinosa, and J. Oliver (1963). Relative excitation of surface waves by earthquakes and underground explosions in California and Nevada, J. Geophys. Res. 68, 3501-3513.

Burdick, L. J., and G. Mellman (1976). Inversion of the body waves from the Borrego Mountain earthquake to the source mechanism, Bull. Seism. Soc. Am. 66, 1485-1499.

Canitez, N., and M. N. Toksöz (1972). Static and dynamic study of earthquake source mechanism: San Fernando earthquake, J. Geophys. Res. 77, 2583-2594.

Geller, R. J. (1976). Scaling relations for earthquake source parameters and magnitudes, Bull. Seism. Soc. Am. 66, 1501-1523.

Gibowicz, S. J. (1975). Variation of source properties: the Inangahua, New Zealand, aftershocks of 1968, Bull. Seism. Soc. Am. 65, 261-276.

Gibowicz, S. J., and T. Hatherton (1975). Source properties of shallow earthquakes in New Zealand and their tectonic associations, Geophys. J. 43, 589-605.

Hanks, T. C., and M. Wyss (1972). The use of body-wave spectra in the determination of seismic-source parameters, Bull. Seism. Soc. Am. 62, 561-589.

Hanks, T. C., J. A. Hileman, and W. Thatcher (1975). Seismic moments of the larger earthquakes of the Southern California region, Bull. Geol. Soc. Am. 86, 1131-1139.

Harkrider, D. G. (1964). Surface waves in multilayered elastic media: I. Rayleigh and Love waves from buried sources in a multilayered elastic halfspace, Bull. Seism. Soc. Am. 54, 627-658.

Harkrider, D. G. (1970). Surface waves in multilayered elastic media: II. Higher mode spectra and spectral ratios from point sources in plane layered earth models, Bull. Seism. Soc. Am. 60, 1937-1987.

Jungels, P. H., and G. A. Frazier (1973). Finite element analysis of the residual displacements for an earthquake rupture: Source parameters for the San Fernando earthquake, J. Geophys. Res. 78, 5062-5083.

Kanamori, H. (1971). Focal mechanism of the Tokachi-Oki earthquake of May 16, 1968: Contortion of the lithosphere at a junction of two trenches, Tectonophysics 12, 1-13.

Kanamori, H., and D. L. Anderson (1975). Theoretical basis of some empirical relations in seismology, Bull. Seism. Soc. Am. 65, 1073-1095.

Langston, C. A. (1976). A body wave inversion of the Koyna, India, earthquake of December 10, 1967, and some implications for body wave focal mechanisms, J. Geophys. Res. 81, 2517-2529.

Mikumo, T. (1973). Faulting process of the San Fernando earthquake of February 9, 1971, inferred from static and dynamic near field displacements, Bull. Seism. Soc. Am. 63, 249-269.

Mitchell, B. J., L. W. B. Leite, Y. K. Yu, and R. B. Herrmann, (1976). Attenuation of Love and Rayleigh waves across the Pacific at periods between 15 and 110 seconds, Bull. Seism. Soc. Am. 66, 1189-1201.

Niazi, M. (1969). Source dynamics of the Dasht-e-Bayaz earthquake of August 31, 1968, Bull. Seism. Soc. Am. 59, 1843-1861.

North, R. G. (1974). Source dimensions of events in western Turkey, Semiannual Technical Summary, Seismic Discrimination, Lincoln Laboratory, MIT, Lexington.

Ohnaka, M. (1976). A physical basis for earthquakes based on the elastic rebound model, Bull Seism. Soc. Am. 66, 433-451.

Scholz, C., M. Wyss, and S. W. Smith (1969). Seismic and aseismic slip on the San Andreas fault, J. Geophys. Res. 74, 2049-2069.

Shimazaki, D. (1975). Nemuro-Oki earthquake of June 17, 1973; A lithospheric rebound at the upper half of the interface, Phys. Earth Planet. Interiors 9, 314-327.

Singh, D. D., B. K. Rastogi, and H. K. Gupta (1975). Surface wave radiation pattern and source parameters of Koyna earthquake of December 10, 1967, Bull. Seism. Soc. Am. 65, 711-731.

Stewart, G. (1978).

Tomblin, J. F., and W. P. Aspinall (1975). Reconnaissance report of the Antigua, West Indies, earthquake of October 8, 1974, Bull. Seism. Soc. Am. 65, 1553-1573.

Trifunac, M. D. (1974). A three-dimensional dislocation model for the San Fernando, California, earthquake of February 9, 1971, Bull. Seism. Soc. Am. 64, 144-172.

Trifunac, M. D., and F. G. Udwadia (1974). Parkfield, California, earthquake of June 27, 1966: A three-dimensional moving dislocation, Bull. Seism. Soc. Am. 64, 511-533.

Tsai, Y. B., and K. Aki (1969). Simultaneous determination of the seismic moment and attenuation of seismic surface waves, Bull. Seism. Soc. Am. 59, 275-287.

Turnbull, L. S. (1976). Determination of seismic source parameters using far-field surface wave spectra, Ph.D. Thesis, The Pennsylvania State University, University Park, Pennsylvania.

Williams, B. R. (1977). Source parameters for large earthquakes from High Gain Long Period body wave spectra, Ph.D. Thesis, University of Michigan, Ann Arbor, Michigan.

Wu, F. T. (1968). Parkfield earthquake of June 28, 1966: Magnitude and source mechanism, Bull, Seism. Soc. Am. 58, 689-709.

Wyss, M., and J. N. Brune (1968). Seismic moment, stress, and source dimensions for earthquakes in the California-Nevada region, J. Geophys. Res. 73, 4681-4694.

Wyss, M., and J. N. Brune (1971). Regional variations of source properties in southern California estimated from the ratio of short- to long-period amplitudes, Bull. Seism. Soc. Am. 61, 1153-1167.

Wyss, M., and T. C. Hanks (1972). Source parameters of the San Fernando earthquake inferred from teleseismic body waves, Bull. Seism. Soc. Am. 62, 591-602.

LIST OF FIGURES

Figure 1 Examples of procedures used in AR(Δ) measurement. (a) Area of aftershock arrival at A to B subtracted from AR(Δ). (b) Area with numerous aftershocks starting at time A to B subtracted from AR(Δ). (c) Area above zero line from A to B is doubled when summing entire trace. Extrapolation of peaks is made for short time spans.

Figure 2 AR value versus epicentral distance Δ. Lines connect stations' AR values for each event.

Figure 3 Representative period models A, B, C versus epicentral distance compared to the 5-step model of Brune et al. (1963).

Figure 4 Increase in duration, D(Δ), of surface wave train with distance due to dispersion; for models A, B' (an intermediate model), B, and C.

Figure 5 Theoretical AR parameter decay with epicentral distance, Δ, for models A, B, C. After correcting AR to standard distance, scale factors are applied.

Figure 6a Fit of small events to A model decay curve from Figure 5.

Figure 6b Fit of intermediate size events to B model decay curve from Figure 5

Figure 6c Fit of large events to C model decay curve from Figure 5. Note increase in spread of data due to radiation pattern and aftershock effects.

Figure 7 Continental crustal events' theoretical and observed envelope function, E_1, in units of 10^{-4} sec/dyne. TL and TR are periods of the Love and Rayleigh radiation patterns. Observed E_1 values from AR measurement are labeled with WWSSN station codes. Strike of fault is the vertical axis.

Figure 8 Oceanic crustal events' theoretical and observed envelope function, E_1, in units of 10^{-4} sec/dyne.

Figure 9 $AR_{3.8°}$ versus M_o calibration curve. Open circles are minimum $AR_{3.8°}$ values. Error bars for M_o are from Table 1 and for AR value depend on type of event.

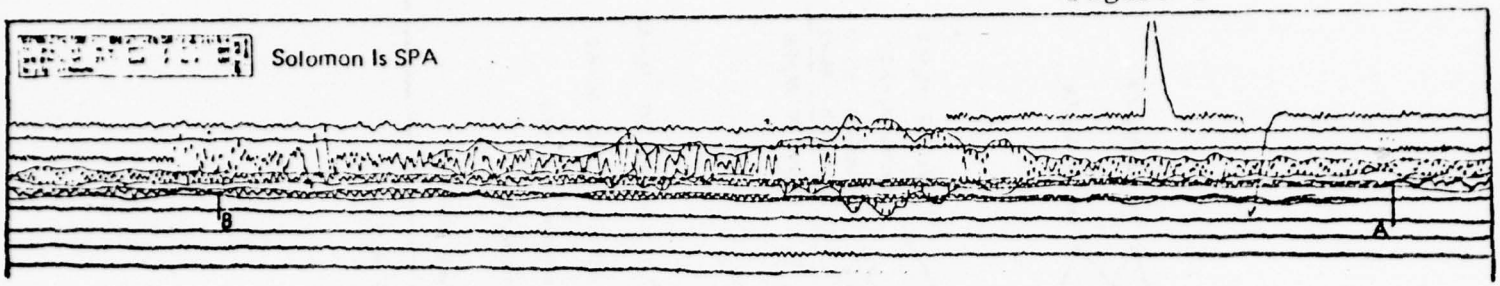
Figure 10 $AR_{3.8°}$ versus M_o calibration curve for station SPA, south pole. AR(SPA) values are triangles.

Figure 11 Theoretical $AR_{3.8°}$ versus M_o relations for various periods with constant crustal response equal to that at 20 sec.

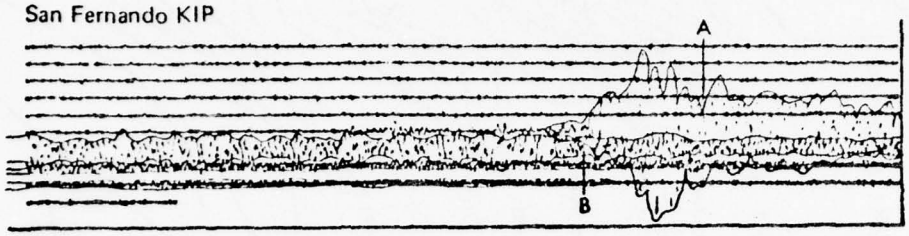
Figure 12 Theoretical $AR_{3.8°}$ versus M_o relations for period dependent crustal response.

Figure 13 Comparison of observed and theoretical calibration curves for $AR_{3.8°}$ vs M_o. Shaded area represents envelope of selected theoretical curves from Figure 14.

Figure 1



a.



b.

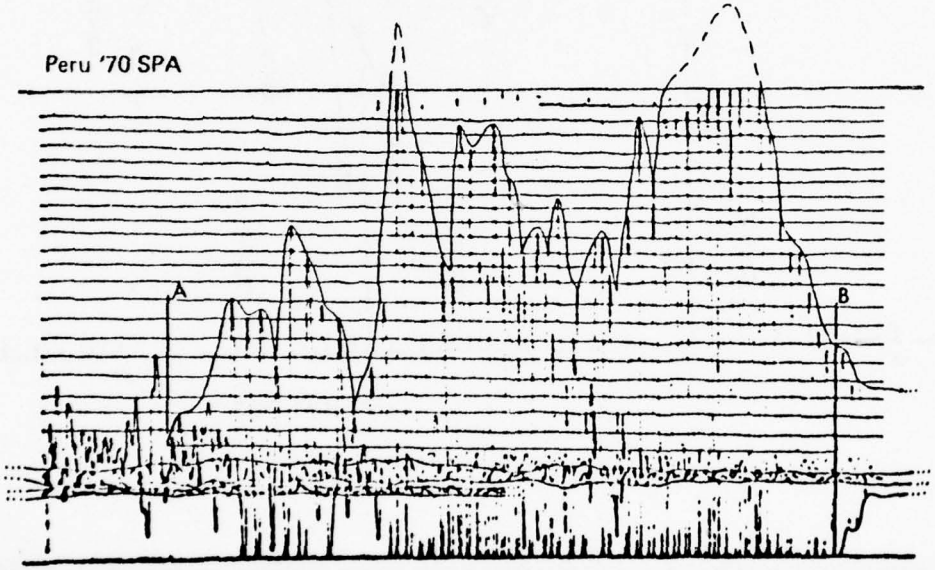


Figure 2

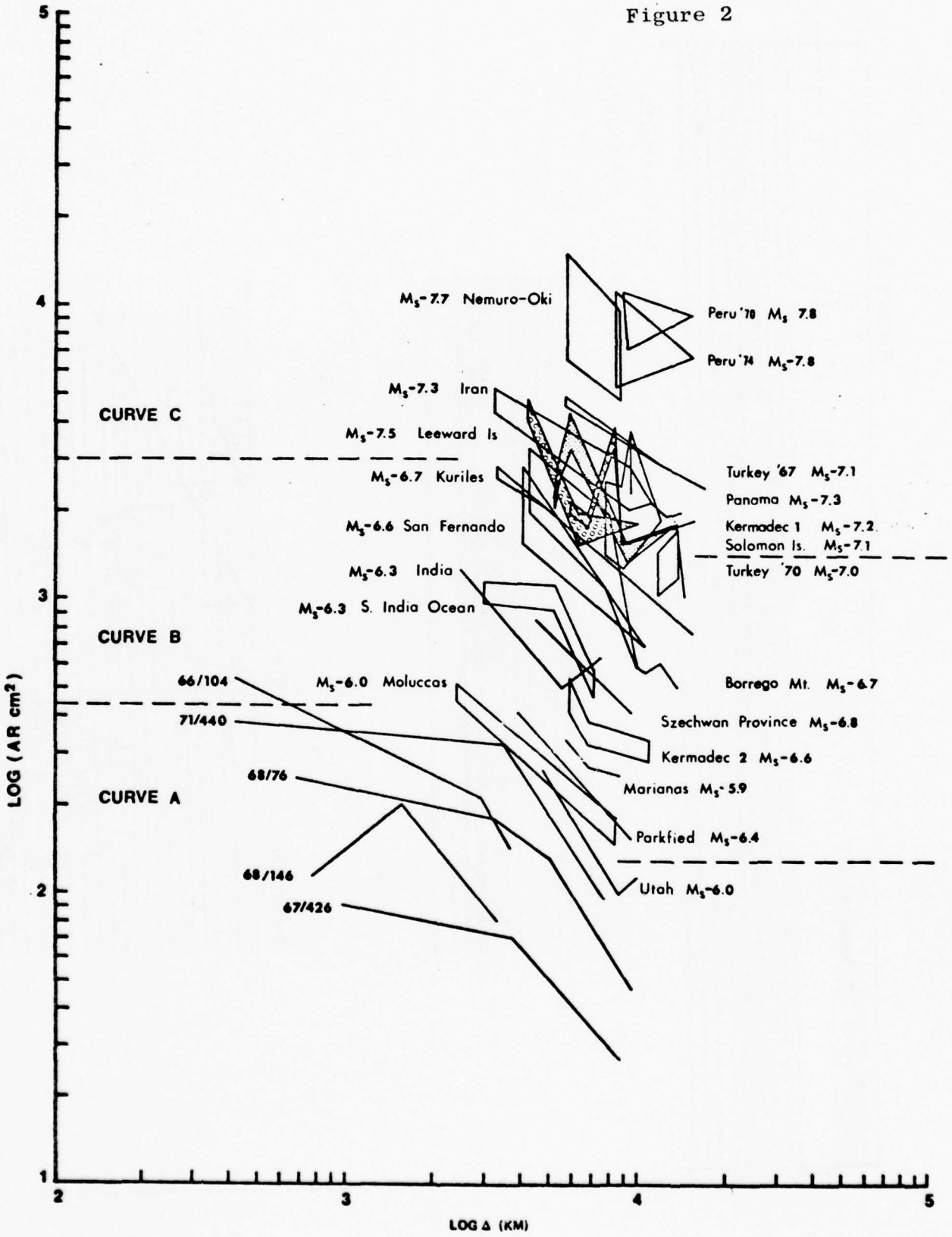

LOG (AR cm²)
LOG Δ (KM)
CURVE C
CURVE B
CURVE A
Ms-7.7 Nemuro-Oki
Peru '78 Ms 7.8
Peru '74 Ms-7.8
Ms-7.3 Iran
Ms-7.5 Leeward Is
Ms-6.7 Kuriles
Turkey '67 Ms-7.1
Panama Ms-7.3
Ms-6.6 San Fernando
Kermadec 1 Ms-7.2
Solomon Is. Ms-7.1
Turkey '70 Ms-7.0
Ms-6.3 India
Ms-6.3 S. India Ocean
Ms-6.0 Moluccas
Borrego Mt. Ms-6.7
66/104
71/440
Szechwan Province Ms-6.8
Kermadec 2 Ms-6.6
68/76
Marianas Ms-5.9
Parkfied Ms-6.4
68/146
Utah Ms-6.0
67/426

Figure 3

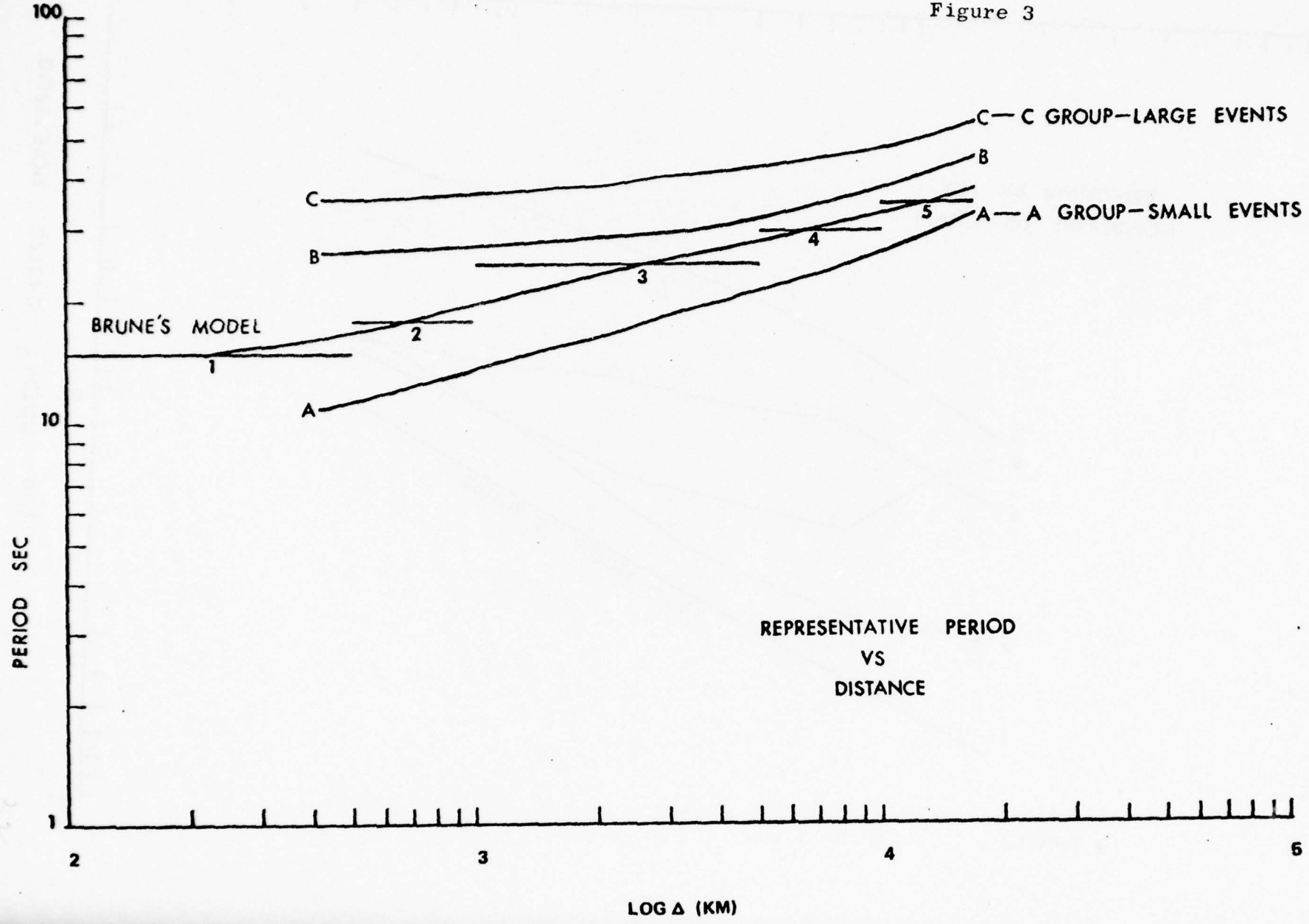

100
10
1
PERIOD SEC
C— C GROUP—LARGE EVENTS
B
A— A GROUP—SMALL EVENTS
C
B
A
BRUNE'S MODEL
1
2
3
4
5
REPRESENTATIVE PERIOD
VS
DISTANCE
2
3
4
5
LOG Δ (KM)

Figure 4

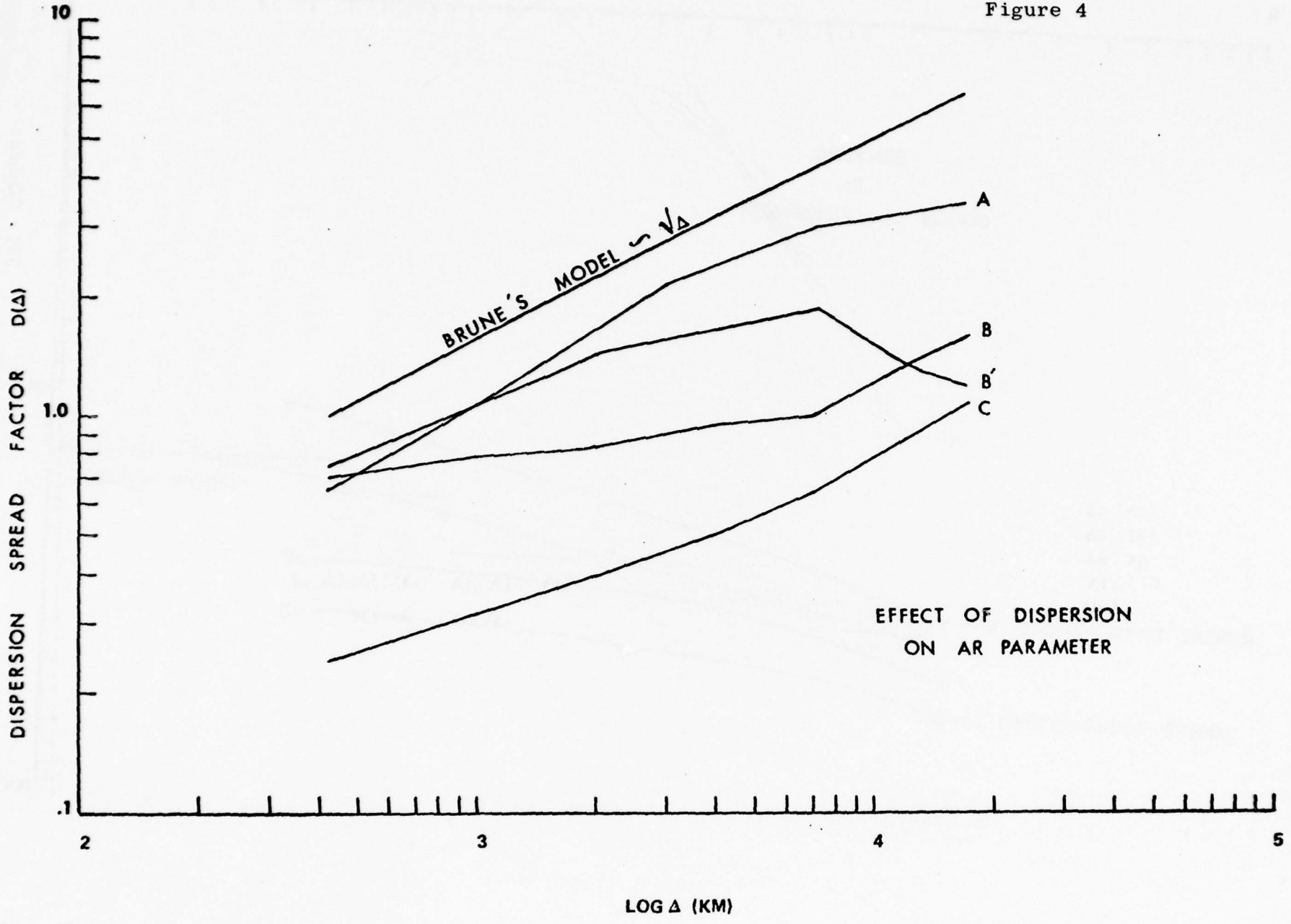
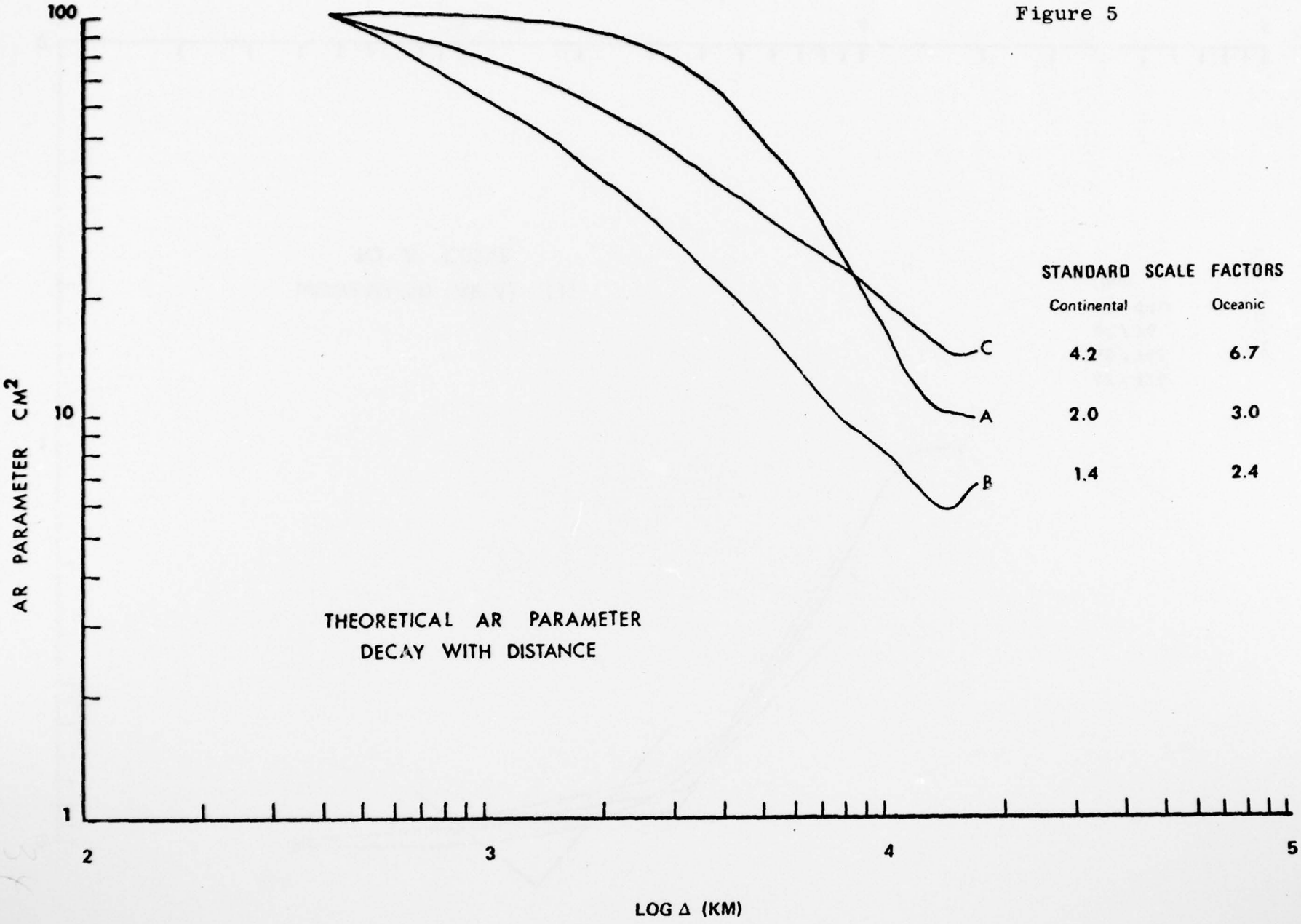

10
1.0
.1
DISPERSION SPREAD FACTOR D(Δ)
BRUNE'S MODEL ~ √Δ
A
B
B'
C
EFFECT OF DISPERSION
ON AR PARAMETER
2
3
4
5
LOG Δ (KM)

Figure 5


100
10
1
AR PARAMETER CM²
2
3
4
5
LOG Δ (KM)
C
A
B
STANDARD SCALE FACTORS
Continental
Oceanic
4.2
6.7
2.0
3.0
1.4
2.4
THEORETICAL AR PARAMETER
DECAY WITH DISTANCE

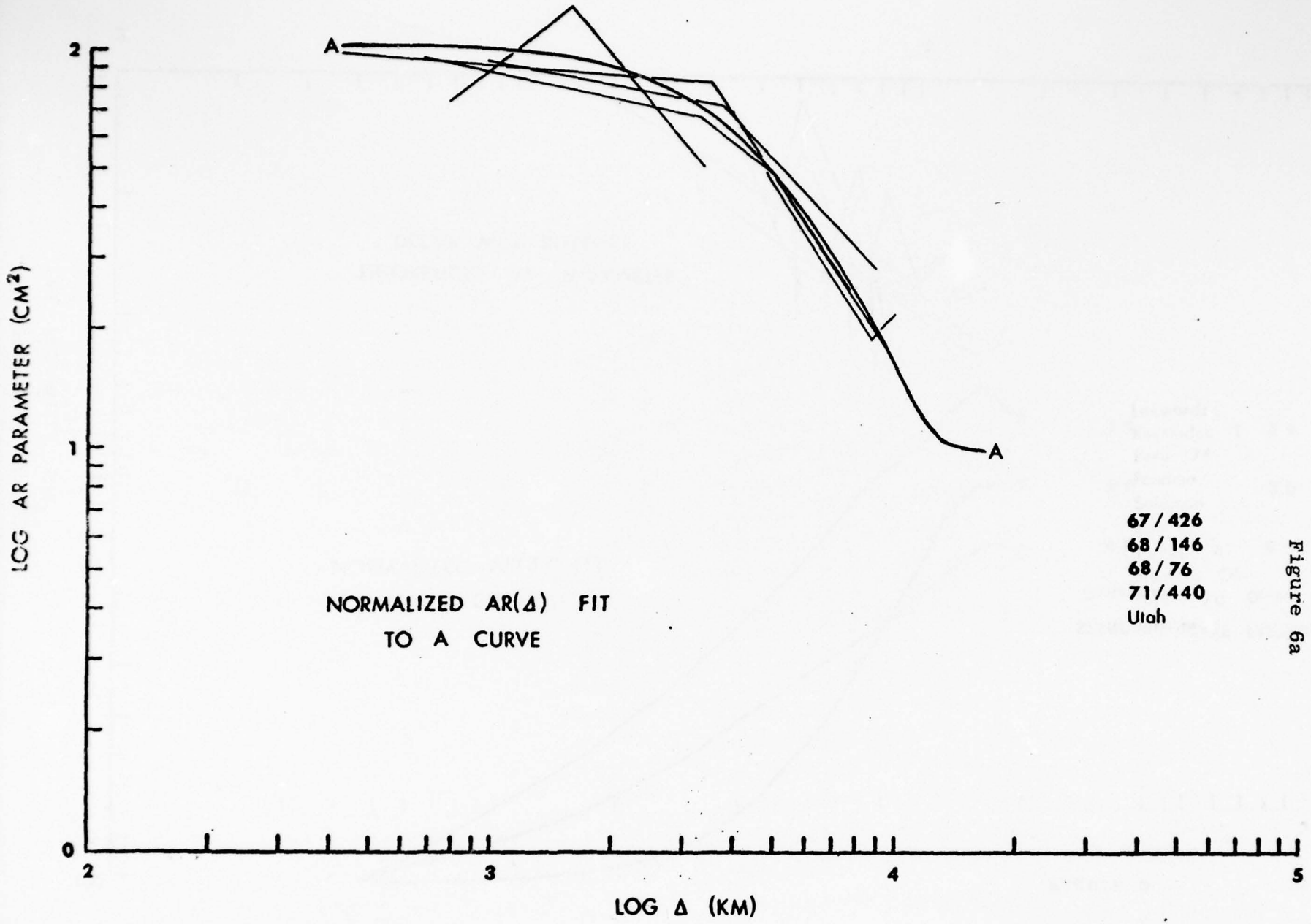

A
A
2
1
0
LOG AR PARAMETER (CM²)
NORMALIZED AR(Δ) FIT
TO A CURVE
67/426
68/146
68/76
71/440
Utah
2
3
4
5
LOG Δ (KM)

Figure 6a

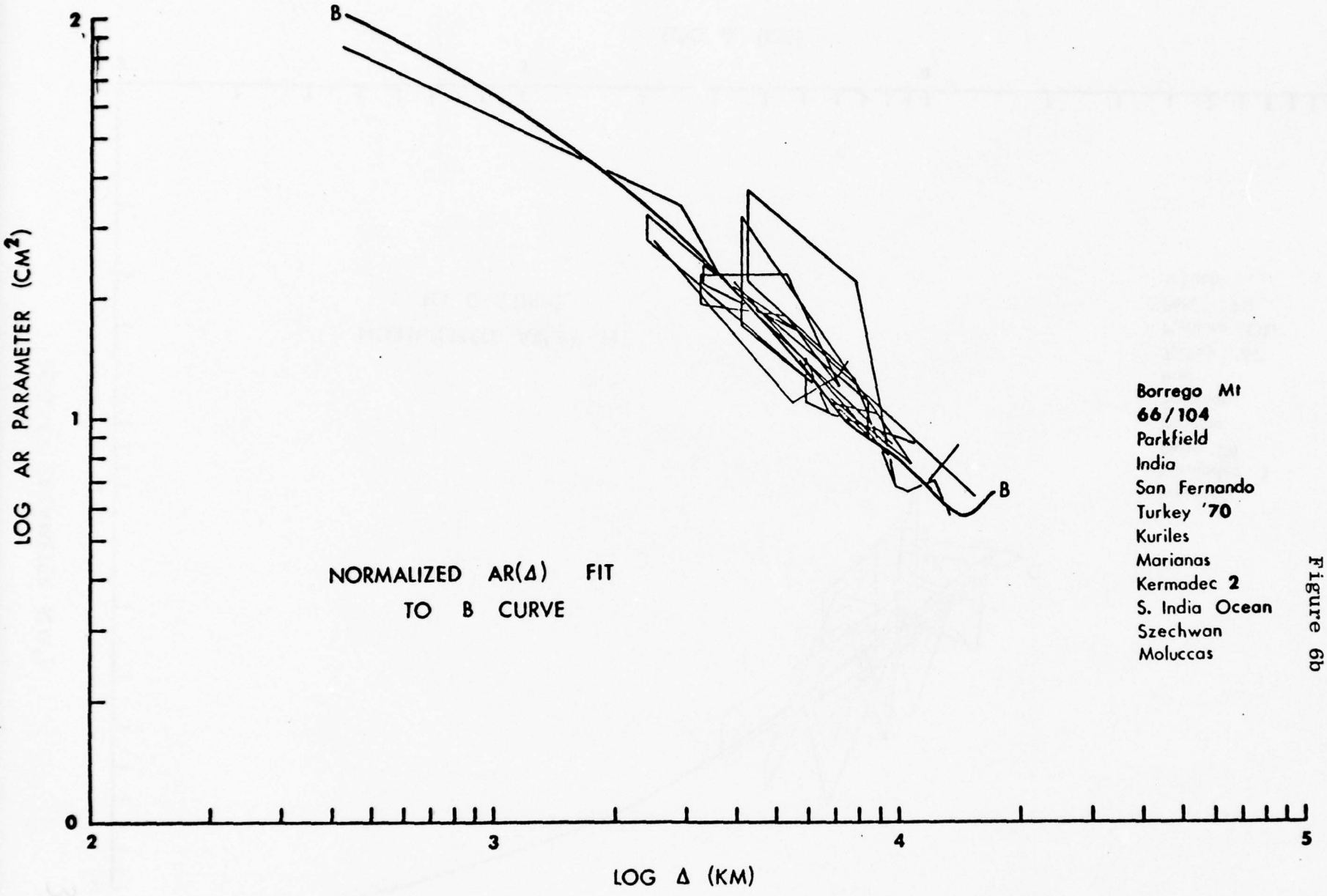

B
B
2
1
0
2
3
4
5
LOG AR PARAMETER (CM²)
LOG Δ (KM)
NORMALIZED AR(Δ) FIT
TO B CURVE
Borrego Mt
66/104
Parkfield
India
San Fernando
Turkey '70
Kuriles
Marianas
Kermadec 2
S. India Ocean
Szechwan
Moluccas

Figure 6b

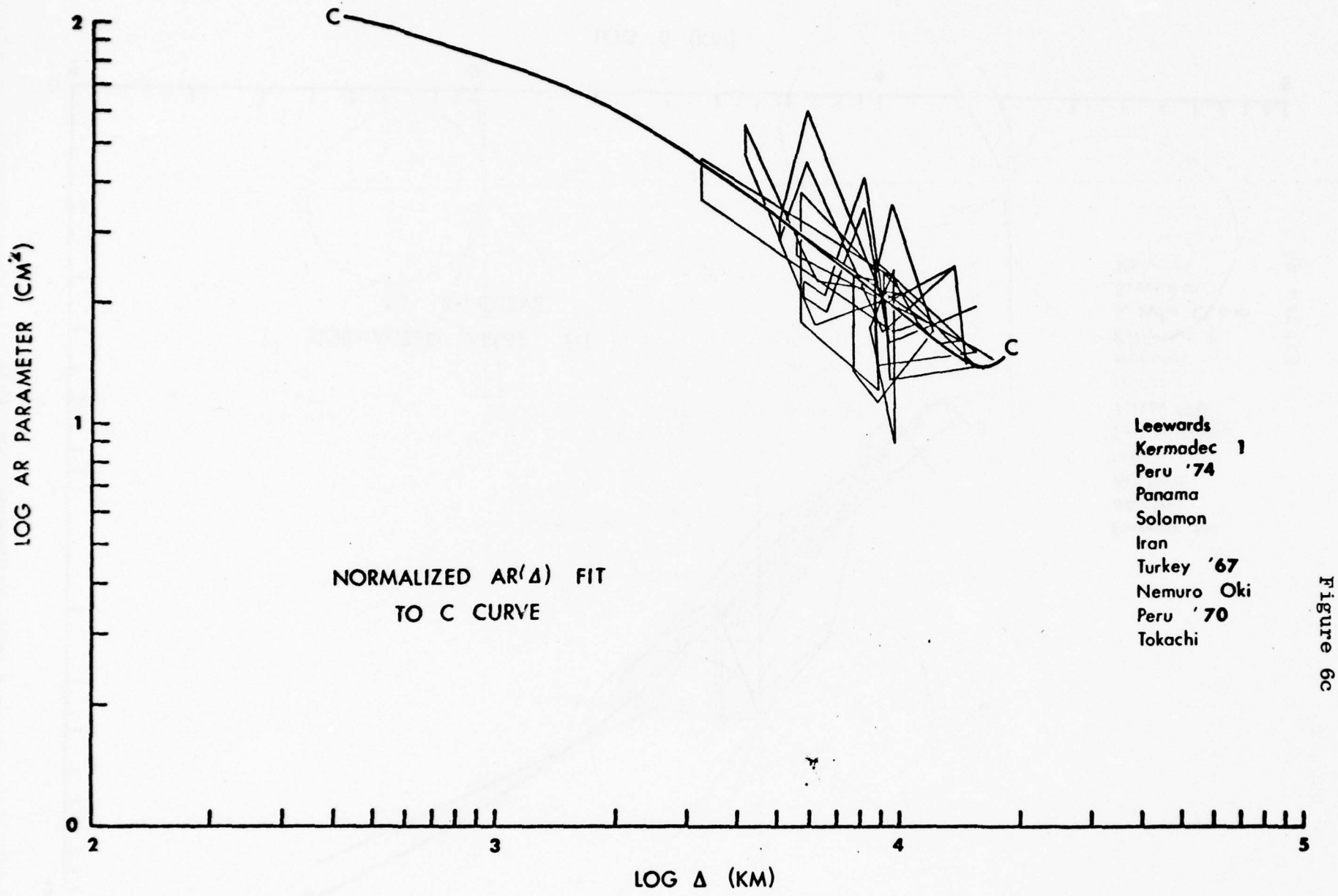

C
C
2
1
0
LOG AR PARAMETER (CM²)
NORMALIZED AR(Δ) FIT
TO C CURVE
Leewards
Kermadec 1
Peru '74
Panama
Solomon
Iran
Turkey '67
Nemuro Oki
Peru '70
Tokachi
2
3
4
5
LOG Δ (KM)

Figure 6c

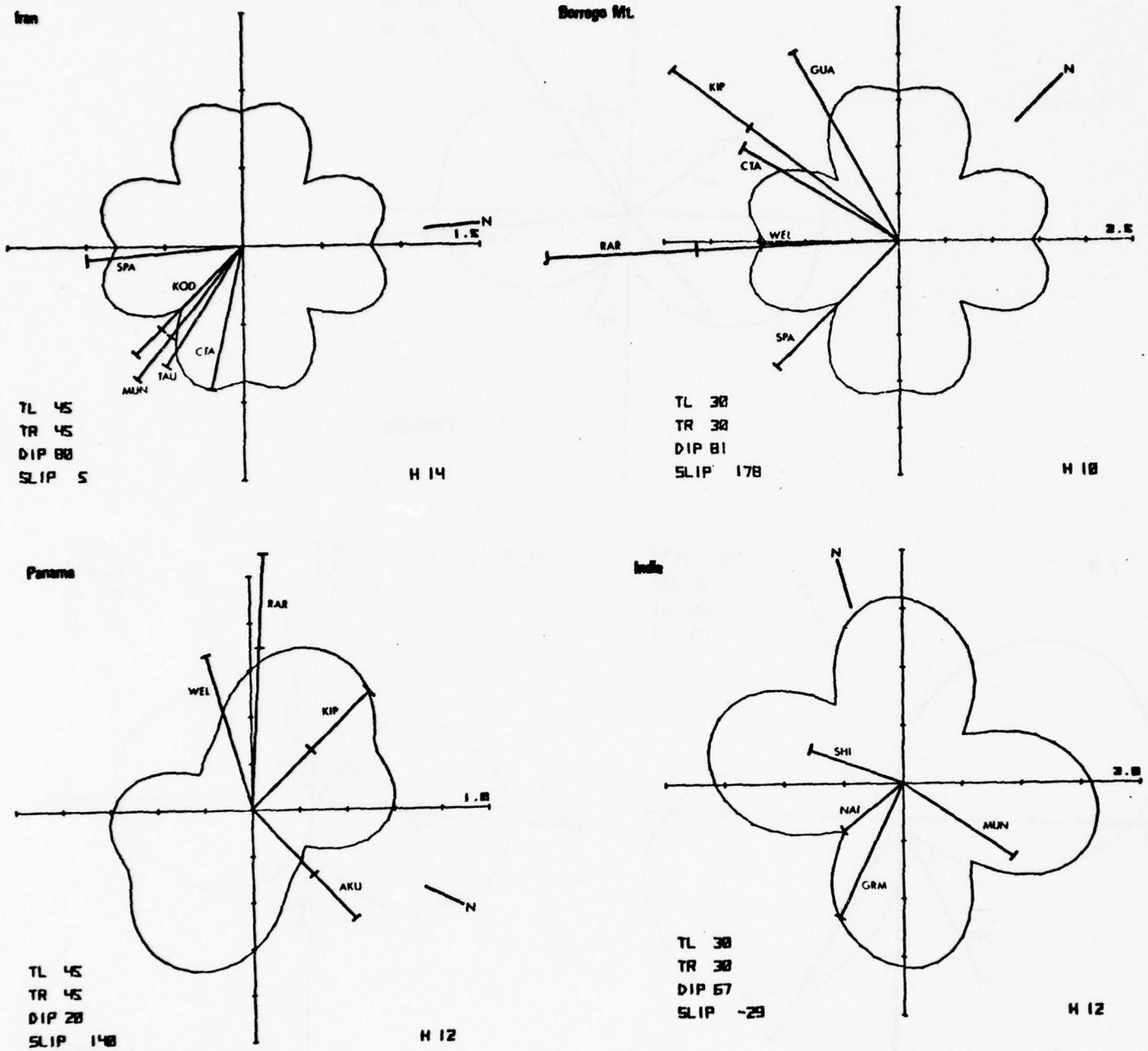
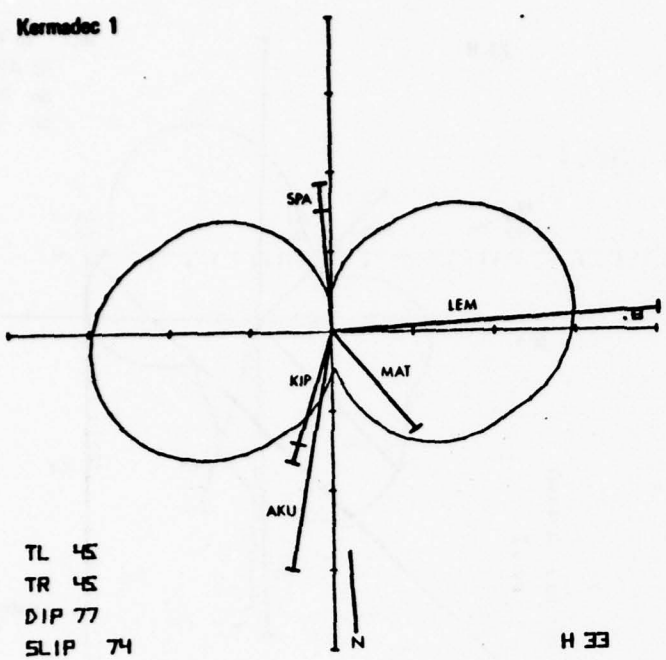
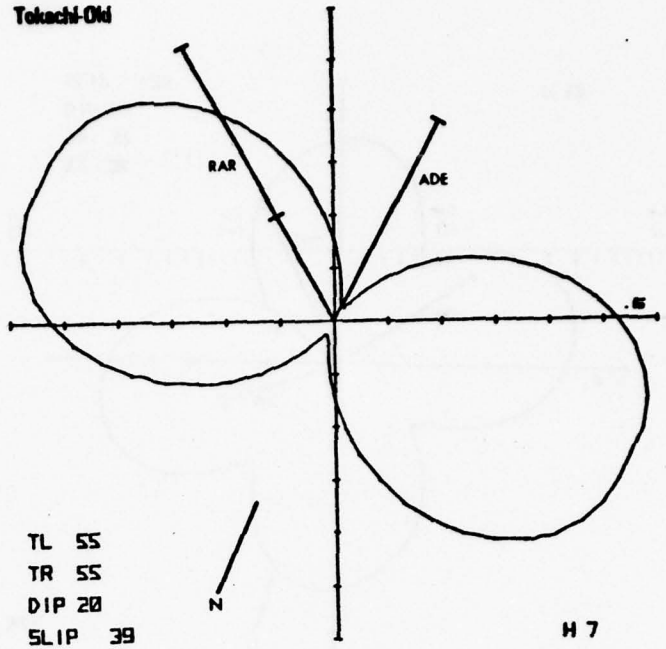

Iran
N
1.5
SPA
KOD
CTA
TAU
MUN
TL 45
TR 45
DIP 80
SLIP 5
H 14
Borrego Mt.
KIP
GUA
N
CTA
WEL
2.5
RAR
SPA
TL 30
TR 30
DIP 81
SLIP 178
H 10
Panama
RAR
WEL
KIP
1.0
AKU
N
TL 45
TR 45
DIP 20
SLIP 148
H 12
India
N
SHI
2.0
NAI
MUN
GRM
TL 30
TR 30
DIP 67
SLIP -29
H 12

Figure 7


Kermadec 1
SPA
LEM
KIP
MAT
AKU
N
TL 45
TR 45
DIP 77
SLIP 74
H 33


Tokachi-Oki
RAR
ADE
N
TL 55
TR 55
DIP 20
SLIP 39
H 7

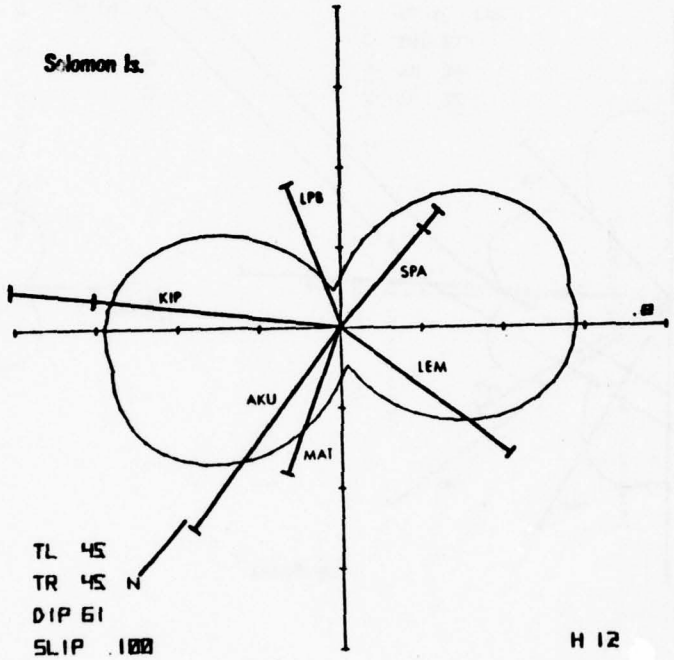

Solomon Is.
LPB
SPA
KIP
LEM
AKU
MAT
N
TL 45
TR 45
DIP 61
SLIP 100
H 12

Figure 8

Figure 9

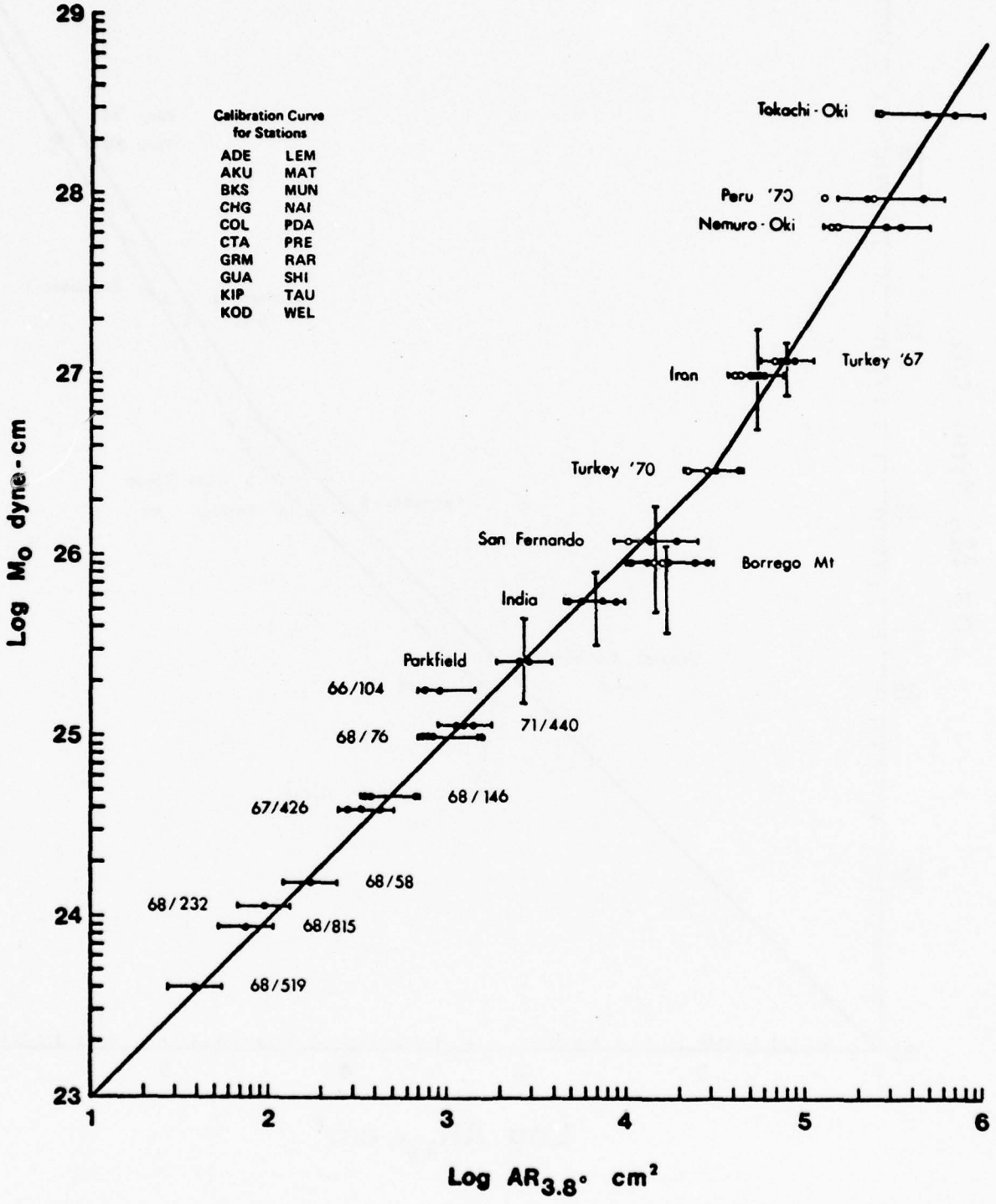

Calibration Curve for Stations
ADE LEM
AKU MAT
BKS MUN
CHG NAI
COL PDA
CTA PRE
GRM RAR
GUA SHI
KIP TAU
KOD WEL
Tokachi-Oki
Peru '70
Nemuro-Oki
Iran
Turkey '67
Turkey '70
San Fernando
Borrego Mt
India
Parkfield
66/104
71/440
68/76
68/146
67/426
68/58
68/232
68/815
68/519
Log Mo dyne-cm
Log AR3.8° cm²
29
28
27
26
25
24
23
1
2
3
4
5
6

Figure 10

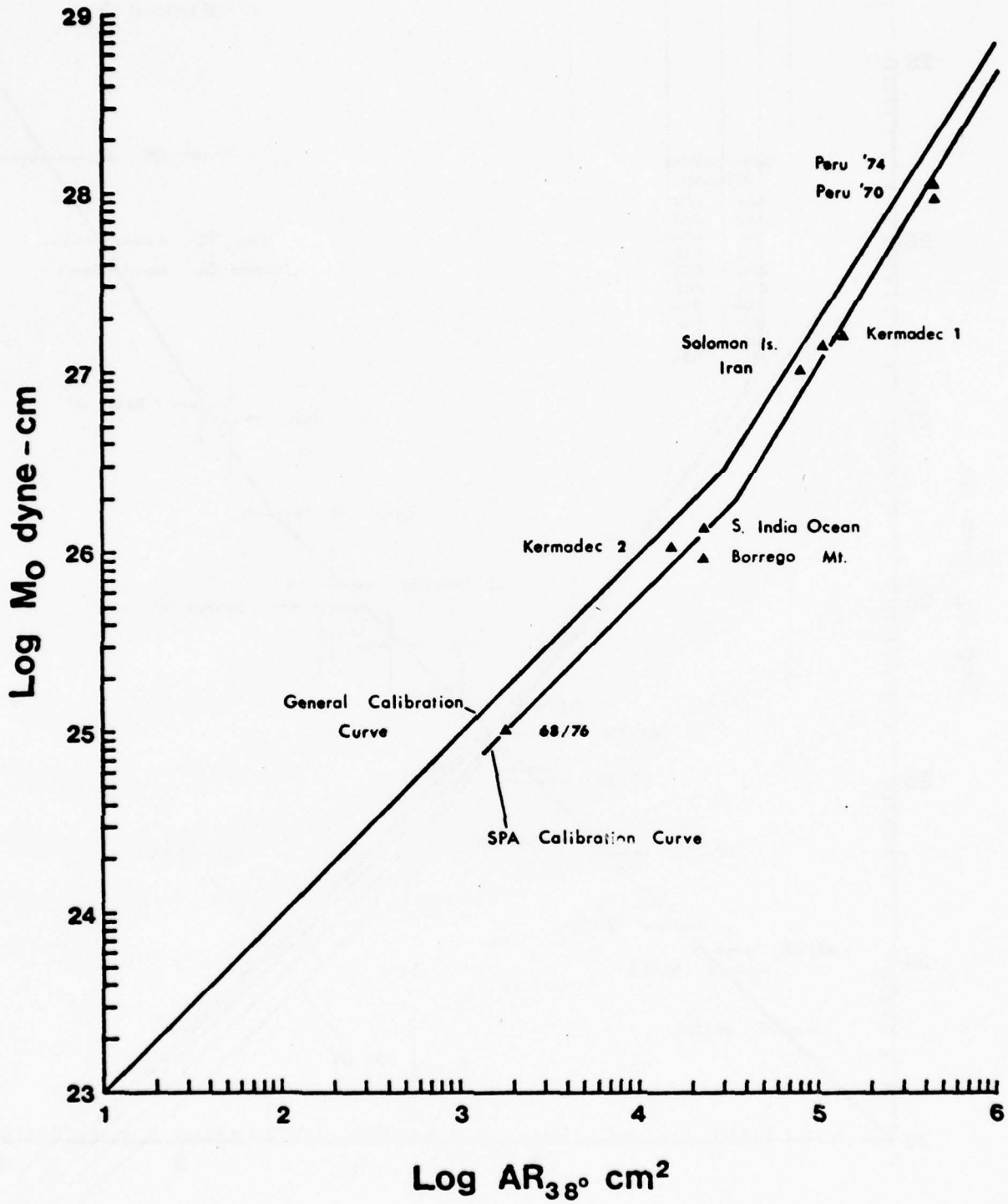

29
28
27
26
25
24
23
Log M_o dyne-cm
1
2
3
4
5
6
Log AR_{38^o} cm^2
Peru '74
Peru '70
Solomon Is.
Iran
Kermadec 1
Kermadec 2
S. India Ocean
Borrego Mt.
General Calibration Curve
68/76
SPA Calibration Curve

Figure 11

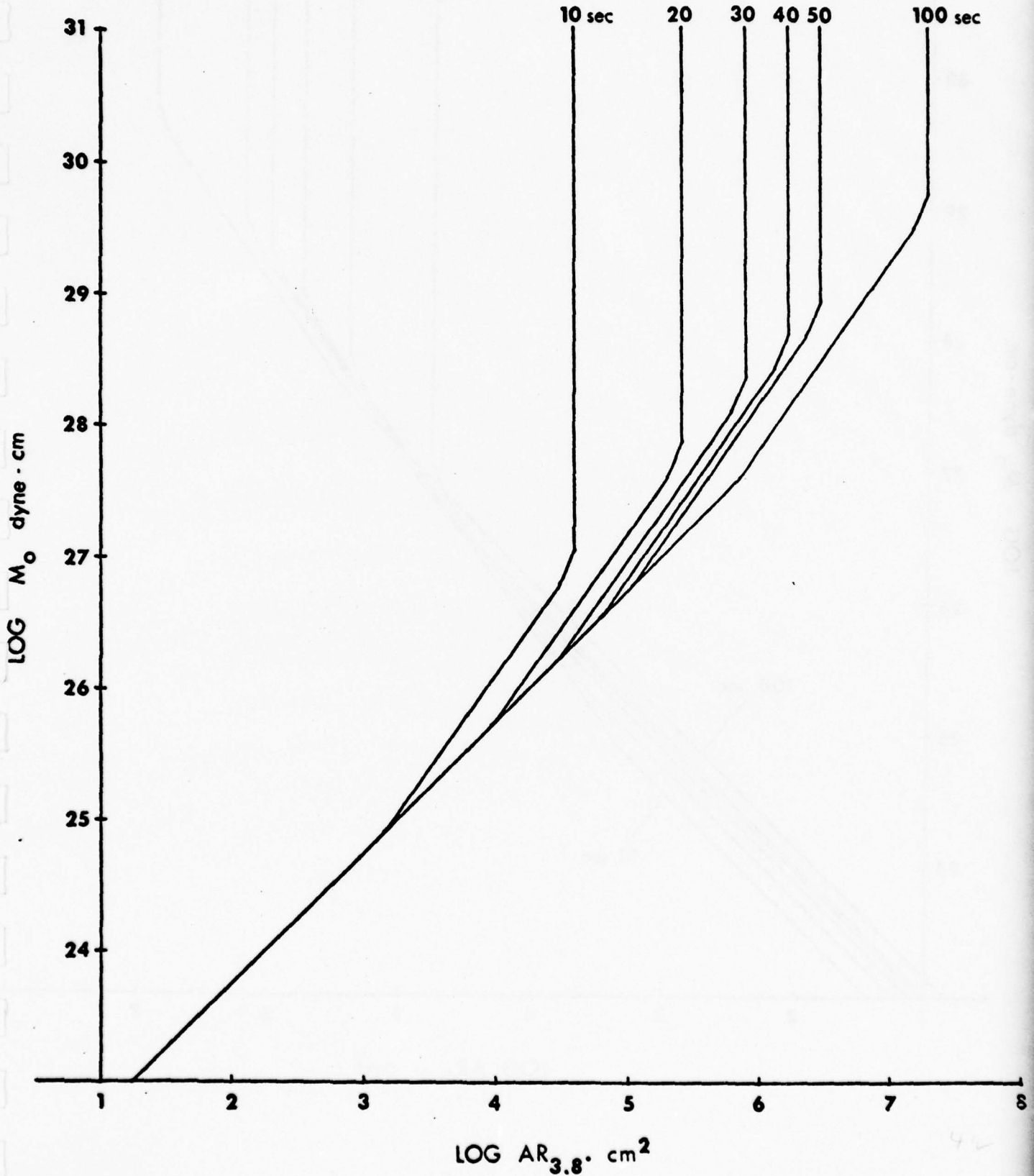

10 sec
20
30
40
50
100 sec
31
30
29
28
27
26
25
24
LOG M_o dyne - cm
1
2
3
4
5
6
7
8
LOG $AR_{3.8}$. cm^2

Figure 12

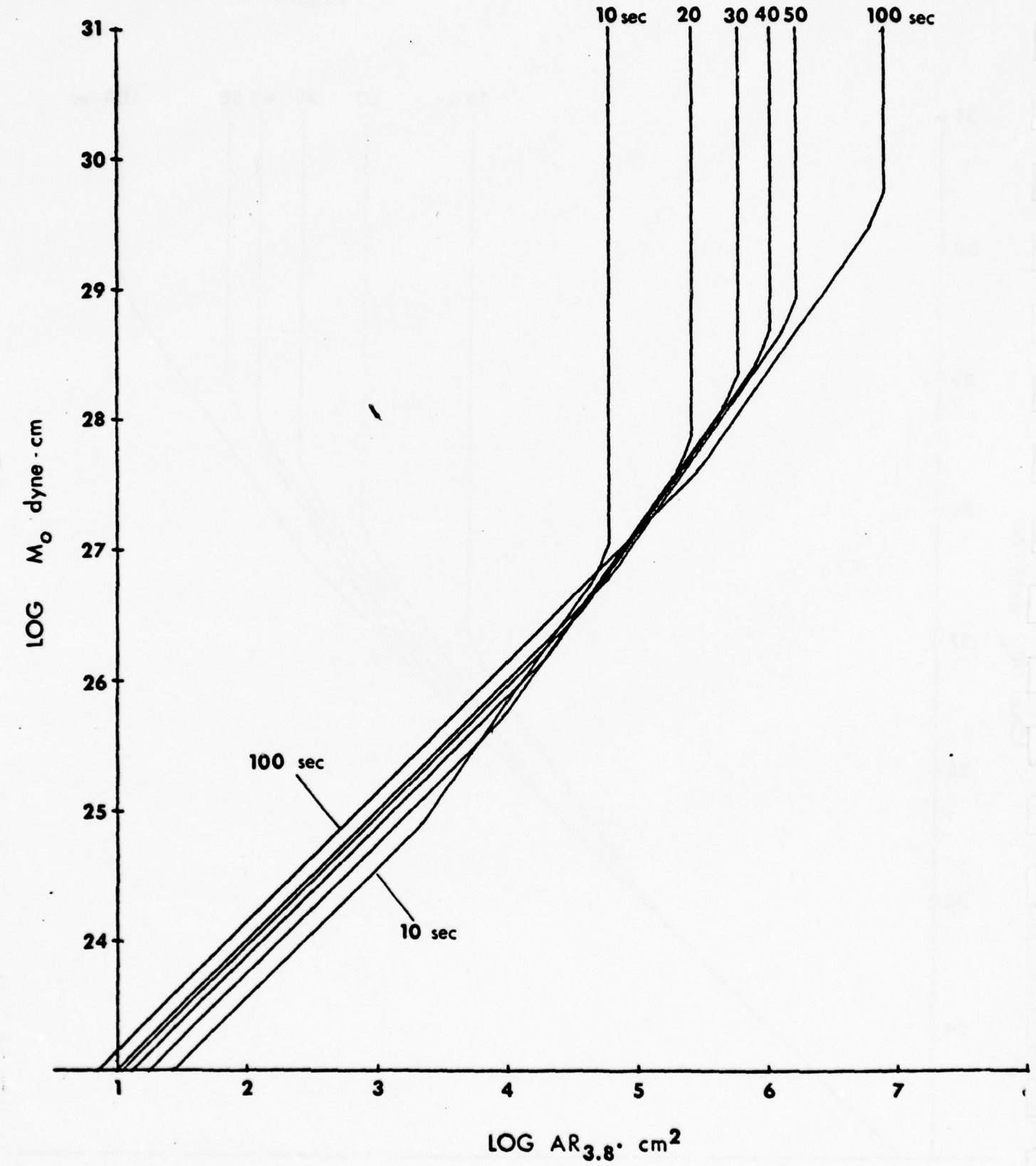
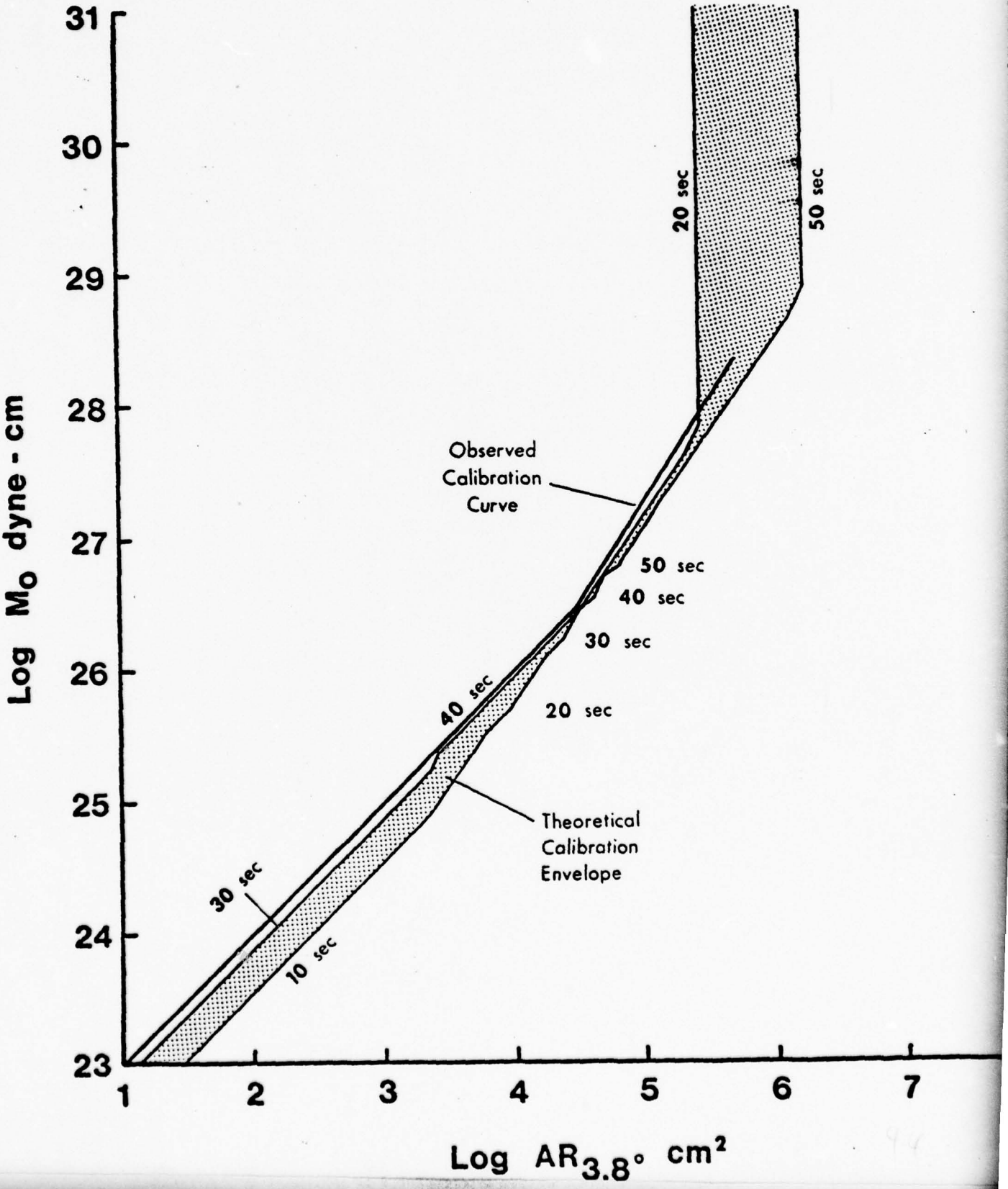

10 sec
20
30
40
50
100 sec
31
30
29
28
27
26
25
24
LOG M_o dyne · cm
100 sec
10 sec
1
2
3
4
5
6
7
LOG $AR_{3.8}$ · cm^2

Figure 13


31
30
29
28
27
26
25
24
23
1
2
3
4
5
6
7
Log M_o dyne - cm
Log $AR_{3.8°}$ cm²
20 sec
50 sec
Observed
Calibration
Curve
50 sec
40 sec
30 sec
20 sec
40 sec
Theoretical
Calibration
Envelope
30 sec
10 sec

APPENDIX II

A TECTONIC-BASED RAYLEIGH WAVE GROUP VELOCITY MODEL FOR PREDICTION OF DISPERSION CHARACTER THROUGH OCEAN BASINS

by

Frederick John Mauk

Department of Geology and Mineralogy
The University of Michigan
Ann Arbor, Michigan 48109

Manuscript submitted to the Journal of Geophysical Research
February 17, 1978

ABSTRACT

A new model to predict Rayleigh wave group velocity dispersion (periods 30 through 100 seconds) through the ocean basins is presented. It is based on a 5°x 5° integration of weighted Rayleigh group velocities for the 2592 geographic grid elements constituting the earth's surface. Percentages (to the nearest 10%) of element coverage by each of twenty tectonic divisions provide the weighting factors. Rayleigh group velocities specific to each of the twelve continental and one oceanic geological division were compiled from the literature. Rayleigh velocities for the remaining seven oceanic divisions were determined by partitioning empirically-derived functional relationships between sea floor age and Rayleigh group velocities.

Dispersion analyses for seventeen random paths through the Pacific Ocean, four for the Indian Ocean and six for the Atlantic Oceans are compared with the model-predicted dispersion curves. Observed-minus-predicted velocity residuals for the Pacific are significantly less than the uncertainty limits. Systematic positive residuals occur in basins of the other major oceans, however. The largest anomaly (0.4 km/sec) occurs in the Brazil Basin. The failure of the Pacific-based model to predict dispersion accurately in these other basins suggests that there may be fundamental differences in crust and upper mantle structure among the world's oceans.

Since petrological differences among the oceans are apparently negligible, perturbations of 'typical' oceanic geotherms by lower thermal influx (possibly reflected in lower spreading rates) and/or

thermal refractions into colder adjacent continental regions may account for the observed velocity differences. Lower temperatures would cause a reduction of partial melting which would result in faster velocities through the region.

Introduction

Analysis of earthquake and explosion generated Love and Rayleigh mode surface waves has contributed significantly to the elucidation of the crust and upper mantle structure of the earth. Although the dispersion of surface waves is determined by the average properties of the crust and mantle over a large depth range, sampling phase and group velocities of dispersed wave trains at a variety of periods has revealed fundamental structural differences between continents and oceans (Oliver, 1962). In addition, variations of observed continental surface wave dispersion character have been correlated convincingly with geological provinces (North, 1976; Goncz and Cleary, 1976; Fix, 1975; Teng, 1974; Biswas and Knopoff, 1974; Adams, 1974; Wu, 1972; James, 1971; Bolt and Niazi, 1964; Brune and Dorman, 1963; Brilliant and Ewing, 1954). Similar variations of oceanic surface wave dispersion character were recognized before sea floor spreading was introduced (Tarr, 1969; Sato and Santo, 1969; Santo, 1966a, 1966b, 1962, 1961a, 1961b, 1960; Papazachos, 1964; Brune and Major, 1962; Kovach, 1961; Shurbet, 1960; Berckhemer, 1956; Oliver, Ewing and Press, 1955; Jardetsky and Press, 1953; Wilson and Baykal, 1948), but without the plate tectonics and ocean floor evolution concepts, a rational differentiation of observed dispersion into provinces was elusive.

The fundamental discovery that the sea floor is created at ocean ridges and evolves both spatially and temporally provided the key to a rational catagorization of the diverse dispersion characteristics previously observed in the ocean basins. The development of the ocean floor spreading framework from marine magnetic anomalies and deep sea drilling has enabled a chronologically detailed mapping of the world's oceans (Pitman, Larson, and Herron, 1974; Herron, Pitman, and Dewey, 1974;

Cooper, Marlow and Scholl, 1976; Johnson, Powell and Veevers, 1976). Equipped with this new information on the age of the ocean floor, and with improved techniques of dispersion analysis (Knopoff, 1972; Landisman, Dziewonski and Sato, 1969), Forsyth (1976, 1975), Yoshii (1975), Leeds (1975), Leeds Knopoff and Kausel (1974a,b) and Knopoff, Schlue and Schwab (1970) have demonstrated the correlation between ocean floor age and variations in both Love and Rayleigh dispersion in the Pacific basins.

The research discussed in this paper is an extension of the characterization of Rayleigh group velocity dispersion through ocean basins. An empirical model based on sea floor age used to predict Rayleigh group velocity dispersion for any path through ocean basins is presented and discussed. The principal model assumption is that Rayleigh group velocities are definable and constitute well-behaved functions in the tectonic evolutionary context of sea floor spreading. Global characterization of Rayleigh group velocities in a 5°x5° tectonic framework requires: first, a regionalized encoding of global tectonic units (e.g. Archean shield, 0-5 million year old oceanic crust, etc.), second, an assignment of a characteristic dispersion through each tectonic unit, and third, a merging of the 5°x5° encoded tectonics with the tectonic-specific group velocities to obtain a global representation of the period-specific Rayleigh group velocity fields. Inversion of the predictive velocity model to obtain a specific crust and upper mantle velocity structure is not intended.

CONSTRUCTION OF THE GLOBAL RAYLEIGH GROUP VELOCITY MATRIX

A fundamental tectonic data matrix was created by dividing the surface of the earth into a grid of 2592 5°x5° elements and encoding the tectonic information for each element derived from maps and published research. Although this grid does not yield elements of equi-

valent area (equatorial ∿ 308,715 km^2, polar ∿13,478 km^2), it does provide a convenient system for subsequent computational manipulation.

Twelve continental and eight oceanic divisions were used for the matrix encoding (See Table 1.). Although many of the tectonic divisions might be subdivided further for specific regions, the selected larger scale designations could be universally recognized and were deemed sufficient for this global study.

The sources of the tectonic data are listed in the appendix. Where possible, detailed tectonic data are used to supplement or to supersede older and/or more generalized data. The Indian Ocean data of Johnson, Powell and Veevers (1976), superseded the data of McKenzie and Sclater (1971), for example. This was the largest scale revision. More frequently, tectonic revisions involved only one or two element adjustments. The tectonic data matrix is amendable as new data become available. The latest update used in this study was March, 1976.

Generally, continental tectonic data are available in abundance. Inaccessability (central Asia), or ice cover (Greenland and Antarctica) may preclude detailed analysis of some regions, but a reasonable approximation of the tectonics could still be effected. Significant gaps in the coverage of the ocean floor do exist, however. Detailed tectonic data for the Arctic Ocean Basin, for example, are sparse. In this case, a postulated model for Arctic evolution proposed by Herron, Dewey and Pitman (1974) was used to fill the gap. Similarly, gaps in the ocean floor coverage in the equatorial Atlantic and Atlantic-Indian Basin are problematic. In these instances, where no direct data exist, tectonic

patterns were inferred on the basis of immediately adjacent element coverage and other tectonic information such as seismicity and transform fault offsets. Finally, the marginal basins often are poorly dated. The majority of them ,however, have deep sea drilling logs and/or subsequent detailed studies to reduce the uncertainty of tectonic assignment. These ill-defined ocean floor tectonics constitute the principal weakness of this aspect of this study. Future improvements in the data coverage should enhance the reliability of this analytic tool.

Figure 1 illustrates the method of encoding the grid elements; in this case, an area in southeast Asia. Each 5°x5° element is inspected for the visually estimated percentage (to the nearest 10%) of the enclosed tectonic divisions. In this example, three of the twenty tectonic divisions are present; shelf sediments 40%, Mesozoic orogeny 30%, and Post-Precambrian undeformed platform 30%. Each of these divisions is assigned a percentage of the total area of the scene and the weights are entered into the tectonic matrix; all other tectonic divisions are assigned weights of zero. The spatial distribution of the tectonic divisions within the grid element is not included in the matrix.

It is possible that a particular path through a grid element will sample only a portion of the enclosed tectonics, and therefore the actual path segment velocity may not be represented accurately by the tectonic based 5°x5° element mean velocity. Since it is likely that a juxtaposition of two or more widely dissimilar tectonic divisions will result in a mutual reequilibration with time, the anomalous influence of the spatial aspect of the tectonic divisions seems remote, except when dealing with most recent tectono-thermal events. Similarly, if paths which are much

greater in length than 500 kilometers are chosen for analysis, they will sample and average element tectonic influence over many elements. The chance of fortuitous local spatial distributions of tectonic divisions significantly perturbing results utilizing the tectonic matrix thus becomes less likely as path length is increased. The tectonic matrix is stored on magnetic tape for easy amendment and access.

Utilization of this tectonic matrix to predict Rayleigh wave group velocities requires the assignment of a group velocity dispersion characteristic to each of the tectonic divisions used in the encoding. One such method is to determine the characteristic dispersion empirically for a given area showing only one tectonic division and assume that the characteristic is relatively invariant.

Although this research is an examination of Rayleigh group velocities across ocean basins, many of the seismograph stations are located at continental margins. Assignment of continental group velocities is required, therefore, to suppress anomalous edge effects and unrealistic velocity gradients at these boundaries. Thus, the assignment of 'average' continental Rayleigh group velocities to all twelve continental divisions is unreasonable. The velocity transition from ocean to continent is significantly different for California versus New Jersey, for example. The group velocities for the twelve continental tectonic divisions are derived from published data. All phase velocity data have been converted to group velocities using the standard formulation.

Frequently, group velocities assigned to a particular tectonic division are the result of several independent investigations throughout the world. Remarkably, the variations in Rayleigh wave group velocities for a given tectonic division generally differ by less than 0.02 km/sec for the period range 20 through 100 seconds. Although additional analy-

ses may result in twelve distinct dispersion characteristics for these tectonic divisions, only six could be differentiated from the current literature. The Archaen and Proterozoic shields were assigned the same velocities for the period range of 20 through 100 seconds based on the analyses of Brune and Dorman (1963) for the Canadian Shield, Bolt and Niazi (1964) for the Australian shields, Bhattacharya (1974) for the Indian shield and Teng (1974) for the Asian shields. Similarly, the Precambrian and post-Precambrian platforms and the shelf sediments were indistinguishable (Brilliant, 1954; Bolt and Niazi, 1964; Ocal, 1965; Knopoff and Mal, 1967; Biswas and Knopoff, 1974; Teng, 1974; Goncz, Hales and Muirhead, 1975; Goncz and Cleary, 1976). Mesozoic orogenic zones were assigned Rayleigh wave group velocities from the combined studies of Alexander (1963), James (1971), Knopoff (1972), Biswas and Knopoff (1974), Fix (1975), and North (1976). The intermontane basin fill division velocities were derived from three studies of the Basin and Range province of the Western United States (Biswas and Knopoff, 1974; Braile, 1975; Keller, 1975). Finally, no data for the divisions early Paleozoic orogeny, late Paleozoic orogeny, and Mesozoic volcanics could be found in the literature. Accordingly, these divisions were assigned mean continental group velocities from Oliver (1962). A summary of the assigned continental group velocities of fundamental mode Rayleigh waves for the period range 20 to 100 seconds is given in table 1.

Data used to construct and to test the functional relationship between sea floor age and Rayleigh group velocities were selected from long period vertical component seismograms of WWSSN and HGLP stations. All seismograms were digitized at 0.56 second increments with an amplitude resolution of .06 millimeters. The length of digitization is dep-

endent on the dispersive character of the original record and generally is three times the length of the included Rayleigh train. This insures an adequate data length for the moving window analysis (Landisman, Dziewonski, and Sato, 1969) to be performed properly and prevents partial loss of visually-obscure low amplitude group arrivals.

Energy levels are mapped in a group velocity versus logaritmic period space using the moving window analysis of Landisman, Dziewonski, and Sato (1969). The arrival time of the peak energy level of a wave packet gives the group velocity at that period when the data have been corrected for instrumental group delay. All records were analyzed with a cosine squared window having width four times the period of interest.

Uncertainty in determining period-specific energy maxima is dependent on the quality of the original seismogram and resolution of the cosine squared window. Generally the velocity uncertainty is approximately 0.02 km/sec in the best cases, but may be as large as 0.10 km/sec at very poorly resolved long periods (greater than 80 sec). All dispersion analyses have been corrected for instrumental group delay using the formulation of Hagiwara (1958) with corrections by Brune (1962).

Other sources of error in group velocity interpretation can be attributed to the seismic source and transmission path. The magnitudes of the source errors are generally inversely proportional to the epicentral distance, thus by using teleseismic events at distances greater than 4000 kilometers, most source-related errors become insignificantly small.

Epicenter mislocation and/or incorrect assignment of origin time are potentially the most significant sources of error to a velocity determination. Utilizing larger magnitude events (greater than M_S 6.0)

and several earthquakes from the same location tend to reduce this uncertainty, however. Mislocation errors are estimated to yield group velocity uncertainties of the order of 0.02 km/sec. This estimate should be quite liberal for most larger magnitude earthquakes, but may be conservative for regions like the Atlantic Indian Rise where azimuthal control of epicenter location is limited.

Group velocity uncertainty attributable to misinterpretation of initial phase from the focal mechanism has been demonstrated by Knopoff and Schwab (1968) to be insignificant for large epicentral distances and the period range discussed in this paper, thus it is not considered as a relevant source of error. Similarly, other source parameters such as fault length, rupture velocity, and stress drop, while affecting the wave-frequency amplitudes are not considered to affect significantly the observed group velocities. Although spceific source parameters, such as depth and rupture velocity can yield far-field surface wave spectral 'holes' (Turnbull, 1976). these energy discontinuities are unrelated to path-associated dispersion and can be disregarded.

Discrimination of tectonic-related group velocity variations through pcean basins presupposes that other path related velocity perturbations can be isolated and removed from the observed data. The effects of horizontal refraction and ocean depth, in fact, may obscure completely the actual group velocity variation due to sea floor evolution. A basic assumption necessary for the computation of the group velocities is that the surface waves travel a minimum distance (great circle) path. This assumption is strictly correct only when the medium is laterally homogeneous or when the great circle path is normal to

the inhomogeneity boundaries. In a medium with lateral structural variations, however, it is possible that the least-time rather than least-distance path is responsible for the arrival on a particular seismogram. Generally the difference between the minimum-time and minimum-distance paths should be a second order effect for group velocities, since the higher velocity of a refracted path tends to be counterbalanced by the increased path length. When the path difference is significant, horizontal refraction effects are manifested as multiple energy arrivals (Capon, 1970,1971), beating (Pilant and Knopoff, 1964), or unusual amplitude fluctuations (McGarr, 1969).

A Significant difference between a minimum-time and minimum-distance path occurs when the velocity gradient normal to the propagation path is large. High crustal and mantle velocity gradients can occur in ocean basins normal to ridge axes (Forsyth, 1975), proximal to unusual thermal perturbations (hot spots) (McGarr, 1969) and at continental margins (Capon, 1970).

The gradient normal to a ridge axis is at a maximum during the first fifteen million years of evolution and/or in basins where the spreading rate is low. The percentage of the sea floor where this can be a problem is relatively small but may account for some of the unusual Atlantic Ocean test results. The influence can be reduced by selecting only paths nearly normal to the ridge axes. If there is significant velocity anisotropy associated with the spreading directions (Bamford and Crampin, 1977; Fuchs, 1977; Schlue and Knopoff, 1977; Forsyth, 1975), then this technique resolves only the velocities in

that direction which may not be representative of a more generalized path. The simplest solution to this problem is to avoid seismograms which are complicated by symptomatic beating and unusual amplitude fluctuations.

McGarr (1969) similarly has demonstrated that surface waves which have propagation paths near hot spots commonly exhibit refractive focusing and defocusing effects. Although this is less of a spatial problem than are the ridge axes, it is a potential problem when the recording station is located on such a perturbation, for example KIP, or if the propagation path is aligned with the perturbed zone. In general the effects of these small regions can be considered insignificant for all but the shortest periods (less than 20 sec), if the propagation paths are chosen to avoid them.

Capon (1970) was able to show that surface waves can undergo considerable refraction at continental margins. The effect was at a maximum at LASA (Montana array) when the waves approached the margin at relatively low angles. The effect is negligible for coastal stations when the angle of approach is nearly ninety degrees.

In summary, the effects of horizontal refraction or departure from a minimum-distance path are difficult to evaluate. By selecting seismograms which exhibit few obvious multi-path characteristics and avoiding paths which are likely to create these effects, the combined horizontal refraction perturbations to group velocities can be considered insignificant.

The influence of the water layer on Rayleigh wave dispersion through ocean basins is perhaps the most significant correction which must be applied to the raw data. It could be argued that the increase in ocean

depth with the thermal contraction of the crust and upper mantle is a correlative to the evolution of the oceanic lithosphere structure (Sclater and Francheteau, 1970; Sclater, Anderson and Bell, 1971). However, there is significant scatter to the topography-age relationship. Failure to correct for ocean depth along a defined path tends to obscure rather than elucidate the continuous evolutionary aspect of the oceanic crust and upper mantle.

Modeling the absolute effect of increasing ocean depth in an evolving crust and upper mantle setting would be the preferred condition. Without a firm understanding of the exact structural evolution, however, this model is not tractable. Assuming a constant crust upper mantle structure and varying only the thickness of the water layer does permit an evaluation of the relative influence of the water layer depth on Rayleigh phase and group velocity dispersion. Since the evolution of the sea floor increases the observed velocities, while the increase in ocean depth decreases the observed velocities, by assuming a constant crust upper mantle structure, the computed influence of the water layer will be an overestimation for older ocean basin regions. To illustrate the effect of the ocean depth, fundamental mode Rayleigh phase and group velocities were calculated for seven ocean models. The basic crust and mantle structure used throughout the calculations is given in table 2. The model differs only in the thickness of the first layer which was varied steowise from zero through six kilometers. The method of calculating phase and group velocity data is that of Harkrider (1964). The results of these calculations are given in table 3. The influence of the ocean layer on the phase and group

velocities increases as the period decreases. Similarly, since the group velocities are more sensitive to structural changes than are the phase velocities, they are significantly more perturbed than are the phase velocities at the corresponding periods. The group velocity correction becomes extremely non-linear as the period decreases, requiring a correction as large as 28% for deep oceans at periods of 20 seconds. Generally the correction is less than 5% or 0.02 km/sec, but this is significant when the variation due to tectonics is of the order of 10%. All observed Rayleigh group velocity dispersions used in this study have been corrected for mean great-circular path ocean depth.

In summary, Rayleigh group velocity data, corrected for instrumental response and mean ocean depth, have a mean RMS residual uncertainty of the order of 0.03 km/sec. The most significant error will be introduced by mislocation of the epicenter and/or incorrect assignment of origin time.

DETERMINATION OF THE GROUP VELOCITY-AGE RELATIONSHIP

Rayleigh group velocity data used to create the group velocity versus age functions were derived from a combination of published dispersion data and some new paths. Dispersion data from the literature could be used only if they satisfied the following criteria: (1) the least-distance path had to be chronologically identifiable in terms of magnetic anomalies and/or deep sea drilling, and limited to a small deviation about the mean age to insure 'pure-path' properties; (2) the seismograms had to be relatively free of significant apparent multipath characteristics; (3) the dispersion curves must be computed by a

moving window-type analysis which is clearly identifiable as instrumentally delay corrected; and (4) the pure path data created by matrix least-squares reduction of mixed path data, such as those by Forsyth (1975),had to have demonstrably stable solutions with clearly stated error limits. A surprisingly small volume of data is available in the literature which meet these criteria. Table 4 lists the published dispersion analyses used in this study. Supplemental new analyses were done to spot check the reliability of the published results and to fill some age gaps. All data compiled were corrected for instrumental and ocean depth group delay.

Even though nearly all group velocity data used in the construction of the age-velocity functions are from the Pacific Ocean, where there is a reasonable distribution of earthquakes and observatories and relatively wide isochronological sea floor segments, determination of mean velocities for a given sea floor age is difficult because of sampling bias in an anisotropic medium. The degree of seismic surface wave velocity anisotropy in the Pacific has been estimated to be between two and ten percent by several authors (Bamford and Crampin, 1977; Fuchs, 1977; Schlue and Knopoff, 1977, Forsyth, 1975). Velocity maxima are parallel with spreading directions and therefore they are normal to sea floor isochrons. Conversely, velocity minima are parallel with ridge axes and therefore are parallel to sea floor isochrons.

Unless an islchronological segment of sea floor is sampled at all azimuths, therefore, an apparent mean velocity will be biased by the particular azimuth-dependent velocities used in the mean computation. Forsyth (1975) determined mean surface wave velocities for temporal-restricted sea floor segments less than 30 million years old which are

relatively free of anisotropy sampling bias. These mean results from the Nazca plate are used for the initial points on the age-velocity functions. All other data points are subject to aniostropy sampling bias which cannot be avoided for the majority of the Pacific basins.

Assuming that the surface wave velocity anisotropy of 2% (Forsyth, 1975) is representative, and that the anisotropy is restricted th the low velocity zone (LVZ) as suggested by Schlue and Knopoff (1977), it is possible to predict how specific observations may be biased. For example, the apparent mean surface wave velocities for sea floor (Nazca) older than 30 million years determined by Forsyth (1975) should be biased toward higher than true mean velocities because sampling must be restricted to paths nearly normal to the South American coastline to avoid significant horizontal refraction effects. Similarly, 'pure path' observations in the older portions of the Pacific (greater than 90 million years) are likely to be biased toward lower than true mean velocities because of the selection of paths which are sub-parallel to sea floor isochrons. Without absolute determination of the anisotropy correction necessary, however, it is not possible to make this correction to the data in advance.

Construction of the functional relationships between sea floor age and period-specific apparent mean group velocities was accomplished by performing stepwise polynomial regressions on the data from table 4 at periods from 30 to 100 seconds in 10 second increments. The results of these analyses are given in figure 2. Although the polynomial regressions were able to fit the data with a high degree of precision, the physical sense of these functions is questionable. The general trend of

these functions is a smooth 'logarithmic-type' curve in which velocity increases with increase in age (30,50,60,70 second curves). The cause of the 40 second period function aberrancy is unknown, but presumed to be a sampling problem since neither the 30 nor the 50 second period functions behave in this erratic fashion. Although the excursions are well within the bounds of a 1-2% anisotropy deviation, preferential sampling of the anisotropic medium is not believed to be responsible for the fluctuations in the 40 second curve. On the other hand, the 1.3% reduction in velocities of the 80, 90, and 100 second period curves in the crustal age region of 90 through 120 million years is believed to be caused by anisotropy sampling bias. All paths sampling sea floor in this age bracket are subparallel to the sea floor isochrons.

The temporal limits of the seven oceanic tectonic divisions (other than island arcs) which are used in this study are indicated by the vertical lines on the age versus apparent mean group velocity functions of figure 2. A set of mean apparent group velocities for periods from 30 through 100 seconds is assigned to each tectonic division by averaging the apparent velocities within each division limit. The assigned apparent mean group velocities for each division are given in table 1. Although there is a set of velocities for a 20 second period, this function was too erratic to be considered meaningful.

THE GLOBAL RAYLEIGH GROUP VELOCITY MATRIX

Apparent mean Rayleigh group velocities through each 5°x5° geographic block are derived by summing the products of the tectonic ele-

ment percentages and the period-specific mean group velocities assigned to each tectonic element; or in matrix notation:

$$\overline{V} = \sum_{i=1}^{n} T_i V_i$$

where $\overline{V}$ is the period-specific mean group velocity matrix with dimensions 8x36x72, T is the tectonic matrix with dimensions 20x36x72 and V is the period-specific, tectonic-specific mean group velocity matrix with dimensions 8x20.

Eight Mercator conformal projections of the contoured mean Rayleigh wave group velocities for the periods 30 through 100 seconds were produced from the velocity matrix. Figures 3,4, and 5 illustrate the velocity contouring for 40, 70, and 100 second Rayleigh waves respectively (13"x26" blackline reproductions of all eight maps are available from the author on request). These maps are a convenient data display providing both a base for nonautomatic 'ray tracing' testing of the model against observed data. All maps are contoured at an interval of 0.05 km/sec. Each map displays the velocity data from 75° north latitude to 75° south latitude. There is a duplication of 65° east longitude through 105° east longitude on the left and right hand margins of the maps. East longitudes 0°, 180°, and 270° and colatitudes 45°, 90° and 135° provide a reference framework on all maps.

TESTS OF THE RAYLEIGH GROUP VELOCITY PREDICTIVE MODEL

PACIFIC OCEAN BASINS

Knopoff (1969) demonstrated that group travel times in inhomogeneous dispersive media are equivalent to the sum of the group velocity delays within each homogeneous path segment. For this study, path segments limited by mapped successive velocity contours are defined as homogeneous divisions and assigned velocities equivalent to the mean of the bounding contours. Paths which cross no mapped velocity contours are assigned velocities dependent on the spatial configuration of the path within the contoured zone. Contoured areas with widths less than 1500 kilometers are assigned velocities equivalent to the mean of the bounding contours. On the other hand, contoured areas with widths exceeding 1500 kilometers, such as those of the western Pacific, are roughly divided into three subregions. The two marginal segments are assigned velocities equivalent to the nearest contour; the central segment is assigned a mean velocity. Thus for example, a path subparallel to a 4.0 km/sec contour located in a wide 'iso-velocity' region, and having the majority of its length within the pne third proximal region would be assigned a velocity of 4.0 km/sec rather than a mean velocity.

In addition, implicit in these analyses is the assumption that all paths are least-distance, and that the composite group velocity along a given path is represented by the sum of the assigned segment group delays. Thus, by overlaying each of the eight Rayleigh velocity contour maps with correctly scaled Mercator conformal projections of least-distance paths, discrete period, path related dispersion curves are computed by summing the product of path segment group velocities and corresponding path length percentages over the total path length.

These predicted dispersion curves, corrected for mean bathymetry, are directly comparable with the instrumental-delay-corrected observed group velocities which are determined for the same path by moving window analysis.

Seventeen random paths were selected for the Pacific Ocean basins. These paths, illustrated in figure 6, collectively sample the Pacific basins in a non-preferential manner with respect to tectonics, possible anisotropy, and bathymetry. Rayleigh group velocities are predicted for each of these paths by the previously discussed technique. These predicted dispersion curves are compared with moving window analyses of path-equivalent observed dispersion curves in figures 7 through 10.

The six dispersion analyses of figure 7 are presented in a format unlike the subsequent comparative diagrams, to illustrate not only the comparison of this model and observed data, but also the comparison of this tectonic-based model with three other standard ocean models. Observed data, corrected for bathymetry effects, are illustrated by the closed circles; uncorrected for bathymetry effects by the open circles. Solid lines represent dispersion analyses predicted by this model; dot and dash lines represent dispersion using the Harkrider-Anderson ocean model (1964); dashed lines represent dispersion using standard ocean model CIT 11A (Kanamori and Abe, 1968); and dotted lines represent dispersion using standard ocean model 8099 (Kanamori and Abe, 1968). Only in figure 7 is the bathymetry correction applied to the observed data. All other diagrams have the bathymetry correction applied to the predicted data to correctly locate it in the observed period versus group velocity space.

Figure 7 clearly demonstrates the inadequacy of previous fixed-structure models to fit the Rayleigh group velocity data. Although the Harkrider-Anderson model may fit Rayleigh group velocity data for old ocean basins (Fig.7,KIP 1) with relatively small residuals, the model fails significantly for a younger oceanic region (Fig. 7, PEL 6). Similarly, fixed structure models like CIT 11A and 8099 may yield small residuals over a very limited spectral band, but fail to fit the observed data over a broader spectrum. On the other hand, the tectonic-based model has an implicitly evolving structure with time, albeit not explicitly stated, which permits it to fit both old and young ocean crust and mantle Rayleigh group velocities over a wide spectrum. This is clearly apparent in figure 7.

The predictive dispersion model significantly overestimates the group velocities for the path PEL 6 (Fig. 7). Interestingly, however, a significant portion of this path traverses the Nazca ridge which has been shown recently by Cutler (1977) to have an anomalously thick crust with modeled low density core extending to at least 20 kilometers. Thus, the apparent failure of the tectonic-based model to predict accurately the dispersion along this path independently illustrates the Nazca Ridge to be an anomalous structure even into the uppermost mantle. Because the predictive model is dependent on surficial tectonics, significant overestimations of observed dispersed Rayleigh group velocities may suggest locations of paleo mantle upwellings which no longer have geophysical expression at the surface. This hypothesis is supported more convincingly if the anomaly extends to longer periods (greater than 40 sec) suggesting a deeper seated cause of the negative velocity residuals.

The remaining dispersion analyses in this paper compare the observed data to the tectonic based model only. The observed data are presented as energy contours in an instrumental group delay corrected group velocity versus logarithmic-period space. Although the entire region is capable of being contoured, only the most significant energy regions are contoured to reduce unnecessary cluttering of the diagrams. Depth-corrected predicted-mean group velocity data for the same great-circular path are presented as solid circles. The diameter of the circle is approximately half the RMS uncertainty of 0.03 km/sec for the determinations. The vertical bars extending from the mean velocities correspond to a 2% velocity uncertainty at 4.0 km/sec (0.08 km/sec). If the degree of surface wave velocity anisotropy in ocean basins does not exceed 2%, as suggested by Forsyth (1975), then these error bars should encompass the possible anisotropy-related scatter. Figures 8 through 10 illustrate the remaining Pacific Ocean tests.

Generally the correspondence of the predicted and observed dispersion data is remarkably high. A systematic overestimation of the 30 and frequently 40 second period group velocities suggests that the depth correction by mean ocean depth may not be adequate. Alternatively this could be a problem with the model, but without performing a stepwise depth correction, the source of this error is unknown. Dispersion curves for paths crossing the Philippine plate are illustrated in figure 10-B, 10-C, and 10-D. Two of these paths cross the width of the plate, the third crosses the length (See figure 6.). Although a predicted dispersion is derived for these paths, all three moving window analyses of the observed data are severely distorted. Energy contours at periods less than 40 seconds indicate the presence of 'spectral holes' and the

resolving kernals at periods greater than 40 seconds are extremely broad, indicating a severe attenuation of longer period waves. Studies by deBremaecker (1958), Hudson and Knopoff (1964), Pilant, Knopoff, and Schwab (1964), and Mal and Knopoff (1966) have shown that transmission and reflection of Rayleigh waves at abrupt velocity contrasts, especially at corners can cause severe distortion of observed Rayleigh waves. Considering that MAT and GUA are both located at critical points for effective Rayleigh wave transmission (deBremaecker, 1958), the lack of resolution on the Philippine plate tests is understandable.

INDIAN OCEAN BASIN

Four paths crossing the Indian Ocean are illustrated in figure 11. The associated dispersion analyses are illustrated in figure 12. Only the Rayleigh group velocity dispersion recorded at MUN (figure 12-D) has consistently small velocity residuals with respect to the model prediction. All other analyses consistently predict group velocities approximately 0.10 km/sec less than those actually observed. Although a systematic regional mislocation error cannot be entirely ruled out as the cause of this anomaly, the simultaneous recording of the same earthquake at CHG (fig. 12-C) and MUN (fig. 12-D) suggests that the error is path related and not the result of mislocation. Since the paths to CHG, KOD, and LEM (figure 12.) sample relatively the same aged material (Johnson, Powell and Veevers, 1976), it is possible that the relatively consistent positive velocity offset is a result of incorrect age assignment. This is a relatively old section of sea floor, however, and the misassignment of age would have to be extreme to account

for the magnitude if the error. Similarly, the magnitude of this error is too large to be the result of an incorrect depth correction. Further discussion of this positive anomaly is deferred to the discussion and speculation section.

ATLANTIC OCEAN BASINS

Six Atlantic Ocean test paths are illustrated in the Mercator conformal projection of figure 13. The dispersion analyses for the three South Atlantic basins tests are illustrated in figures 14A, 14B, and 14C. The dispersion analysis ,14A, is for a path traversing the Cape Basin of the South Atlantic Ocean, and is characterized by positive observed-minus-predicted velocity residuals approximately equivalent to those observed for the Indian Ocean. Both dispersion curves 14B and 14C are for paths either partly (14B) or entirely (14C) confined to the Brazil Basin. Both dispersion curves exhibit extremely large positive residuals with respect to the model; 14C larger than 14B. Since P-wave travel times for both events have essentially no residuals, timing and/or mislocation errors can be discounted. Similarly, there are no input errors in the moving window analyses, thus these anomalies appear to be real and related to the Brazil Basin.

North Atlantic tests are illustrated in figures 14D, 15A, and 15B. Inadequate resolution of the moving window analysis for the recording of the earthquake at TRN (fig. 15A) appear to be characteristic for that station since similar observations have been made by other authors (Weidner, 1972). Since the resolution difficulties preclude interpretation of TRN recordings of mid-Atlantic earthquakes,

this station is unsuitable for surface wave analyses of Atlantic paths. The other two dispersion curves for the North Atlantic, 14D and 15B, are not confined to specific basins but have paths subnormal (14D) and subparallel (15B) to the mid-Atlantic ridge. Both of these paths have characteristic velocity residuals (0.1-0.2 km/sec) larger than those observed for the Cape Basin (0.05-0.1 km/sec) in the South Atlantic or the Indian Ocean (0.05-0.1 km/sec), but significantly less than the residuals observed for the Brazil Basin.

In summary, tests of the tectonic-based Rayleigh wave group velocity predictor have been conducted for many of the major ocean basins. Only in the Pacific basins does the model consistently predict the dispersion curves for given paths with extremely small errors. In all other ocean basins, the model systematically underestimates the observed velocities.

DISCUSSIONS AND SPECULATIONS

The relative success of this Rayleigh group velocity model clearly indicates that the first order variations in observed oceanic dispersion are related to sea floor age. In the Pacific Ocean, there is a 10% increase in the group velocity of Rayleigh waves with a period of 40 seconds over the span of 140 million years. Approximately 6% of this 10% increase occurs within the first 30 million years of evolution. In comparison, there is a 7% increase in group velocity of Rayleigh waves with a period of 90 seconds over the span of 140 million years, with only 3% of the 7% increase occurring within the first 30 million years.

It is gratifying that the Rayleigh predictor model is as successful as it appears to be in the Pacific basins. However, the failures of the model pose intriguing problems. These can be separated into explanations of negative residuals and explanations of positive residuals.

The one path displaying systematic negative observed-minus-predicted Rayleigh group velocity residuals for the Pacific Ocean traverses the Nazca Ridge which has been shown to have an anomalous crustal structure and low density core (Cutler, 1977). This suggests a previously unexpected application of the Rayleigh predictor model, i.e. the search for 'fossil' spreading regions. These ancient thermal perturbations should retain a mantle signature significantly beyond the time that surface expression (topography) of the divergent zone has disappeared (approximately 35 million years). Thus, for example, it may be possible to located the mantle 'root' of the Kula Ridge even though the surface geophysical signature (magnetic anomaly patterns) of the axis of this spreading center has been spatially decoupled. The location of fossil upwelling zones in the mantle, which should be fixed spatially for a longer period of time than their surface correlative features, can offer additional constraints to possible paleoplate reconstructions. This is especially true when episodes of plate motion are characterized by distinct directions of motion which are time dependent, and subsequently deactivated ridges are spatially migrated as has occurred in the Pacific.

The systematic positive velocity residuals with respect to the Rayleigh predictor which occur in all ocean basins except the Pacific

constitute a second intriguing problem. Although the observed higher Rayleigh velocities of the non-Pacific basins may be a function of compositional variation, the relative world-wide homogeneity of sampled oceanic lithosphere (Chung, 1976) does not support this proposition. Spatial variability of mantle heat flux (Pollack and Chapman, 1977a,b) appears to be a more likely cause of the Rayleigh group velocity variation.

Two alternative explanations for the lower Atlantic and Indian Ocean crust and upper mantle thermal structure, and thus higher Rayleigh group velocities, are possible. Either there may be a lower initial thermal input, or there is a mechanism for extraction of the heat which is not present in the Pacific. If the former explanation is correct as suggested by Pollack and Chapman (1977b), then the reduction of partial melting due to reduced oceanic geothermal gradients is a relatively time-invariant influence and provides a constant offset of the group velocity versus age functions of figure 2. Thus, for example, paths through equivalently aged lithosphere in the Atlantic versus the Pacific would display consistently higher velocities in the former basins than the latter, and regardless of age, the offset would be the same.

Alternatively, the Atlantic and Indian Oceans differ from the Pacific in another important aspect, i.e. the former basins have been locations occupied, perhaps repeatedly, by continental lithosphere, whereas the latter has apparently remained an oceanic lithosphere realm throughout its existence. The cooler cratonic lithosphere, proposed

by Pollack and Chapman (1977b) to be in excess of 300 kilometers thick, has a profound influence on the thermal structure of the lower crust and upper mantle. The degree of influence should be proportional to the distance from the spreading center to the cratonic margin. If the proximity to cratonic elements rather than lower spreading center temperatures is the cause of the higher Rayleigh group velocities in ocean basins occupied by continents prior to drifting, then the group velocity versus age functions (figure 2.) would be influenced in a temporally lessening manner. The oldest ocean basins, closest to the initial rifting would be most pronouncedly affected, while the present mid-Atlantic ridge should show little or no influence of craton proximity on its geotherms. This could explain why the Brazil, and possibly Angola Basins would have very fast Rayleigh group velocities since they were closest to cratonic elements contemporaneous with the breakup of Gondwana. Similarly, the basins of the North Atlantic would have fast Rayleigh velocities due to the proximity with North American and African cratonic regions. However, these basins should be slower than the Brazil Basin since there was a younger tectonically disturbed lithospheric buffer between these cratons and the incipient spreading center.

Additional testing of the Atlantic and Indian Ocean basins to attempt to differentiate between these alternative explanations for positive residuals from the Rayleigh predictor model is a currently active research effort at the University of Michigan. In all likelihood, the higher velocities characteristic of the non-Pacific ocean basins might be the result of a combination of lower initial thermal flux and thermal diffraction due to continental proximity influence.

APPENDIX Sources of Tectonic Data

Continents

North America: Tectonic Map of North America (1969), United States Geological Survey, scale 1:5,000,000 compiled by P. B. King.

South America: Geologic Map of South America (1964), Commission of the Geologic Map of the World, scale 1:5,000,000, General coordinator A.R. Lamego; Tectonic Map of Brazil (1971), Ministry of Mines and Energy, National Department of Mineral Production, Brazil, scale 1:5,000,000, coordinator E.O. Ferreira.

Antarctica : Geologic Map of Antarctica (1971), American Geographical Society, scale 1,5,000,000, compiled by C. Craddock.

Africa : International Tectonic Map of Africa (1968), Association of African Geologic Surveys and United Nations Educational Scientific and Cultural Organization, scale 1:5,000,000, coordinator G. Choubert.

Australia : Tectonic Map of Australia and New Guinea (1971), Geological Society of Australia, scale 1:5,000,000, Sidney.

Europe and Asia : Tectonic Map of Eurasia (1966), Geologic Institute of the Academy of Sciences of the U.S.S.R., scale 1: 5,000,000, chief editor A.L. Yanshin.

Oceans

General: Magnetic Lineations of the Oceans (1974), Geologic Society of America, compiled by W. C. Pitman III, R. L. Larson, and E. M. Herron.

Arctic: Herron, E. M., J. F. Dewey, and W. C. Pitman III (1974), 'Plate Tectonics Model for the Evolution of the Arctic', Geol. (2), p. 377-380.

Sources of Tectonic Data continued

Indian: Johnson, B. D., C. Mca. Powell, and J. J. Veevers (1976), 'Spreading History of the Eastern Indian Ocean and Greater India's Northward Flight from Antarctica and Australia', Geol. Soc. Amer. Bull. (87), p. 1560-1566.

Marginal Basins: Sclater, J.G., U.G. Ritter, and F. S. Dixon (1972), 'Heat Flow in the Southwestern Pacific', Jour. Geophys. Res. (77), p. 5697-5704.; Sclater, J.G. (1972), 'Heat flow and Elevation of the Marginal Basins of the Western Pacific', Jour. Geophys. Res. (77), p. 5705-5719. ; Cooper, A.K., M.S. Marlow, and D.W. Scholl (1976), ' Mesozoic Magnetic Lineations in the Bearing Sea Marginal Basin', Jour. Geophys. Res. (81), p. 1916-1934.; Lawver, L. A., J. R. Curray, and D.G. Moore (1975), ' Magnetics in the Adaman Sea and the Effect of High Sedimentation Rates', E.O.S. (56), p. 1064.; Packham, G.H., and D. A. Falvey (1971), 'An Hypothesis for the Formation of Marginal Seas in the Western Pacific', Tectonophys. (11), p. 79-110.; VanderVoo, R., F.J. Mauk, and R.B. French (1976), 'Permian Triassic Continental Configurations and the Origin of the Gulf of Mexico', Geol. (3), p. 177-179.; Initial Reports of the Deep Sea Drilling Project Volumes Prepared for the National Science Foundation under Contract C-482.

ACKNOWLEDGEMENTS

This research was supported by the Advanced Research Projects Agency of the Department of Defense and was monitored by the Air Force Office of Scientific Research under contract number F44620-73-C-0060. I would like to acknowledge Dr. Adam Dziewonski for supplying me with a copy of his moving window analysis program, without which this study could not have been done. Special thanks are due to Dr. David Chapman and Mr. Steven Henry who assisted in the compilation of the global tectonic data file. Finally, conversations and criticisms of Dr. James T. Wilson, Dr. Henry N. Pollack, Dr. Rob Vander Voo, Dr. David Chapman, and Dr. Arthur Tarr proved invaluable to the continuity of this research.

REFERENCES

Adams, R. D. (1974), Dispersion Wave Studies in Antarctica, Wellington New Zealand Seismol. Obs. Bull., No. S-194.

Alexander, S.S. (1963), Surface Wave Propagation in the Western U. S., Ph.D. Thesis, Calif. Inst. Tech., Pasadena, Cal.

Bamford, D. and S. Crampin (1977), Seismic Anisotropy - The State of the Art, Geophys. Jour., 49, 108.

Berckhemer, H. (1956), Rayleigh Wave Dispersion and Crustal Structure in the Eastern Atlantic Ocean, Bull. Seis. Soc. Amer., 46, 83.

Bhattacharya, S. N. (1974), The Crust-Mantle Structure of the Indian Peninsula from Surface Wave Dispersion, Geophys. Jour., 36, 273.

Biswas, N. N. and L. Knopoff (1974), The Structure of the Upper Mantle under the United States from the Dispersion of Rayleigh Waves, Geophys. Jour., 36, 515.

Bolt, B. A. and M. Niazi (1964), Dispersion of Rayleigh Waves Across Australia, Geophys. Jour., 8, 21.

Braile, L. W. and G. R. Keller (1975), Fine Structure of the Crust Inferred from Linear Inversion of Rayleigh Wave Dispersion, Bull. Seis. Soc. Amer., 65, 71.

Brilliant, R. M. and M. Ewing (1954), Dispersion of Rayleigh Waves across the United States, Bull. Seis. Soc. Amer., 44, 149.

Brune, J. and J. Dorman (1963), Seismic Waves and Earth Structure in the Canadian Shield, Bull. Seis. Soc. Amer., 53, 167.

Capon, J. (1970), Analysis of Rayleigh Wave Multipath Propagation at LASA, Bull. Seis. Soc. Amer., 60, 1701.

Cooper, A.K., M. S. Marlow, and D. W. Scholl (1976), Mesozoic Magnetic Lineations in the Bearing Sea Marginal Basin, Jour. Geophys. Res., 81, 1916.

Cutler, S.T. (1977), Geophysical Investigation of the Nazca Ridge, E.O.S. 58, 1230.

deBremaecker, J. C. (1958), Transmission and Reflection of Rayleigh Waves at Corners, Geophys., 23, 253.

Fix, J. E. (1975), The Crust and Upper Mantle of Central Mexico, Geophys. Jour., 43, 453.

Forsyth, D. W. (1975), The Early Structural Evolution and Anisotropy of the Oceanic Mantle, Geophys. Jour., 43, 103.

Fuchs, K. (1977), Seismic Anisotropy of the Subcrustal Lithosphere as Evidence for Dynamical Processes in the Upper Mantle, Geophys. Jour., 49, 167.

Goncz, J.H., A. L. Hales, and K J. Muirhead (1975), Analysis to Extended Periods of Rayleigh and Love Wave Dispersion across Australia, Geophys. Jour., 41, 81.

_____ and J. R. Cleary (1976), Variations in the Structure of the Upper Mantle beneath Australia from Rayleigh Wave Observations, Geophys. Jour., 44, 507.

Hagiwara, T. (1958), A Note on the Theory of the Electromagnetic Seismograph, Bull. Earthq. Res. Inst., 36, 139.

Harkrider, D. G. (1964), Surface Waves in Multilayered Elastic Media: I. Rayleigh and Love Waves from Buried Sources in a Multilayered Half-Space, Bull. Seis. Soc. Amer., 54, 627.

Herron, E. M., J. F. Dewey, and W.C. Pitman (1974), Plate Tectonics Model for the Evolution of the Arctic, Geology, 2, 377.

Hudson, J. A. and L. Knopoff (1964), Transmission and Reflection of Surface Waves at a Corner 2. Rayleigh Waves (Theoretical), Jour. Geophys. Res., 69, 281.

James, D. E. (1971), Andean Crustal and Upper Mantle Structure, Jour. Geophys. Res., 76, 3246.

Jardetsky, W.S. and F. Press (1953), Crustal Structure and Surface Wave Dispersion, Part III. Theoretical Dispersion Curves for Sub-Oceanic Rayleigh Waves, Bull.Seis. Soc. Amer., 43, 137.

Johnson, B.D., C. MCA, Powell, and J. J. Veevers (1976), Spreading History of the Eastern Indian Ocean and Greater India's Northward Flight from Antarctica and Australia, Geol. Soc. Amer. Bull., 81, 1560.

Kanamori, H. and K. Abe (1968), Deep Structure of Island Arcs as Revealed by Surface Waves, Bull. Earthq. Res. Inst., 46, 1001.

Keller, G. R., et.al. (1975), Upper Crustal Structure of the Eastern Basin-Range, Northern Colorado Plateau, and Middle Rocky Mountains for Rayleigh Wave Dispersion, E.O.S., 56, 402, (Abstract).

Knopoff, L., S. Mueller, and W. L. Pilant (1966), Structure of the Crust and Upper Mantle in the Alps from Phase Velocity of Rayleigh Waves, Bull. Seis. Soc. Amer., 56, 1009.

____ and A.K. Mal (1967), Phase Velocities of Surface Waves in the Transition Zone of Continental Margins, Jour. Geophys. Res., 72, 1769.

____ and F. Schwab (1968), Apparent Initial Phase of a Source of Rayleigh Waves, Jour. Geophys. Res., 73, 755.

____ (1972), Observation and Inversion of Surface Wave Dispersion, Tectonophys., 13, 497.

____, J. W. Schlue, and F. A. Schwab (1970), Phase Velocities of Rayleigh Waves across the East Pacific Rise, Tectonophys., 10, 321.

Kovach, R. and F. Press (1961), Rayleigh Wave Dispersion and Crustal Structure in the Eastern Pacific and Indian Oceans, Geophys. Jour., 4, 202.

Landisman, M. A. Dziewonski and Y. Sato (1969), Recent Improvements in the Analysis of Surface Wave Observations, Geophys. Jour., 17, 369.

Leeds, A.R., E.G. Kausel, and L. Knopoff (1974), Variations of Rayleigh Wave Phase Velocities across the Pacific Ocean, Sci., 186, 139.

____ (1974), Variations of Upper Mantle Structure under the Pacific Ocean, Sci., 186, 141.

____ (1975), Lithospheric Thickness in the Western Pacific, Phys. Earth and Planet. Int., 11, 61.

Mal, A. K. and L. Knopoff (1966), Transmission of Rayleigh Waves at a Corner, Bull. Seis. Soc. Amer., 56, 455.

McGarr, A (1969), Amplitude Variations of Rayleigh Waves - Horizontal Refractions, Bull. Seis. Soc. Amer., 59, 1307.

North, R. G. (1976), The Effects of Lateral Heterogeneity upon Rayleigh Wave Propagation across Eurasia, E.O.S., 57, 287, (abstract).

Ocal, N. (1965), The Dispersion of Surface Waves and Crustal Structure in African Continent, Pure and Appl. Geophys., 60, 74.

Oliver, J., M. Ewing, and F. Press (1955), Crustal Structure and Surface Wave Dispersion 4, Atlantic and Pacific Basins, Geol. Soc. Amer. Bull., 66, 913.

_____ (1962), A Summary of Observed Surface Wave Dispersion, Bull. Seis. Soc. Amer., 52, 81.

Papazachos, B. C. (1964), Dispersion of Rayleigh Waves in the Gulf of Mexico and Caribbean Sea, Bull. Seis. Soc. Amer., 54, 1137.

Pilant, W., L. Knopoff, and F. Schwab (1964), Transmission and Reflection of Surface Waves at a Corner 3. Rayleigh Waves (Experimental), Jour. Geophys. Res., 69, 291.

Pitman, W.C., R. L. Larson, and E. M. Herron (1974), Magnetic Lineations of the Oceans, Geol. Soc. Amer. Map.

Pollack, H. N. and D. S Chapman (1977, a), Mantle Heat Flow, Jour. Geophys. Res., 34, 174.

_____ (1977, b), On Regional Variations of Heat Flow, Geotherms, and Lithospheric Thickness, Jour, Geophys. Res., 38, 279.

Santo, T. A. (1961), Division of the Southwest Pacific into Several Regions in Each of which Rayleigh Waves have the Same Dispersive Character, Bull. Earthq. Res. Inst., 39, 603.

_____(1960), Rayleigh Wave Dispersion across the Ocean Basin around Japan, Part II, Bull. Earthq. Res. Inst., 38, 385.

_____(1961, b), Rayleigh Wave Dispersion across the Oceanic Basin around Japan, Part III on the Crust of the Southwest Pacific Ocean, Bull. Earthq. Res. Inst., 39, 1.

_____(1962, a), Dispersion of Surface Waves along Various Paths to Uppsala, Sweden: Part I Continental Paths, Annali di Geofisica, 15, 245.

_____(1962, b), Dispersion of Surface Waves along Various Paths to Uppsala, Sweden: Part II Arctic and Atlantic Oceans, Annali di Geofisica, 15, 273.

_____(1966, a), Lateral Variations of Rayleigh Wave Dispersive Character: Part III Atlantic Ocean, Africa, and Indian Ocean, Pure and Appl. Geophys., 63, 40.

_____ and Y. Sato (1966, b), World-Wide Survey of Regional Characteristics of Group Velocity Dispersion of Rayleigh Waves, Bull. Earthq. Res. Inst., 44, 939.

Sato, Y. and T. Santo (1969), World-Wide Distribution of the Group Velocity of Rayleigh Waves as Determined by Dispersion Data, Bull. Earthq. Res. Inst., 47, 31.

Schlue, J. W., and L. Knopoff (1977), Shear Wave Polarization Anisotropy in the Pacific Basin, Geophys. Jour., 49, 145.

Sclater, J. G. and J. Francheteau (1970), The Implications of Terrestrial Heat Flow Observations on Current Tectonic' and Geochemical Models of the Crust and Upper Mantle of the Earth, Geophys. Jour., 20, 509.

_____, Anderson, R. N. and M. L. Bell (1971), Elevation of Ridges and Evolution of the Central Eastern Pacific, Jour. Geophys. Res. , 76, 7888.

Shurbet, D. H. (1960), The Effect of the Gulf of Mexico on Rayleigh Wave Dispersion, Jour. Geophys. Res., 65, 1251.

Tarr, A. C. (1969), Rayleigh Wave Dispersion in the North Atlantic Ocean, Caribbean Sea, and Gulf of Mexico, Jour. Geophys. Res., 74, 1591.

Teng, Ta-Liang (1974), Surface Wave Studies on Crustal and Mantle Structure of China, Univ. Southern Calif., Geophys. Lab. Tech. Rpt. 74-2.

Turnbull, L. (1976), Determination of Seismic Source Parameters Using Far Field Surface Wave Spectra, PhD Thesis, Pennsylvania State University, State College, Pennsylvania.

Weidner, D. J. (1972), Rayleigh Waves from Mid-Ocean Earthquakes: Source and Path Effects, PhD. Thesis, Mass. Inst. Technol., Cambridge Mass., 256.

Wilson, J. T. and D. Baykal (1948), Crustal Structure of the North Atlantic Basin as Determined from Rayleigh Wave Dispersion, Bull. Seis. Soc. Amer., 38, 41.

Wu, F. T. (1972), Mantle Rayleigh Wave Dispersion and Tectonic Provinces, Jour. Geophys. Res., 77, 6445.

Yoshii, T. (1975), Regionality of Group Velocities of Rayleigh Waves in the Pacific and Thickening of the Plate, Earth and Planet. Sci. Let., 25, 305.

CAPTIONS FOR FIGURES

Figure 1. 5°x 5° grid element tectonic encoding method

Figure 2. Apparent Mean Rayleigh Group Velocity Versus Sea Floor Age. Numerical designations on each curve indicate the period of the wave in seconds. Vertical bars separate tectonic divisions

Figure 3. 40 Second Period Rayleigh Wave Group Velocities. Contour interval is 0.05 km/sec.

Figure 4. 70 Second Period Rayleigh Wave Group Velocities. Contour interval is 0.05 km/sec.

Figure 5. 100 Second Period Rayleigh Wave Group Velocities. Contour interval is 0.05 km/sec.

Figure 6. Mercator Conformal Projection of Pacific Ocean Test Paths.

Figure 7. Six Pacific Dispersion Analyses. Closed circles indicate data corrected for bathymetry, open circles indicate data uncorrected. Solid lines are dispersions predicted from this model. Dot and Dash Lines are dispersions with Harkrider-Anderson Ocean Model (1964). Dotted lines are dispersions with standard ocean model 8099, Dashed lines are dispersions with standard ocean model CIT 11A.

Figure 8. Pacific Ocean Tests. A. KIP-12.5 S, 77.8 W, epicentral distance 9514 km.; B. LON-8.4 S, 154.0 E, epicentral distance 10230 km.; C. KIP-53.0 N, 171.1 E, epicentral distance 4384 km.; D. AFI-39.8 N, 143.1 E, epicentral distance 7553 km.

Figure 9. Pacific Ocean Tests. A. KIP-14.7 S, 175.6 E, epicentral distance 4429 Km.; B. KIP-15.7 S, 172.64 W, epicentral distance 4397 km.

CAPTIONS FOR FIGURES CONTINUED

Figure 10. Pacific Ocean and Philippine Plate Tests. A. KIP-14.8 S, 174.8 W, epicentral distance 4400 km.; B MAT-1.2 N, 126.3 E, epicentral distance 4094 km.; C. GUA-5.1 N, 126.8 E, epicentral distance 2198 km.; D. GUA-1.2 N, 126.3 E, epicentral distance 2455 km.

Figure 11. Mercator Conformal Projection of Indian Ocean Test Paths.

Figure 12. Indian Ocean Tests. A. KOD-47.9 S, 99.7 E, epicentral distance 6796 km.; B. LEM-26.1 S, 84.3 E, epicentral distance 3261 km.; C. CHG-41.7 S, 79.9 E, epicentral distance 6954 km.; D. MUN-41.7 S, 79.9 E, epicentral distance 3384 km.

Figure 13. Mercator Conformal Projection of Atlantic Ocean Test Paths.

Figure 14. South and North Atlantic Tests. A. SDB-58.5 S, 13.6 W, epicentral distance 5307 km.; B. NAT-54.4 S, 2.5 E, epicentral distance 6416 km.; C. NAT-11.7 S, 14.0 W, epicentral distance 2421 km.; D. TLO-10.6 N, 63.4 W, epicentral distance 6653 km.

Figure 15. North Atlantic Tests. A. TRN-15.3 N, 45.9 W, epicentral distance 1756 km.; B. AKU-00.9 S, 22.1 W, epicentral distance 7384 km.

Table 1. A. Continental Tectonic Divisions and Associated Velocities

Tectonic Element	Rayleigh Wave Group Velocity (km/sec)								
	20 (sec)	30 (sec)	40 (sec)	50 (sec)	60 (sec)	70 (sec)	80 (sec)	90 (sec)	100 (sec)
Archean Shield	3.070	3.420	3.700	3.940	4.070	4.100	4.100	4.080	4.040
Proterozoic Shield	3.070	3.420	3.700	3.940	4.070	4.100	4.100	4.080	4.040
Precambrian Undeformed sediments	3.050	3.300	3.650	3.800	3.920	3.950	3.960	3.970	3.950
Early Paleozoic Orogeny	3.000	3.300	3.650	3.780	3.820	3.830	3.820	3.820	3.800
Late Paleozoic Orogeny	3.000	3.300	3.650	3.780	3.820	3.830	3.820	3.820	3.800
Post-Precambrian Undeformed sediments	3.050	3.300	3.650	3.800	3.920	3.950	3.960	3.970	3.950
Mesozoic Orogeny	3.000	3.400	3.700	3.730	3.660	3.660	3.650	3.650	3.600
Cenozoic Folding	3.000	3.300	3.650	3.780	3.820	3.830	3.820	3.820	3.800
Cenozoic Volcanics	3.000	3.300	3.650	3.780	3.820	3.830	3.820	3.820	3.800
Intermontane Basin Fill	3.290	3.350	3.500	3.605	3.630	3.680	3.692	3.696	3.692
Mesozoic Volcanics	3.000	3.300	3.650	3.780	3.820	3.830	3.820	3.820	3.800
Shelf Sediments	2.650	3.300	3.620	3.740	3.880	3.950	3.960	3.970	3.950

Table 1. B. Oceanic Tectonic Divisions and Associated Velocities

Tectonic Element	Rayleigh Wave Group Velocity (km/sec)								
	20 (sec)	30 (sec)	40 (sec)	50 (sec)	60 (sec)	70 (sec)	80 (sec)	90 (sec)	100 (sec)
Anomaly 0-5	3.815	3.815	3.740	3.725	3.665	3.645	3.640	3.630	3.630
Anomaly 5-6	3.880	3.920	3.883	3.818	3.768	3.728	3.715	3.693	3.678
Anomaly 6-13	3.958	4.000	3.985	3.915	3.875	3.820	3.803	3.770	3.743
Anomaly 13-25	4.038	4.103	4.053	3.998	3.958	3.900	3.898	3.818	3.790
Late Cretaceous Sea Floor 63-100 my	4.143	4.160	4.113	4.068	4.020	3.968	3.913	3.855	3.828
Early Cretaceous Sea Floor 100-140 my	4.200	4.188	4.150	4.110	4.055	4.000	3.950	3.860	3.845
Jurassic Sea Floor Older than 140 my	4.150	4.200	4.115	4.120	4.068	4.010	3.949	3.885	3.840
Island Arcs	3.500	3.680	3.760	3.780	3.810	3.800	3.800	3.750	3.740

Table 2. Standard Oceanic Crust and Upper Mantle Model

Layer Thickness (kilometers)	V_p km/sec	V_s km/sec	Rho g/cm^3
5.0	1.52	0.0	1.03
1.0	2.10	1.00	2.10
2.5	6.41	3.70	3.06
2.5	6.411	3.702	3.07
3.0	8.11	4.61	3.40
5.5	8.12	4.61	3.40
17.5	8.12	4.61	3.40
20.0	8.01	4.56	3.37
20.0	7.95	4.56	3.37
20.0	7.71	4.40	3.37
20.0	7.68	4.34	3.33
20.0	7.77	4.34	3.33
20.0	7.85	4.34	3.33
20.0	8.10	4.45	3.33
20.0	8.12	4.45	3.33
20.0	8.12	4.45	3.35
20.0	8.12	4.45	3.36
20.0	8.12	4.45	3.37
20.0	8.12	4.45	3.38
20.0	8.24	4.45	3.39
10.0	8.30	4.53	3.44
20.0	8.36	4.56	3.50
25.0	8.75	4.795	3.68
20.0	9.15	5.04	3.88
10.0	9.43	5.217	3.90
20.0	9.76	5.40	3.92
25.0	9.77	5.40	3.93
25.0	9.78	5.40	3.95
25.0	9.78	5.40	3.96
25.0	9.78	5.40	3.99

Table 3. Phase and Group Velocities for the standard ocean model of table 2 varying the thickness of layer 1 (water layer) from 0 through 6 kilometers.

Period (sec)	0 km/sec		1 km/sec		2 km/sec		3 km/sec		4 km/sec		5 km/sec		6 km/sec	
	C	U	C	U	C	U	C	U	C	U	C	U	C	U
20	4.083	4.036	4.069	4.005	4.053	3.966	4.033	3.911	4.005	3.817	3.961	3.625	3.873	3.138
25	4.089	4.087	4.078	4.063	4.066	4.036	4.052	4.001	4.035	3.952	4.014	3.877	3.982	3.745
30	4.096	4.113	4.077	4.095	4.068	4.074	4.057	4.049	4.045	4.017	4.031	3.974	4.013	3.912
35	4.081	4.123	4.073	4.107	4.065	4.090	4.057	4.071	4.047	4.048	4.036	4.019	4.024	3.981
40	4.075	4.121	4.069	4.108	4.062	4.093	4.054	4.078	4.046	4.060	4.037	4.033	4.028	4.011
45	4.070	4.112	4.064	4.100	4.058	4.089	4.051	4.075	4.044	4.060	4.037	4.043	4.029	4.023
50	4.066	4.100	4.060	4.090	4.055	4.079	4.049	4.067	4.043	4.055	4.036	4.040	4.030	4.024
55	4.063	4.086	4.058	4.077	4.053	4.067	4.048	4.057	4.042	4.046	4.036	4.033	4.030	4.019
60	4.062	4.071	4.057	4.063	4.052	4.056	4.047	4.045	4.042	4.034	4.037	4.024	4.031	4.012
65	4.062	4.056	4.057	4.048	4.053	4.040	4.048	4.031	4.043	4.022	4.038	4.013	4.033	4.012
70	4.063	4.041	4.058	4.033	4.054	4.025	4.050	4.018	4.045	4.009	4.041	4.001	4.036	3.991
75	4.065	4.025	4.061	4.018	4.057	4.011	4.052	4.003	4.048	3.996	4.044	3.988	4.039	3.979
80	4.068	4.008	4.064	4.002	4.060	3.995	4.056	3.988	4.052	3.981	4.048	3.974	4.044	3.966
85	4.072	3.991	4.069	3.985	4.065	3.979	4.061	3.973	4.057	3.966	4.053	3.959	4.049	3.952
90	4.078	3.974	4.074	3.968	4.071	3.962	4.067	3.957	4.063	3.950	4.059	3.944	4.056	3.937
95	4.084	3.956	4.081	3.951	4.077	3.945	4.074	3.940	4.070	3.934	4.067	3.928	4.063	3.922
100	4.092	3.937	4.088	3.932	4.085	3.927	4.081	3.922	4.078	3.916	4.075	3.911	4.071	3.905
105	4.100	3.918	4.097	3.913	4.094	3.908	4.090	3.903	4.087	3.898	4.084	3.893	4.080	3.887
110	4.110	3.898	4.107	3.894	4.103	3.889	4.100	3.884	4.097	3.879	4.094	3.874	4.090	3.869
115	4.120	3.878	4.117	3.874	4.114	3.870	4.111	3.865	4.108	3.860	4.105	3.856	4.101	3.851
120	4.132	3.858	4.129	3.854	4.126	3.850	4.123	3.845	4.120	3.841	4.117	3.837	4.113	3.832

Table 4 Published Data Used to Construct the Group Velocity Versus Age Relationship

Forsyth, D. W. (1975), The Early Structural Evolution and Anisotropy of the Oceanic Mantle, Geophys. Jour., 43, 103-162.

Kausel, E. G. (1972), Regionalization of the Lithosphere and Asthenosphere of the Pacific Ocean, Ph.D. Thesis, Columbia University, New York.

Knopoff, L., J. W. Schlue, and F. A. Schwab (1970), Phase Velocities of Rayleigh Waves across the East Pacific Rise, Tectonophys., 10, 321.

Kovach, R. L. and F. Press (1961), Rayleigh Wave Dispersion and Crustal Structure in the Eastern Pacific and Indian Oceans, Geophys. Jour., 4, 202.

Leeds, A. R., E. G. Kausel, and L. Knopoff (1974), Variations of Rayleigh Wave Phase Velocities across the Pacific Ocean, Sci., 186, 139.

Leeds, A. R. (1975), Lithospheric Thickness in the Western Pacific, Phys. Earth and Planet. Int., 11, 61.

Santo, T. A. (1961), Division of the Southwest Pacific into Several Regions in each of which Rayleigh Waves have the same Dispersive Character, Bull. Earthq. Res. Inst., 39, 309.

Yoshii, T. (1975), Regionality of Group Velocities of Rayleigh Waves in the Pacific and Thickening of the Plate, Ear. and Planet. Sci. Lett., 25, 305.

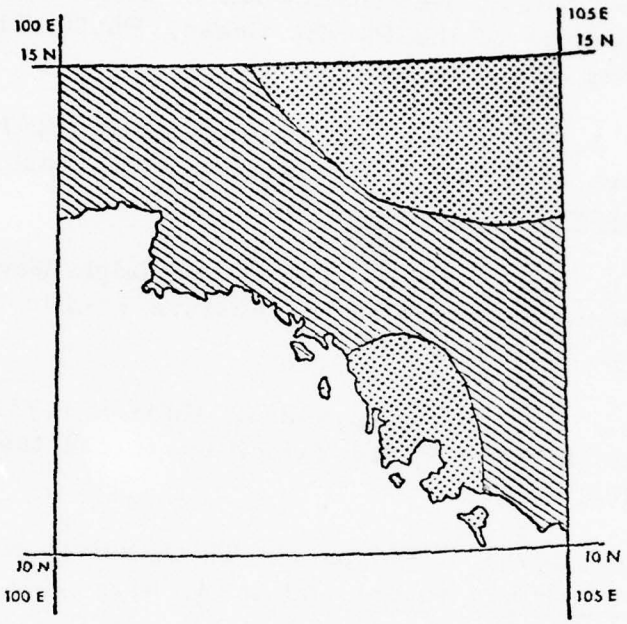

100 E
15 N
105 E
15 N
10 N
100 E
10 N
105 E
Post Precambrian Undeformed
Mesozoic Orogeny / Folding
Shelf Sediments

Figure 1.

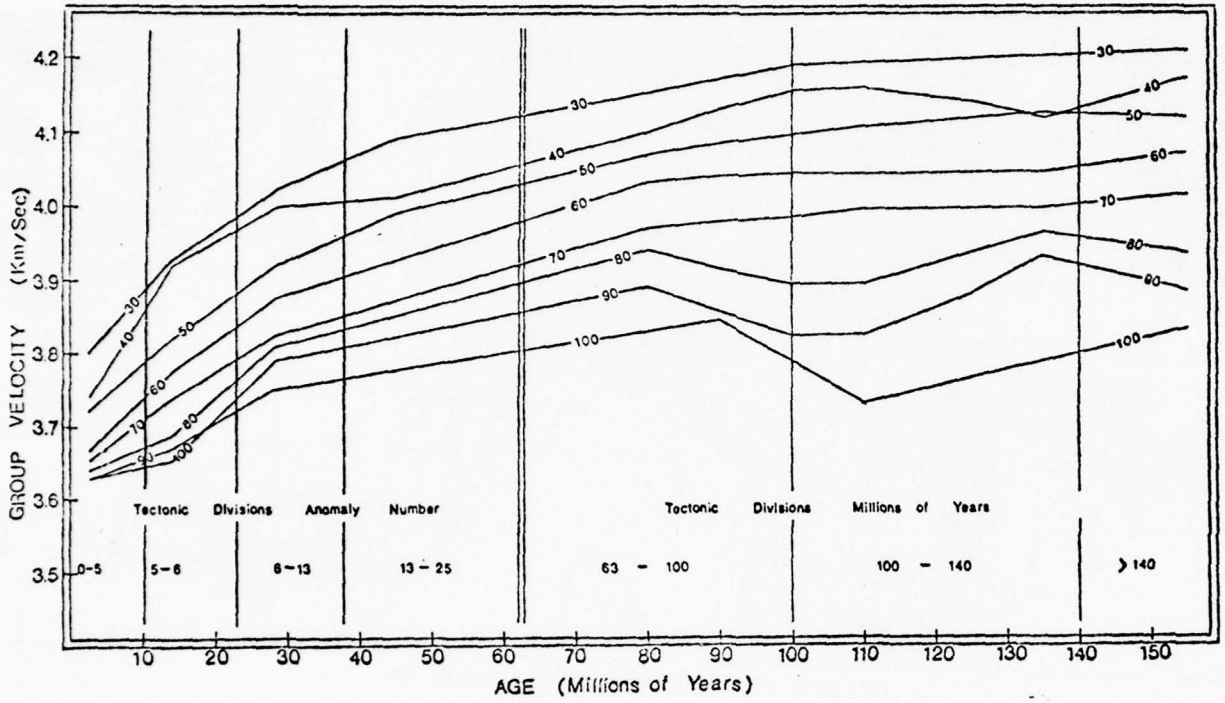

GROUP VELOCITY (Km/Sec)
4.2
4.1
4.0
3.9
3.8
3.7
3.6
3.5
30
40
50
60
70
80
90
100
Tectonic Divisions
Anomaly Number
Tectonic Divisions
Millions of Years
0-5
5-6
6-13
13-25
63 - 100
100 - 140
> 140
10 20 30 40 50 60 70 80 90 100 110 120 130 140 150
AGE (Millions of Years)

Figure 2.

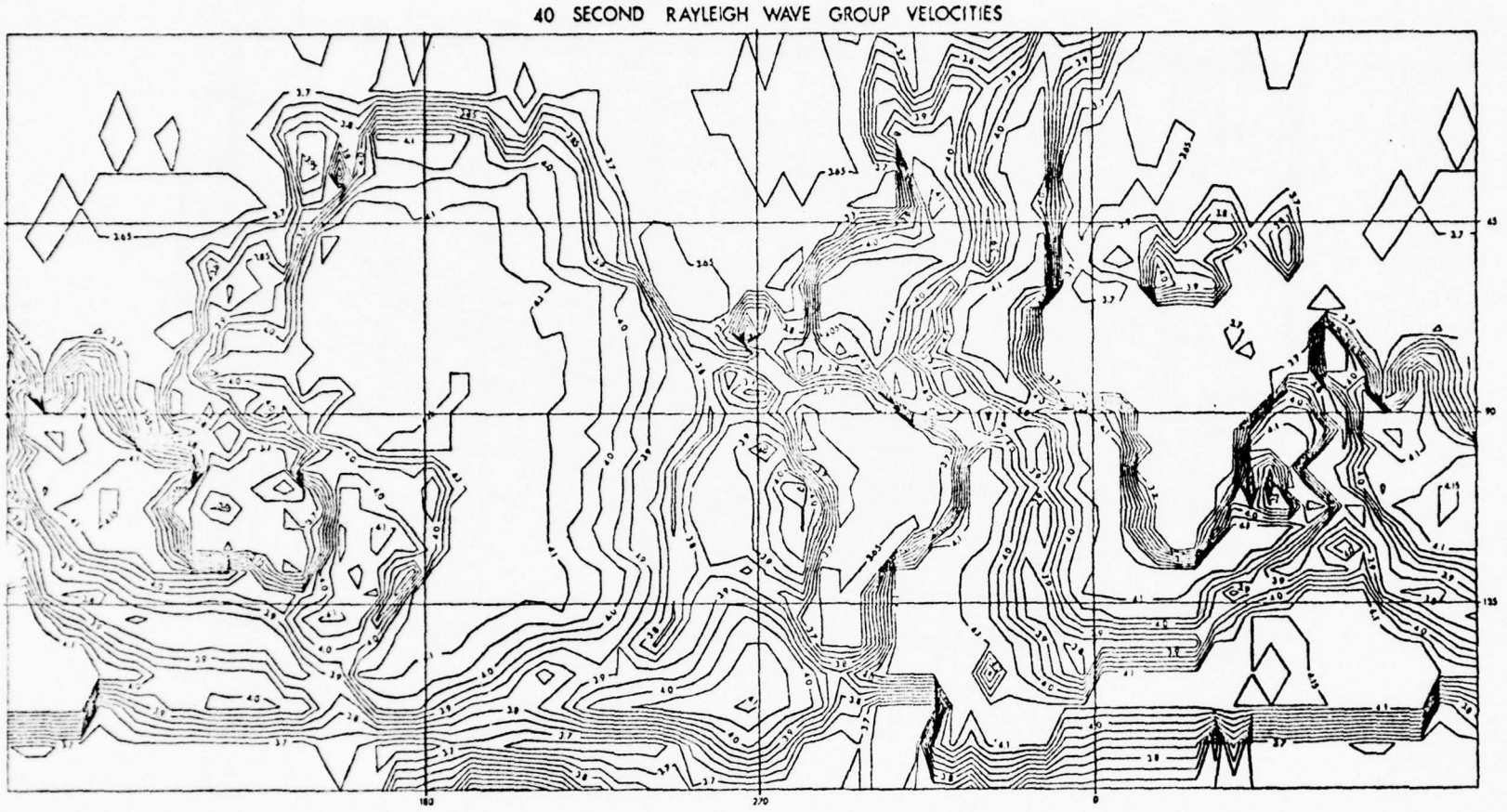


Figure 3.

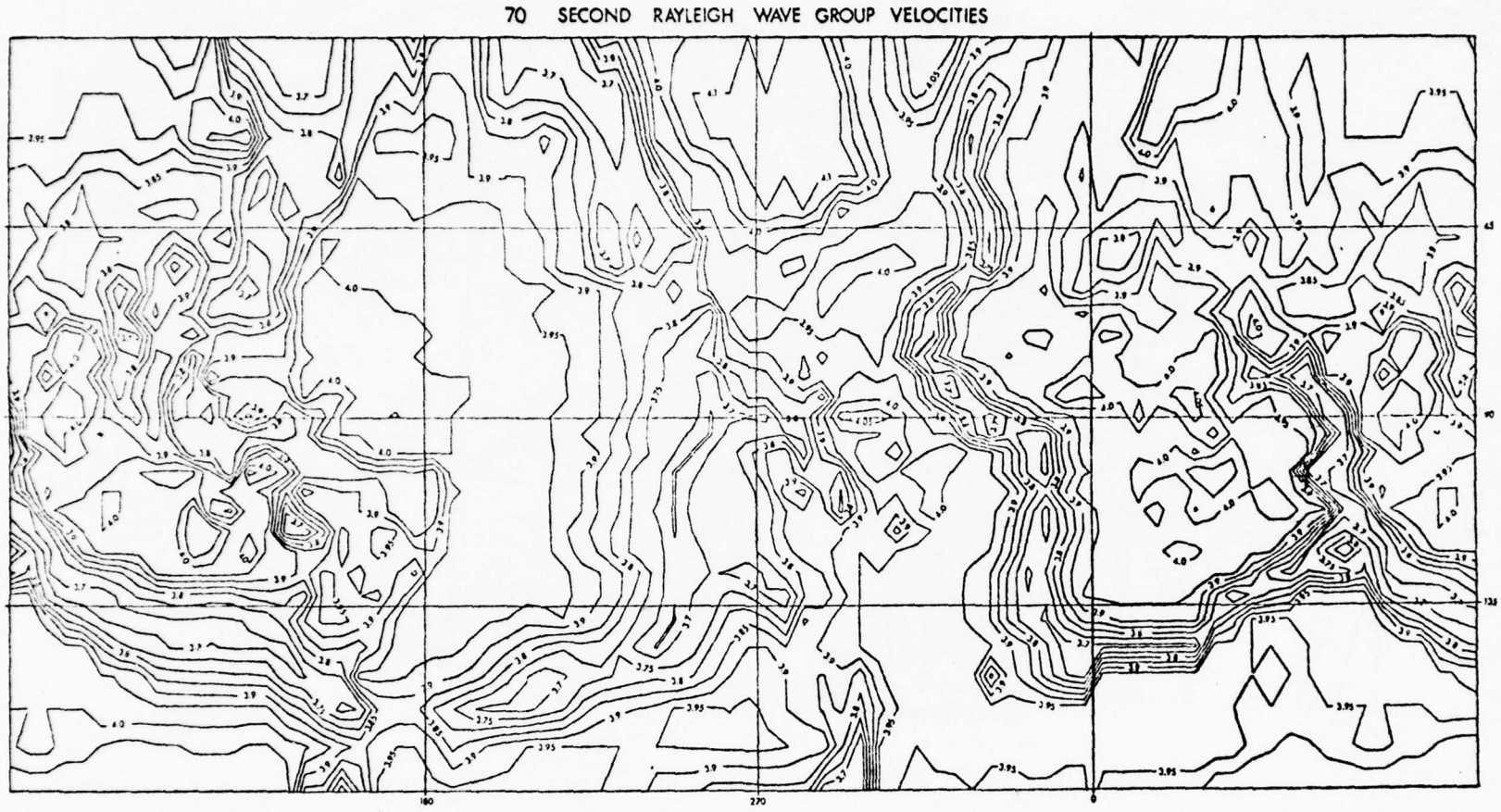
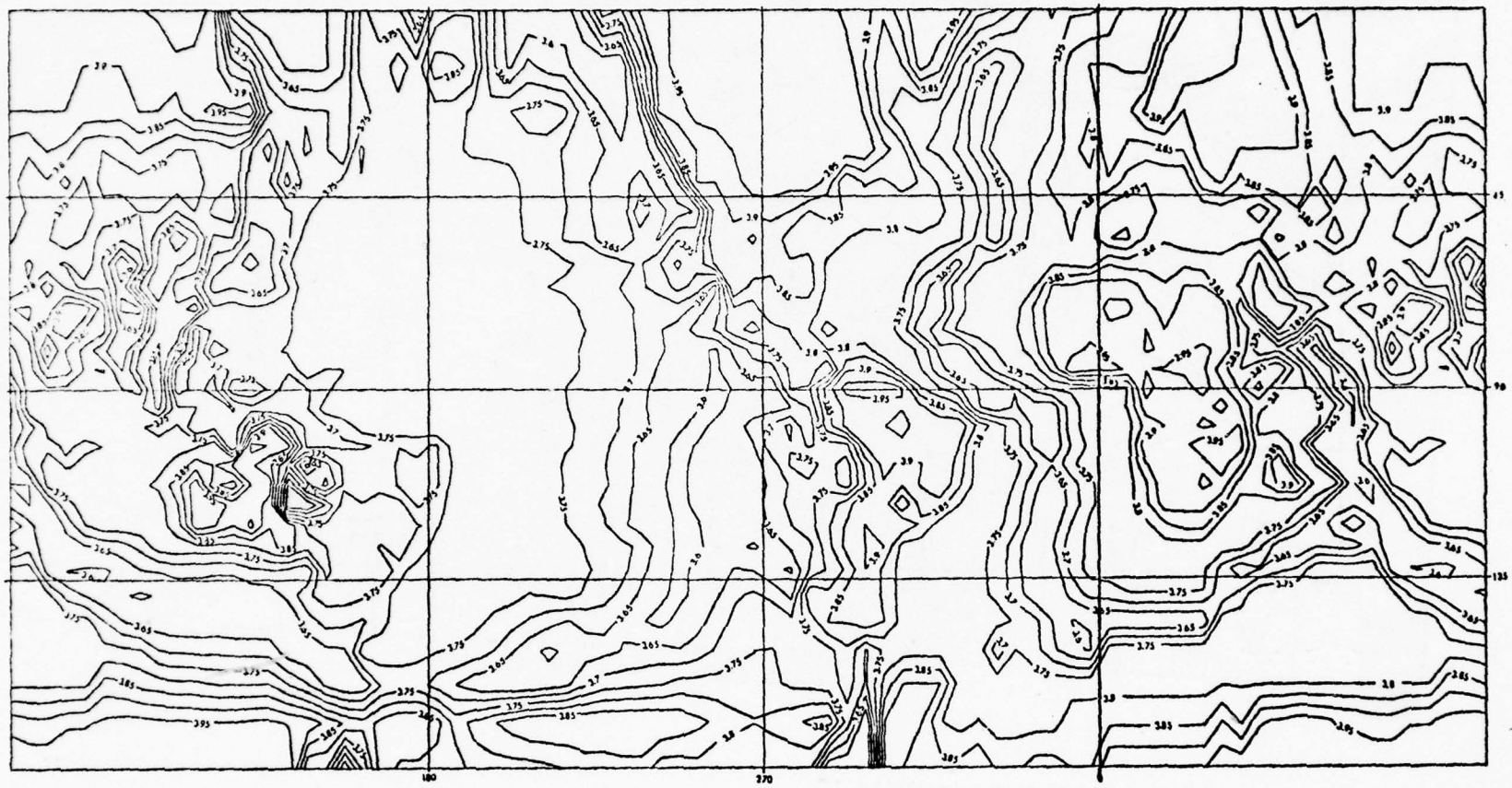


Figure 4.

100 SECOND RAYLEIGH WAVE GROUP VELOCITIES



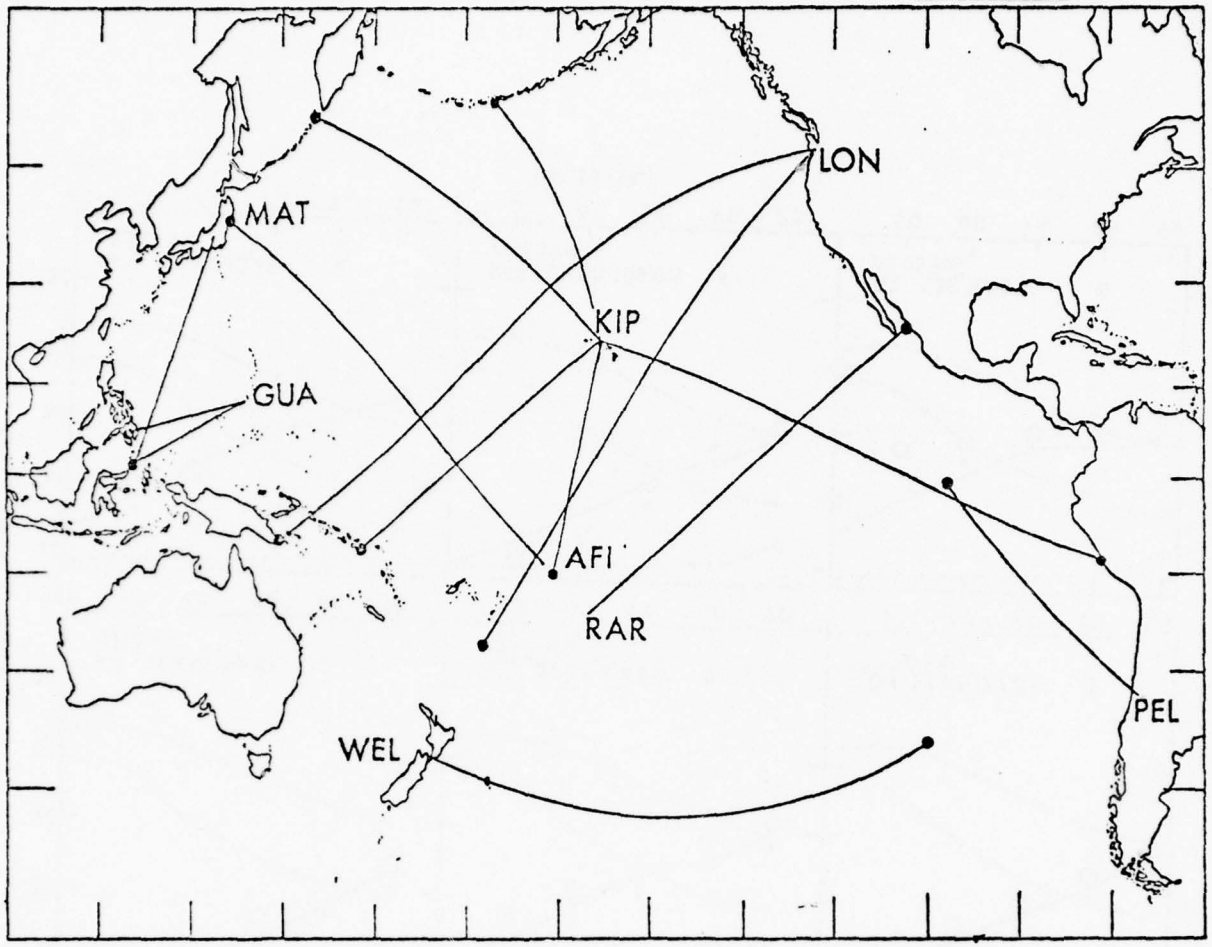


Figure 6.

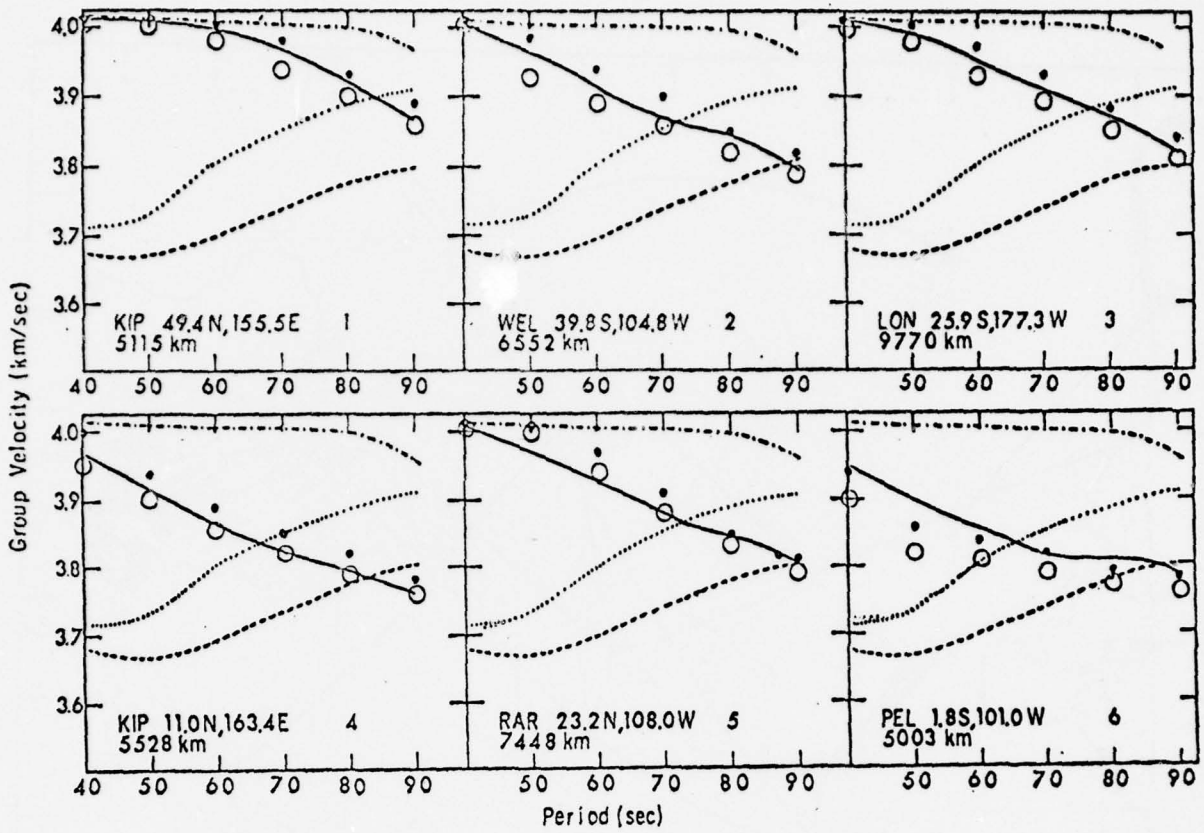

Group Velocity (km/sec)
4.0
3.9
3.8
3.7
3.6
KIP 49.4N,155.5E 1
5115 km
WEL 39.8S,104.8W 2
6552 km
LON 25.9S,177.3W 3
9770 km
KIP 11.0N,163.4E 4
5528 km
RAR 23.2N,108.0W 5
7448 km
PEL 1.8S,101.0W 6
5003 km
40 50 60 70 80 90
Period (sec)

Figure 7.

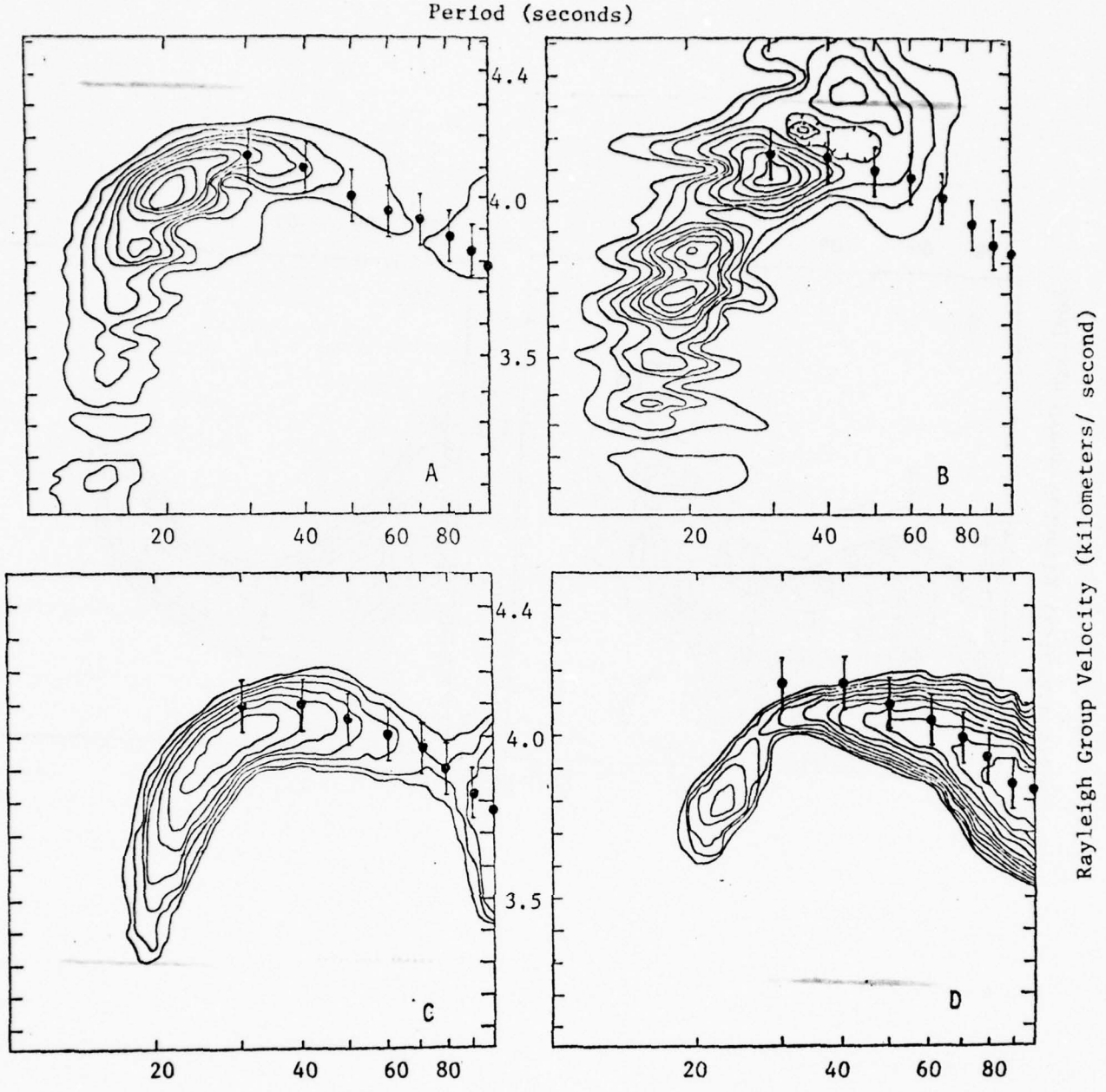
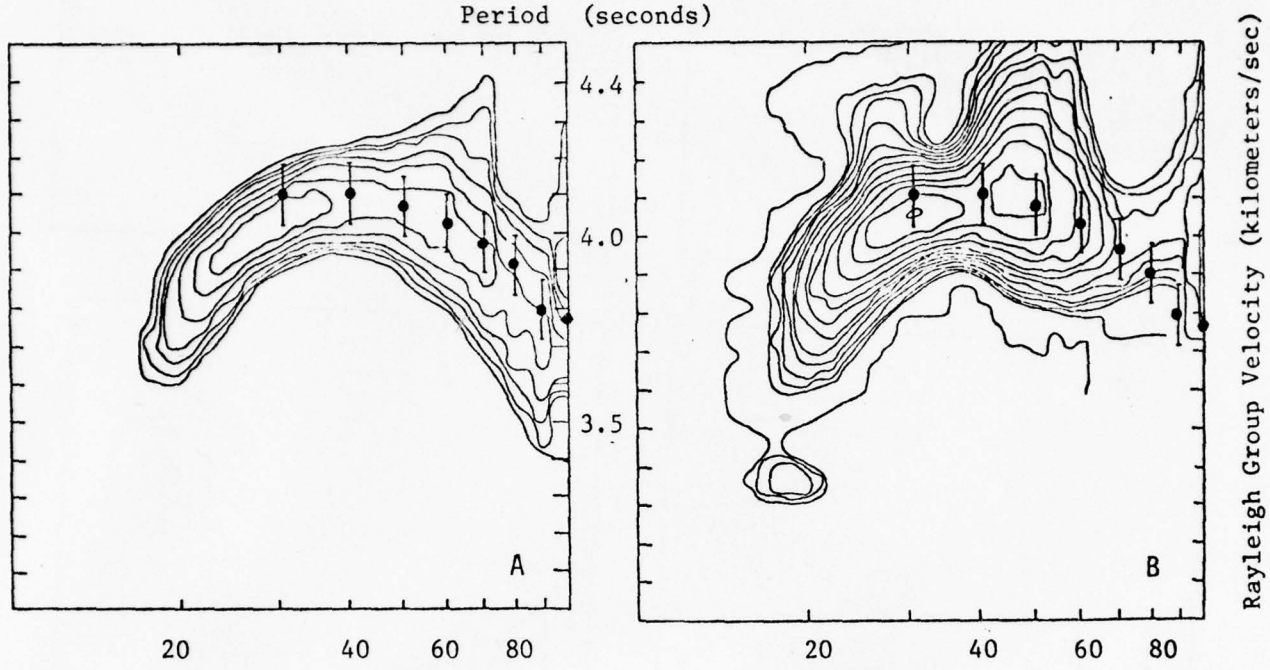
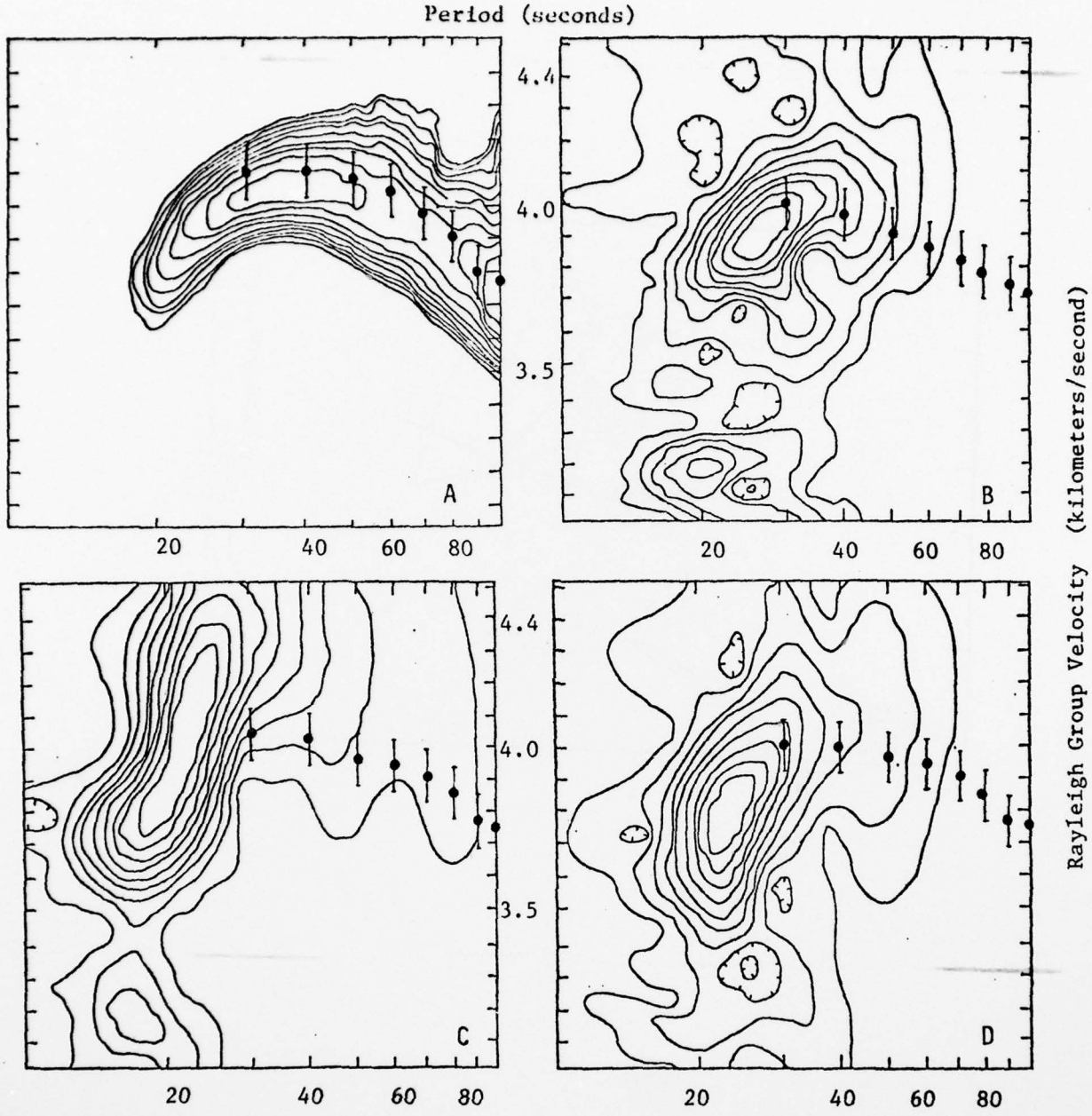
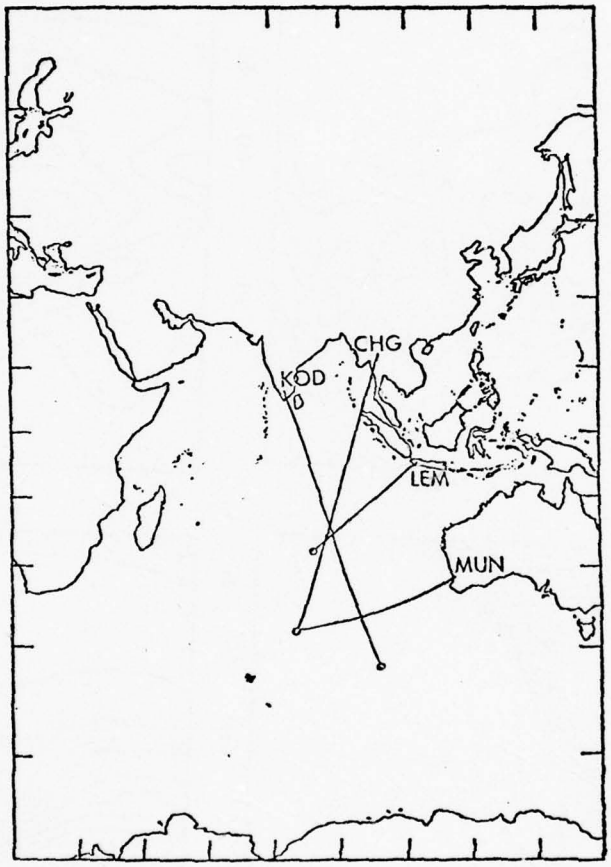

Period (seconds)
4.4
4.0
3.5
A
B
C
D
20
40
60
80
Rayleigh Group Velocity (kilometers/ second)

Figure 8.


Period (seconds)
4.4
4.0
3.5
A
B
20
40
60
80
20
40
60
80
Rayleigh Group Velocity (kilometers/sec)


Period (seconds)
4.4
4.0
3.5
A
B
C
D
20
40
60
80
Rayleigh Group Velocity (kilometers/second)


CHG
KOD
LEM
MUN

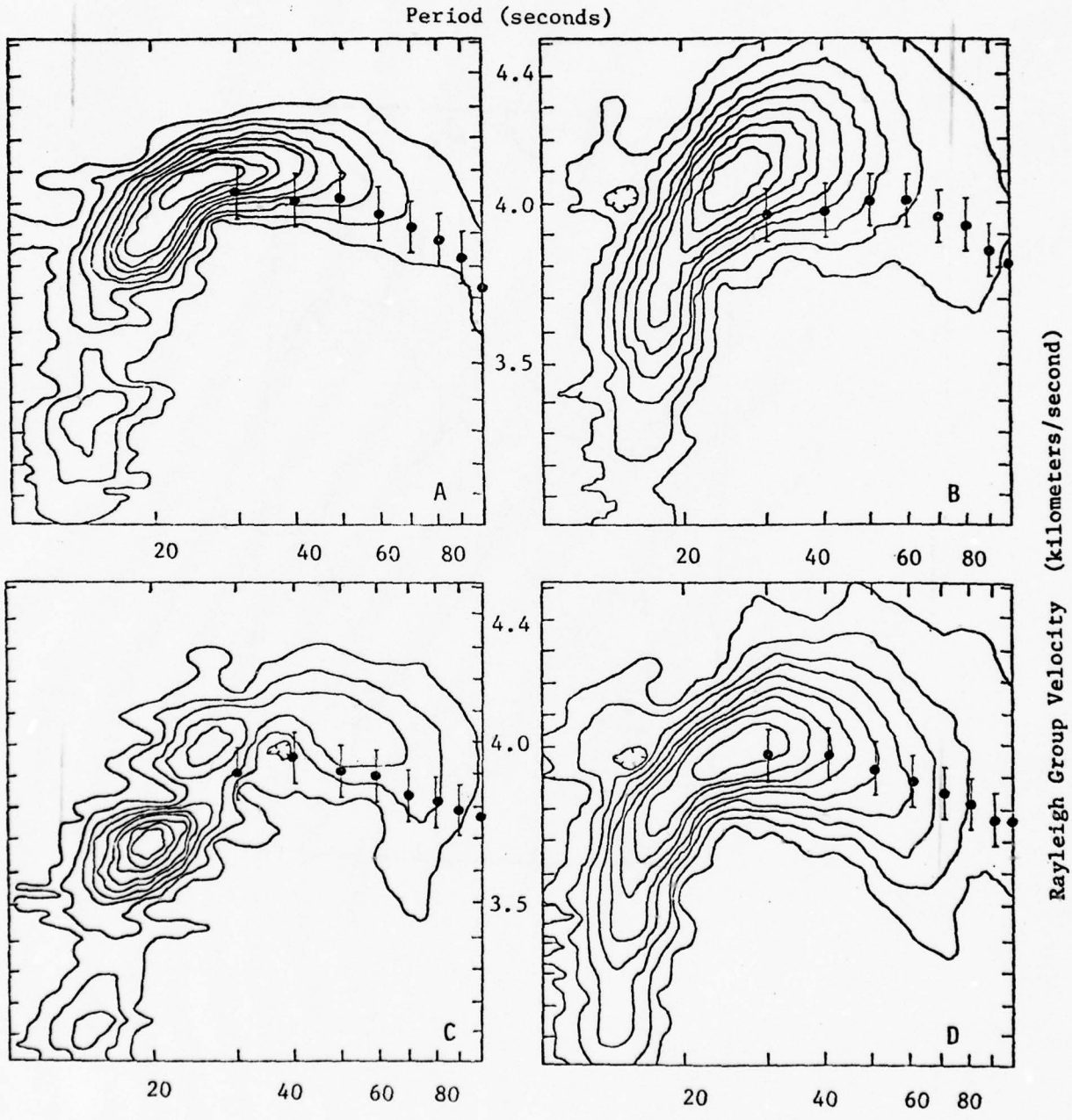

Period (seconds)
4.4
4.0
3.5
A
B
C
D
20
40
60
80
Rayleigh Group Velocity (kilometers/second)

Figure 12.

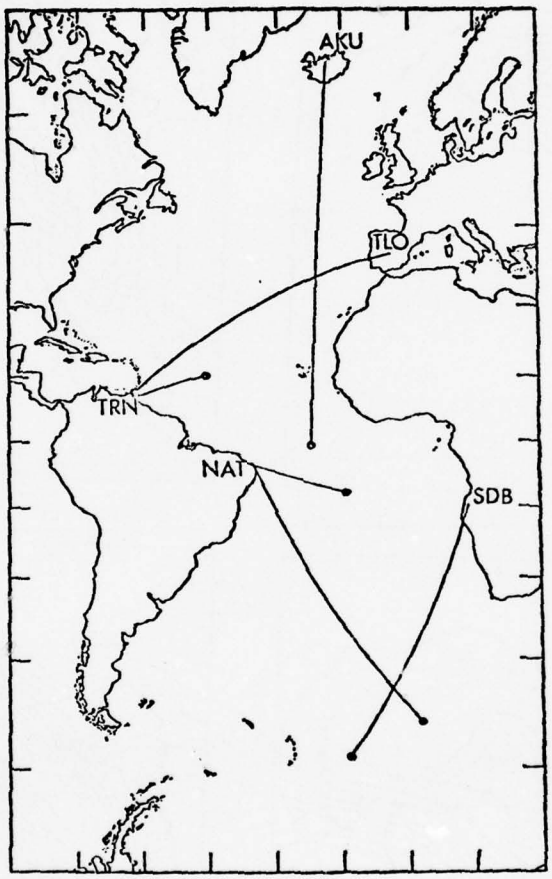


Figure 13.

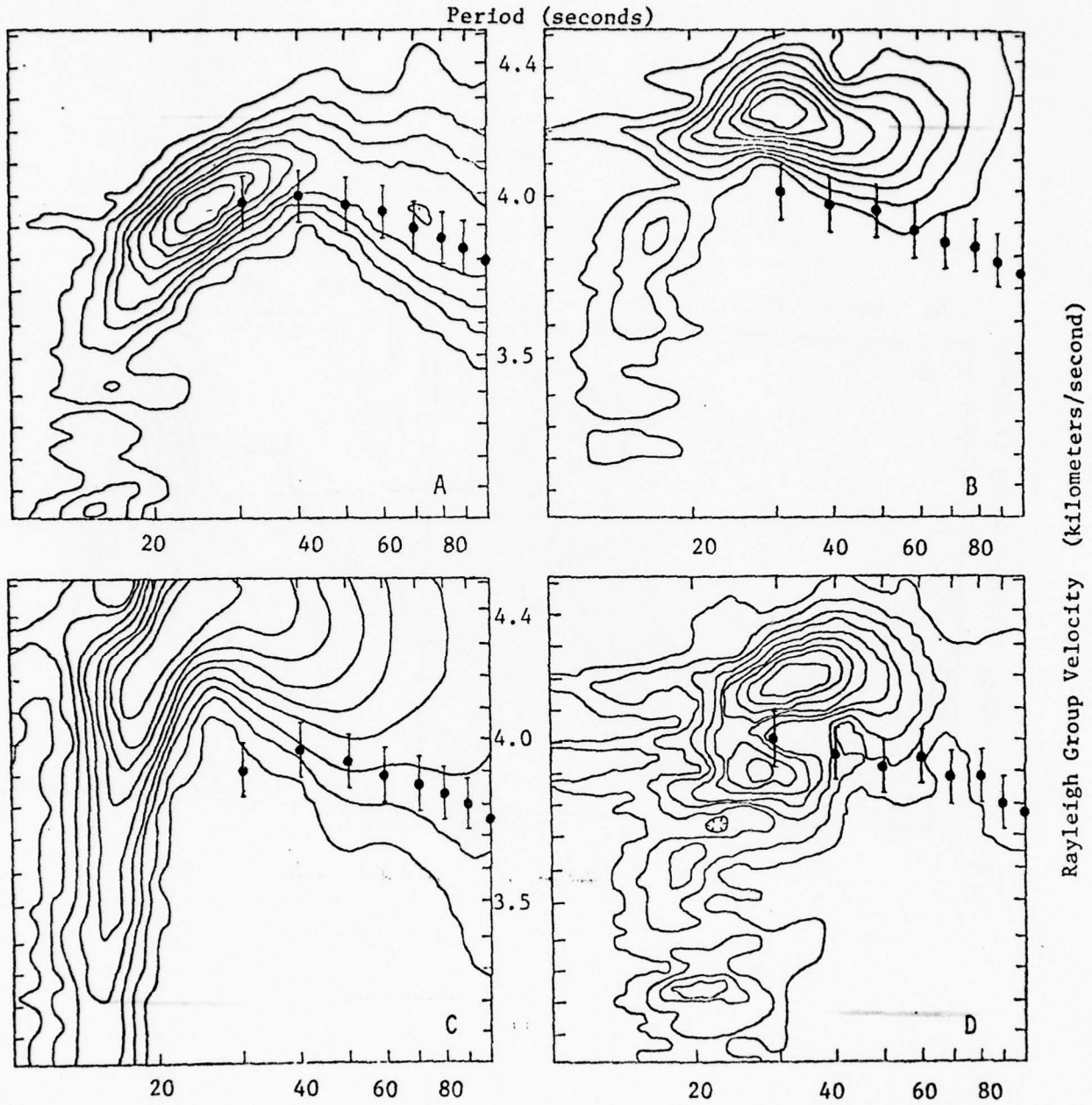

Period (seconds)
4.4
4.0
3.5
A
B
C
D
20
40
60
80
Rayleigh Group Velocity (kilometers/second)

Figure 14.

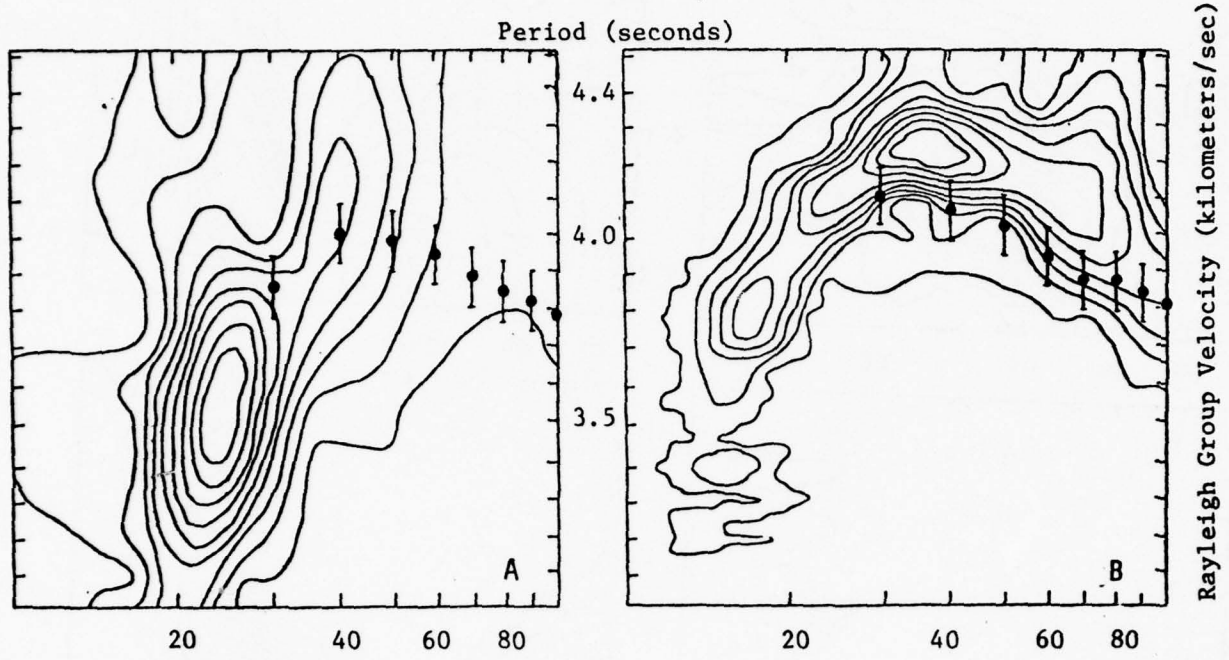

Period (seconds)
4.4
4.0
3.5
A
B
20
40
60
80
20
40
60
80
Rayleigh Group Velocity (kilometers/sec)

Figure 15.

APPENDIX III

(1) Pa and Sa Phases Revisited by Frederick J. Mauk submitted for the 47th Annual Meeting of the Eastern Section of the Seismological Society of America

"Examination of four months of seismograms from the White Pine HGLP observatory has revealed the occurrence of vertical mode Pa and Sa phases for an azimuthally restricted population of teleseismic events. These earthquakes range in distance from 30 to 106 degrees and in depth from 30 to 60 kilometers. The predominant periods are 15 and 25-30 seconds for Pa and Sa, respectively. The apparent velocities of both Pa and Sa show strong dependence on the type of lithosphere through which the waves pass. Pa ranges from 8.05 km/sec to 8.28 km/sec and Sa from 4.38 km/sec to 4.54 km/sec. The predominant north-south azimuths to the events yielding Pa and Sa display a remarkable correlation with regions of thick lithosphere proposed by Chapman and Pollack (1975). This suggests that the "whisper gallery" effect of Press and Ewing (1955) rather than the low velocity zone wave guide of Caloi (1953) is the propagation mechanism."

CHARACTERISTICS OF HGLP BODY WAVE SPECTRA

B. Radovich Williams (Dept. of Geology and Mineralogy, Univ. of Michigan, Ann Arbor, Michigan 48109)

Body wave FFT and Maximum Entropy spectra recorded on the 11 station HGLP network for several large events ($m_b > 6.0$) in 1974 have been determined. This is part of a study to relate the regionally controlled M_s-m_b value to corner frequency, and to rise time estimated from seismic moment (Kanamori, 1972). The FFT spectra for P and SH, corrected for instrument response, are consistent with theories that predict a low frequency rise and flattening of spectra. The PP phase spectra are very similar to P implying little path distortions at these long periods, and suggests PP can be used for source parameter studies at $\Delta > 100°$. The position of the corner frequency with the HGLP, FFT spectra is no more accurate than with the WWSSN estimates due to poor resolution at long periods inherent in the FFT method. The Maximum Entropy spectra are also calculated for this data set and show a smoother low frequency rise than the FFT data, but do not enhance the flattening. This suggests that long period noise may be covering the position of the corner frequency and pass band filters are being designed to suppress this effect.

1. 032499WILLIAMS
2.1976 Spring Annual Meeting
3.Seismology
4.No
5. No
6. none previously presented
7. Bill to keyline address
8.

SEISMIC MOMENTS FROM BRUNE'S AR METHOD AND DETERMINATIONS FOR INTER-INTRAPLATE EVENTS

Barbara R. Williams (Department of Geology and Mineralogy, University of Michigan, Ann Arbor, MI 48109)

Seismic moments of 20 shallow earthquakes in 1974-1975 with $5.0<M_S<8.0$ have been calculated using a modified Brune's AR parameter method. Several major events in this data set are of an intraplate nature, i.e. not on well defined plate boundaries, including the Leeward Is. 1974 event with new $M_O = 2.2 \times 10^{26}$ dyne-cm, the Utah-Idaho 1975 event with $M_O = 8 \times 10^{24}$, and the Tadzhik-Sinkiang 1974 event with $M_O = 1.7 \times 10^{26}$. On an M_O vs M_S diagram, these data tend to show higher apparent stresses ($n\bar{\sigma} \geq 100$ bars) for the intraplate events, as Kanamori and Anderson (1975) have found in their data. The Brune's AR method has been calibrated using 12 events with independent M_O estimates that have been recorded on WWSSN long period stations over predominantly oceanic paths. A total of 15 stations in Pacific, Atlantic, and Indian Oceans, at epicentral distances up to 17000 km are used - at least two stations per event. An epicentral distance correction based on a more detailed Q structure than Brune's, as well as an added correction for instrument response must be applied to give a nearly linear M_O vs AR relation. Aftershocks are the largest source of error and give moment estimates with a factor of 2 error for events with moment $\leq 10^{27}$ dyne-cm and a factor of 3 error with moment determinations $> 10^{27}$ dyne-cm.

1. 032499WILLIAMS
2. Eastern Section of SSA, 1976
3. Seismology
4. No
5. No
6. 5%
7. Bill to keyline address
8.

RAYLEIGH OCEANIC GROUP VELOCITY DISPERSION: A PREDICTIVE MODEL DERIVED FROM TECTONICS

Frederick J. Mauk (Department of Geology and Mineralogy, University of Michigan, Ann Arbor, MI 48109)

A functional relationship between sea floor age and group velocities of fundamental mode Rayleigh waves for periods from 30 to 100 seconds has been empirically determined. This 10% systematic increase in group velocity with increase in age is used to define a bathymetry corrected age-velocity matrix. Multiplication of this age-velocity matrix and a 5° x 5° matrix encoded with sea floor age has yielded Rayleigh group velocity contour maps at periods of 30, 40, 50, 60, 70, 80, 90, and 100 seconds for the world's oceans. Comparison between predicted and observed group velocity dispersions using these maps yields velocity residuals consistently less than 0.02 km/sec.

1. Fred Mauk
   Dept. of Geology
   and Mineralogy
   University of Mich.
   Ann Arbor, MI 48109
2. Seismological Society
   Eastern Section Meeting
3. Surface Waves
4. No
5. No
6. 0%
7. Department of Geology
   and Mineralogy
   University of Mich.
   Ann Arbor, MI 48109
8. P.O. number requested

PREDICTION OF OCEANIC RAYLEIGH WAVE GROUP VELOCITIES: ONE HIT AND SEVERAL NEAR MISSES

Frederick J. Mauk (University of Michigan, Department of Geology and Mineralogy, Ann Arbor, Michigan 48109)

A fundamental mode oceanic Rayleigh wave group velocity predictor based on sea floor age has been described by Mauk (EOS, vol 50, no. 10, 1976). Application of this empirical model to random paths across the Pacific basins yield group velocity residuals for periods from 30 to 100 seconds which are consistently less than 0.02 km/sec. Similar random path tests of the Pacific-derived model have been conducted for the North Atlantic, South Atlantic and Indian Oceans. Observed group velocities for these three ocean basins were consistently faster, frequently greater than 0.20 km/sec, than predicted by the model. The largest residuals occurred in the North Atlantic Ocean, the smallest in the Indian Ocean. This suggests that models of Rayleigh group velocities based solely on sea floor age are incomplete. The additional requisite model correction to predict accurately the group velocities for all ocean basins appears to be embodied in the spreading rates. Since the functional relationship between group velocities and sea floor age appears to be related to the thermal evolution of the oceanic lithosphere, the observed velocity variations among these ocean basins suggests that the mantle heat flow into the base of the lithosphere is non-uniform.

027797MAUK

1977 Spring Meeting

Seismology

None

No

No

5% at Midwest Meeting

Bill to:
Department of Geology and Mineralogy, Univ. of Mich., Ann Arbor, Michigan 48109

(1) Pa and Sa Phases Revisited by Frederick J. Mauk submitted for the 47th Annual Meeting of the Eastern Section of the Seismological Society of America

> "Examination of four months of seismograms from the White Pine HGLP observatory has revealed the occurrence of vertical mode Pa and Sa phases for an azimuthally restricted population of teleseismic events. These earthquakes range in distance from 30 to 106 degrees and in depth from 30 to 60 kilometers. The predominant periods are 15 and 25-30 seconds for Pa and Sa, respectively. The apparent velocities of both Pa and Sa show strong dependence on the type of lithosphere through which the waves pass. Pa ranges from 8.05 km/sec to 8.28 km/sec and Sa from 4.38 km/sec to 4.54 km/sec. The predominant north-south azimuths to the events yielding Pa and Sa display a remarkable correlation with regions of thick lithosphere proposed by Chapman and Pollack (1975). This suggests that the "whisper gallery" effect of Press and Ewing (1955) rather than the low velocity zone wave guide of Caloi (1953) is the propagation mechanism."

(2) A Finite Element Model of Recent Turkey Plate Movements by Barbara Radovich Williams presented at the AGU meeting in Washington, D.C., June, 1975 and submitted for publication to the Journal of Geophysical Research.

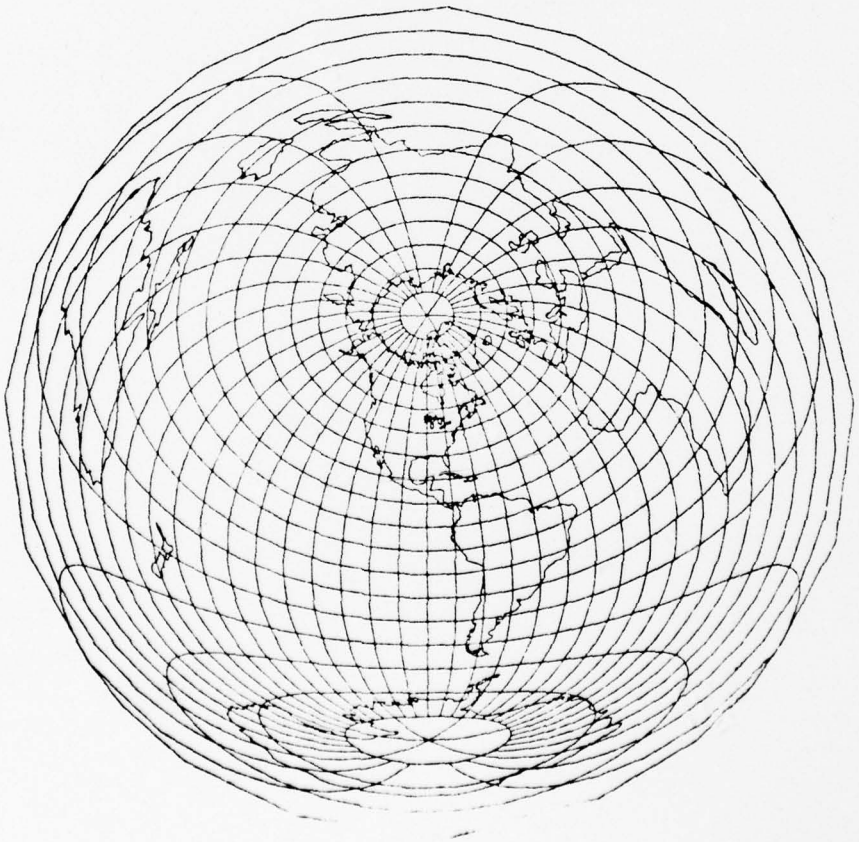
> "Plate tectonics in the eastern Mediterranean shows the African and Arabian plates moving northward with respect to Eurasia and the Turkish and Aegean microplates moving rapidly in a direction perpendicular to these major plate motions in a westerly direction. Construction of a finite element model of the plates in this region, with the microplates loaded only on their edges, verifies McKenzie's hypothesis that the Arabian and African plates colliding with Eurasia are wedging the Turkish microplate westward. The motions of the microplates in the model are very sensitive to the boundary conditions, and the Turkish part of the model moves westward only when the Turkey and Arabian plates are uncoupled from Eurasia. An easterly movement of the microplates occurs when the boundaries of the model are coupled to Eurasia. The smaller microplate areas of the model seem to act more like the ideal of a rigid plate than the larger major plate areas. The Border zone activity, on the south border of the Turkish microplate, is predicted to be inversely proportional to the activity on the Anatolian Fault. In general the fit to the observed plate motions for the Turkish microplate are good but the model shows that the Aegean part of the model may fit the observed seismic zones without really moving to the southwest, but rotating counterclockwise."

APPENDIX IV

THE UNIVERSITY OF MICHIGAN

Catalog of Events
for
The White Pine High Gain Long Period Seismograph Station
1 July 1974 through 30 April 1975

Compiled by
Frederick J. Mauk
and
Steven G. Henry



Preface

The following pages contain a listing of seismic events recorded at the White Pine High Gain Long Period Observatory for the period July 1974 through April 1975. During this period the observatory was in a state of instrumental flux both in amplifier type and recording mode. To appear in the listing, all events had to exceed a recorded signal to noise ratio of 2:1 in Rayleigh wave signature. Only vertical seismograms are available for this time period. The exact arrival times of body phases for these events have not been included to encourage other interpreters to examine the seismograms more thoroughly. All of these early grams may be obtained for study by writing to the Seismological Observatory, Department of Geology and Mineralogy, University of Michigan, Ann Arbor, Michigan 48104 or calling (313) 763-8069.

A brief description of the station is included in this catalog, but data users are encouraged to read the semi-annual Technical Reports "Installation and Operation of a High Gain Long Period Seismograph Station" ARPA Order No. 1827, Contract No. F44620-73-C-0060 for details regarding alteration of the system.

Station Description

Seismic Station WPM is comprised of a three component high gain (100 K) long period (T_o = 30 sec) seismic system. The station is divided into a subsurface instrument vault and a surface recording facility which are linked via a hard wire telemetry system.

The seismometers have been installed 89 meters below the surface in a vault provided in section 31-A of the White Pine Copper Company mine, White Pine, Michigan (see locator map on page 4). They are sitting in specially constructed pressure-temperature sealed tanks on the uppermost horizon of the Copper Harbor Formation at an elevation of 193.5 meters (see geologic column on page 5). All signals from the seismometers are electronically amplified and FM multiplexed to assigned carrier frequencies to transmit them to the surface recording site. Remote boom repositioning and calibration of the instruments is accomplished from a subsurface control panel located in vault 1 (see subsurface station schematic and floor plan on page 6). All recording of the seismic signals is done at the surface installation.

Tests of the subsurface station site environmental stability have shown: (1) it is located in a portion of the mine exhibiting low cavity convergence (< 0.002 inches/year); (2) it is located in an area having little microseismic activity but exhibiting substantial 4 hertz background noise during active mining periods; (3) it is not microbarometrically stable and exhibits a seasonal fluctuation in humidity ranging from 99% in the summer to 65% in the winter; (4) it is thermally stable to $\pm$ 1°F at 55°F but does exhibit a seasonal decrease of 5°F during winter months.

The surface recording facility is located in the north end of the Bechtel Building of the White Pine Copper Company. Signals received from the subsurface are demultiplexed and separated and

then recorded in both analog and digital form. Analog signals are recorded directly on helicorders. Simultaneously, velocity and displacement analog information is transformed to a digital format and recorded on magnetic tape with the Astrodata data logger system. All digital tapes must be processed by the Albuquerque Seismological Center before they are computer compatible.

Helicorder records are changed daily; magnetic tape, bimonthly. All processing of the data is done at the University of Michigan Seismological Observatory.

Station Facilities

Location
White Pine Copper Company
White Pine, Michigan 49971

Station Abbreviation
WPM

Station Director
Dr. James T. Wilson

Station Address
c/o Fred Mauk
Seismological Observatory
Department of Geology and Mineralogy
C.C. Little Building
University of Michigan
Ann Arbor, Michigan 48104

Telephone
Mine (906)885-5111, ext. 321
UofM (313)763-4069

Geographic Coordinates
45°45'05.5" North latitude
89°33'17.75" West longitude

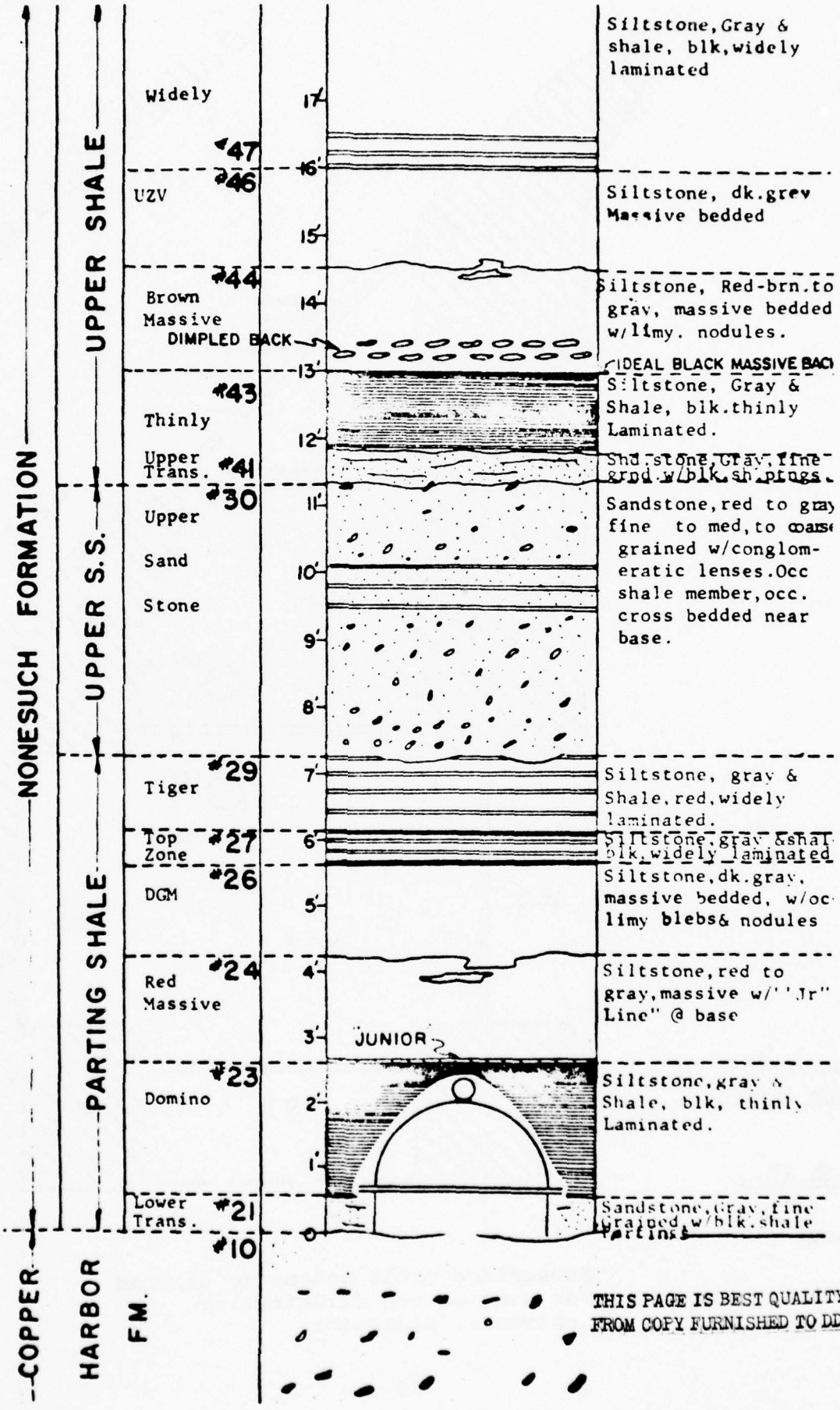
Station Elevation
193.5 meters

Depth of Sensors
89 meters

History of Station
The White Pine high gain long period seismograph station was established in the White Pine Copper Company mine during 1973 and 1974 with funds provided by the Advanced Research Projects Agency under Contract No. F44620-73-C-0060. First installed as an experimental station in 1973, WPM became the eleventh HGLP observatory in 1974. For further installation information, refer to ARPA Technical Reports Contract No. F44620-73-C-0060.

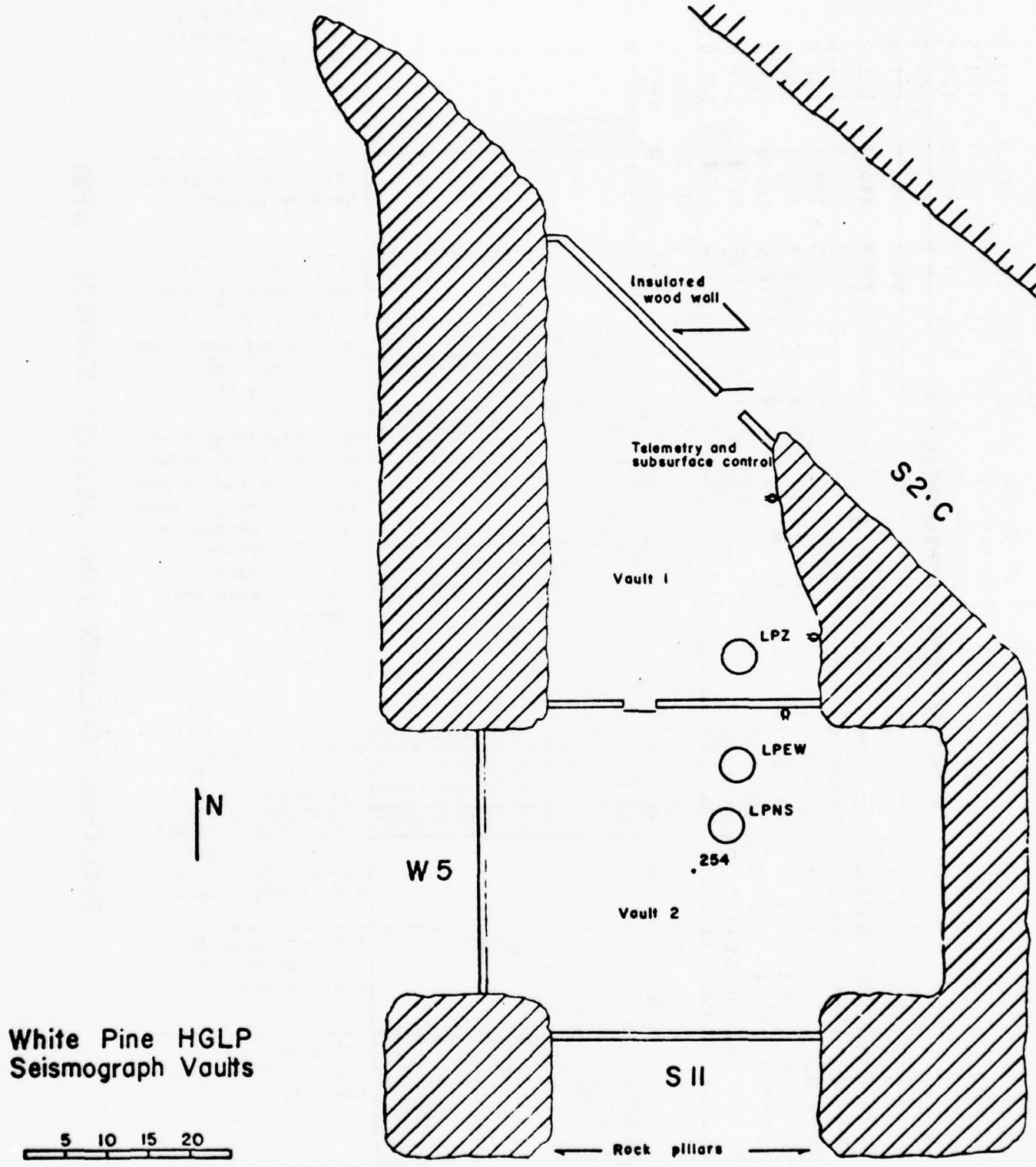


Locator Map



- GEOLOGIC COLUMN FOR SEISMIC STATION WPM -

THIS PAGE IS BEST QUALITY PRACTICABLE
FROM COPY FURNISHED TO DDC



Subsurface vault schematic diagram for station WPM illustrating instrument placement

All events for the period July 1974 through November 1975 were recorded with a Geotech 7505A long period seismometer (To=30 seconds). The signal was amplified using a Geotech AS-650 solid state long period amplifier and multiplexed for telemetry purposes. The signal was demultiplexed using a Geotech XD-410 discriminator and recorded at two gain levels on Esterline Angus S-601-S Strip Chart recorders. The gains are split by one order of magnitude 8k and 88k. The timing system is a Springnether TS-100. All events from December 1974 through April 1975 were recorded on a Geotech RV-301-B rectilinear helicorder at a gain of 5k. The timing system is a Geotech TG-120. For further information refer to Technical Reports ARPA Order NO. 1827 contract No. F4462D-73-C-0060.

EVENTS RECORDED AT THE HGLP SEISMIC STATION WPM

MONTH: July 1974

Day	PDE #	Origin Time (UCT) Hr Mn Sec	Geographic Coordinates Latitude	Longitude	Region and Comments	Depth Km	Mb	Ms	Δ°	Az	Baz	Box #
01	48	07 28 31.2	75.7N	6.8E	Greenland Sea	N	4.6	5.0	46.8	290.6	19.8	2
01	49	16 51 51.5	22.1S	64.7W	Salta Province Argentina	13	5.5	5.9	72.2	342.2	155.6	1
01	46	23 11 14.5	22.6S	10.7W	South Atlantic Ridge	N	5.6	5.6	99.0	316.9	113.3	2
02	49	07 15 46.1	54.1S	140.2E	West of Macquarie	N	5.4	5.4	147.9	82.4	238.1	2
02	46	16 41 05.8	42.2N	75.6E	Alma-Ata Region	N	5.0		90.5	349.9	10.8	2
02	50	19 34 10.4	16.0S	75.1W	Off Coast of Peru	N	4.8	4.8	63.8	348.8	164.3	2
02	50	23 26 26.6	29.1S	176.0W	Kermadec Island Region	N	6.8	7.2	108.2	46.2	246.8	2
03	50	23 25 09.3	29.1S	176.1W	Kermadec Island Region	N	6.2	6.6	108.2	46.3	246.8	1
04	50	19 30 42.1	45.1N	94.0E	Mongolia	N	6.1	6.7	88.5	2.6	357.3	1
04	48	22 01 54.6	59.8S	150.7W	South Pacific Cordillera	N	5.3		117.2	42.5	209.8	1
05	47	04 58 55.4	44.8S	80.0W	Off Coast of Southern Chile	N	5.2	5.1	91.6	353.3	173.1	2
05	50	18 04 14.9	29.2S	176.2W	Kermadec Island Region	N	5.4	5.3	108.4	46.3	246.8	1
05	48	20 09 34.6	14.8N	81.7W	Caribbean Sea	23	5.2		32.6	349.7	165.4	1
07	50	07 43 27.0	18.9N	46.1W	North Atlantic Ridge	N	4.4		45.2	318.0	112.9	1
08	51	05 45 37.0	36.4N	141.1E	Near East Coast Honshu	35	6.0	6.0	85.5	32.3	321.1	3
09	49	02 32 17.6	36.7N	28.4E	Dodecanese Is. Turkey	69	5.0		80.1	322.0	46.0	3
09	48	06 18 31.4	6.6S	155.1E	Solomon Islands	48	4.6		111.9	42.1	284.2	3
10	48	16 00 00.1A	37.068N	116.032W	Southern Nevada	0	5.7		21.7	55.3	253.0	3
11	47	05 34 22.1	13.1N	145.4E	Mariana Islands	53	5.3		102.6	35.4	304.9	3
11	52	17 56 18.5	71.6N	4.1 W	Jan Mayen Island Region	N	5.0		45.2	284.8	26.5	3
13	55	01 18 22.8	7.7N	77.7W	Panama-Colombia Border	12	6.4	7.3	40.3	347.2	161.3	4
13	61	02 02 21.7	7.8N	77.5W	Panama-Colombia Border	N	4.8		40.2	346.9	161.0	4
13	55	02 12 39.6	7.6N	77.7W	Panama-Colombia Border	N	5.0		40.3	347.0	161.2	4
13	59	03 45 18.2	7.7N	77.8W	Panama-Colombia Border	38	4.7		40.2	347.3	161.5	4
13	57	10 38 06.8	7.7N	77.6W	Panama-Colombia Border	12	4.9		40.3	347.2	161.3	4
13	55	11 44 05.9	8.0N	77.5W	Panama-Colombia Border	39	4.8		40.0	347.1	161.2	4
13	55	13 00 53.3	7.5N	77.6W	Panama-Colombia Border	N	4.9	4.6	40.4	347.2	161.2	4
13	55	17 48 53.9	8.0N	77.5W	Panama-Colombia Border	20	4.8		40.0	347.1	161.2	4
13	55	23 08 41.9	7.1N	77.7W	Panama-Colombia Border	23	5.3	4.3	40.8	347.5	161.8	3

Az and Baz measured CW from North

EVENTS RECORDED AT THE HGLP SEISMIC STATION WPM

MONTH: July 1974

Day	PDE #	Origin Time (UCT) Hr Mn Sec	Geographic Coordinates Latitude	Longitude	Region and Comments	Depth Km	Mb	Ms	Δ°	Az	Baz	Box #
13	56	23 40 40.2	7.5N	77.8W	Panama-Colombia Border	59	4.4		40.4	347.5	161.8	3
14	56	00 34 42.4	7.5N	77.3W	Panama-Colombia Border	58	4.6		40.5	347.0	161.1	3
14	55	01 48 43.6	7.8N	77.6W	Panama-Colombia Border	26	5.2	4.5	40.1	347.2	161.4	3
14	55	02 13 50.4	7.7N	77.6W	Panama-Colombia Border	15	5.9	5.0	40.2	347.1	161.5	3
14	52	09 37 36.8	8.7S	122.6E	Flores Island Region	123	5.8		133.1	30.3	313.6	3
14	50	18 48 42.9	28.3S	178.1W	Kermadec Islands Region	183	5.3		109.0	46.6	248.7	3
15	53	01 24 03.2	36.4N	71.6E	Afganistan-USSR Border	117	4.4		95.5	347.2	15.0	6
15	51	03 38 14.2	3.2S	139.4E	West New Guinea	59	5.2		119.3	36.6	300.0	6
15	55	19 11 51.7	7.9N	77.5W	Panama-Colombia Border	7	4.8		40.1	346.9	160.9	6
15	55	23 11 27.8	7.5N	77.6W	Panama-Colombia Border	N	5.3	4.4	40.4	347.3	161.5	6
16	53	02 46 06.1	7.7N	77.4W	Panama-Colombia Border	N	4.6		40.3	347.1	161.2	5
16	48	04 30 21.5	28.9N	113.1W	Baja California	N	4.6		25.5	39.3	233.8	3
16	55	06 38 45.8	45.8N	111.4W	Montana	N	4.4		15.0	78.6	274.2	3
16	52	16 01 16.6	37.3N	32.7W	Azores Islands Region	N	4.7	4.4	42.6	301.5	81.5	6
17	53	02 44 24.1	54.2N	161.1E	East Coast Kamchatka	N	4.7	4.3	62.9	46.8	321.4	6
18	53	11 04 43.2	15.2S	173.6W	Tonga Islands	N	5.9	5.8	96.8	43.5	255.2	5
18	55	18 29 50.7	45.8S	76.3W	Off Coast of S.Chile	N	5.1	5.4	92.9	350.8	170.6	5
18	51	19 21 24.6	17.1N	98.4W	Guerrero Mexico	48	5.6	5.2	30.4	11.8	196.5	5
18	54	22 59 01.6	31.3S	177.7W	Kermadec Island Region	N	5.0	5.2	110.7	47.3	246.2	5
19	48	02 02 51.3	32.8S	71.7W	Near Coast of Cen.Chile	44	5.2	4.5	80.8	347.5	164.7	5
19	51	17 45 43.9	6.1S	154.9E	Solomon Islands	N	5.3	4.8	111.7	42.0	248.7	5
19	53	18 44 53.4	42.2N	142.6E	Hokkaido Japan	38	4.8		80.0	33.6	323.3	5
19	54	20 40 29.6	14.3N	92.3W	Near Coast Chiapas, Mex.	59	4.5		32.4	3.3	184.6	5
19	54	23 44 38.2	29.8S	175.8W	Kermadec Islands Region	44	5.1	4.8	108.5	46.3	246.1	5
20	55	12 57 02.0	8.1N	77.5W	Panama-Colombia Border	N	4.8	3.9	39.9	346.8	160.9	9
20	54	19 15 59.0	49.9N	126.5E	Vancouver Island Region	N	4.0		24.5	83.2	291.0	9
20	49	19 30 13.8	0.8S	127.4E	Halmahera	N	5.2	4.9	123.9	30.0	313.3	9
21	51	08 20 35.3	14.3N	92.1W	Near Coast Chiapas, Mex.	70	5.3		32.4	3.0	184.2	10
21	52	22 33 38.2	11.3N	86.1W	Near Coast of Nicaragua	87	5.2		35.5	355.7	173.8	7

Az and Baz measured CW from North

EVENTS RECORDED AT THE HGLP SEISMIC STATION WPM

MONTH: July 1974

Day	PDE #	Origin Time (UCT) Hr Mn Sec	Geographic Coordinates Latitude	Longitude	Region and Comments	Depth Km	Mb	Ms	Δ°	Az	Baz	Box #
22	52	16 03 30.4	12.8N	71.1W	Near N.Coast Colombia	N	4.6	4.7	37.3	338.7	149.0	7
23	49	00 28 13.3	20.7S	174.3W	Tonga Islands	N	5.0	5.0	101.2	44.2	251.8	7
23	50	06 45 12.6	16.6S	173.6W	Tonga Islands	46	5.5	4.3	97.8	43.6	254.2	7
23	51	10 58 47.5	19.5S	169.3E	New Hebrides Islands	162	5.6		111.3	46.5	263.9	7
23	52	15 28 34.8	19.5N	104.3W	Near Coast Jalisco, Mex.	109	4.9		29.7	20.4	208.6	7
24	53	08 27 35.9	31.3S	177.8W	Kermadec Islands Reg.	N	5.4	5.8	110.8	47.3	246.2	7
24	51	20 23 01.2	13.0N	144.9E	Mariana Islands	78	5.4		103.0	35.1	305.3	6
25	52	14 29 11.1	26.7S	114.1W	Easter Islands Region	N	5.3	4.6	76.3	17.0	202.3	6
25	51	17 17 38.9	6.1S	153.1E	New Britian Region	N	5.5	5.3	112.9	41.6	286.2	6
26	49	08 59 47.8	16.3S	70.9W	Southern Peru	157	5.0		65.0	345.8	160.0	6
26	49	13 01 02.5	3.6S	128.9E	Ceram	25	5.6	5.4	125.5	31.8	310.0	6
26	52	20 37 17.8	51.1N	170.5W	Fox Islands, Aleutians	N	4.9		50.7	61.3	306.5	8
27	56	04 26 47.0	55.5N	166.4E	Komandorsky Is. Region	N	5.3	5.4	59.8	50.6	320.2	8
27	55	11 44 51.0	27.2N	111.3W	Gulf of California	N	4.3		25.9	35.4	228.5	8
27	55	21 24 39.0	37.1N	32.6W	Azores Islands Region	N	4.8		42.7	301.7	81.7	8
28	54	11 34 59.7	46.3N	153.3E	Kuril Islands	52	5.9		72.1	40.1	319.5	8
28	51	07 52 59.0	29.2S	177.7W	Kermadec Islands	63	4.8		109.3	46.7	247.8	8
28	53	16 33 55.6	46.2N	153.2E	Kuril Islands	49	4.9	5.0	72.2	40.0	319.5	8
28	53	18 00 45.4	46.4N	153.4E	Kuril Islands	46	4.9	4.6	72.0	40.2	319.5	8
28	50	20 15 08.2	31.3S	177.8W	Kermadec Island Region	14	4.9	5.1	110.8	47.3	246.2	8
29	56	07 16 26.1	46.1N	153.1E	Kuril Islands	N	5.9	6.2	72.3	39.9	319.5	9
29	59	03 15 16.7	46.2N	153.1E	Kuril Islands	38	5.7	5.8	72.3	40.0	319.5	9
29	52	14 21 16.2	46.2N	152.9E	Kuril Islands	36	4.9		72.4	39.8	319.6	8
30	51	05 12 40.6	36.4N	70.8E	Hindu Kush Region	211	6.5		95.4	346.7	15.6	9
30	53	22 39 44.5	46.2N	153.2E	Kuril Islands	42	5.0	4.7	72.2	40.0	319.5	RPT
31	56	22 31 18.2	28.4S	176.6W	Kermadec Islands	58	4.8		108.1	46.2	247.7	9

Az and Baz measured CW from North

EVENTS RECORDED AT THE HGLP SEISMIC STATION WPM

MONTH: August 1974

Day	PDE #	Origin Time (UCT) Hr Mn Sec	Geographic Coordinates Latitude	Longitude	Region and Comments	Depth Km	Mb	Ms	Δ°	Az	Baz	Box #
01	52	05 07 59.0	56.5N	152.3W	Kodiak Island Region	10	5.2	6.1	38.8	77.0	308.2	2
01	52	05 55 38.2	56.7N	152.1W	Kodiak Island Region	N	5.7	6.3	38.7	77.4	308.5	2
03	52	04 08 13.8	35.4N	80.6E	Kashmire Tibet Border	20	5.0		97.7	353.2	8.1	2
04	52	21 08 52.9	24.4S	69.8W	Northern Chile	68	5.2		73.0	345.9	161.2	3
05	53	13 19 39.5	28.0N	53.5E	Southern Iran	11	5.3		98.4	335.3	32.5	3
05	53	14 13 01.3	16.6S	167.6E	New Hebrides Islands	42	5.1		110.6	45.8	267.5	3
06	54	02 37 42.3	60.2N	153.3W	Southern Alaska	136	5.0		38.6	80.9	314.2	3
06	54	12 59 55.6	56.6N	152.5W	Kodiak Island Region	16	4.5	4.7	38.9	77.0	308.4	3
06	53	16 49 22.2	46.8N	150.4E	Kurile Islands	166	5.2		73.1	38.5	321.6	3
06	53	18 38 13.1	21.8S	175.2W	Tonga Islands	48	5.7	5.7	102.7	44.6	251.8	3
07	54	00 52 14.9	73.5N	6.9E	Greenland Sea	N	4.6		47.6	292.4	22.6	1
07	54	01 47 48.1	73.5N	6.7E	Greenland Sea	N	4.5		47.6	292.2	22.6	1
07	54	08 23 36.8	56.6N	152.3W	Kodiak Island Region	N	4.9	5.3	38.8	77.2	308.3	1
07	55	15 30 29.5	56.7N	152.4W	Kodial Island Region	N	4.6		38.9	77.2	308.5	1
08	53	01 25 15.8	73.2N	6.2E	Greenland Sea	N	5.0	5.2	47.6	292.0	23.1	1
09	53	10 18 56.7	12.9N	144.1E	South of Mariana Islands	37	4.6	4.5	103.7	34.7	306.1	1
11	54	01 13 55.5	39.5N	73.8E	Tadzhik-Sinkiang Region	9	6.4	7.3	92.8	348.6	12.8	4
11	54	07 02 08.5	39.4N	73.9E	Tadzhik-Sinkiang Region	N	5.2	5.4	93.0	348.7	12.8	5
11	54	09 08 58.5	39.2N	73.9E	Tadzhik-Sinkiang Region	29	5.1		93.2	348.7	12.8	5
11	54	21 56 29.9	39.6N	73.6E	Tadzhik-Sinkiang Region	N	4.8		92.7	348.5	12.9	4
11	54	20 05 30.1	39.5N	73.7E	Tadzhik-Sinkiang Region	9	5.9	6.1	92.8	348.6	12.9	4
12	54	02 52 42.6	16.0S	179.4W	Fiji Island Region	70	5.7		101.4	44.5	258.8	7
12	56	05 26 24.9	6.4S	130.0E	Banda Sea	128	5.4		127.4	33.4	307.2	7
12	57	10 06 52.5	16.0S	179.3W	Fiji Islands Region	23	4.9	5.0	101.3	44.5	258.7	7
12	57	11 23 12.5	41.5N	142.0E	Hokkaido, Japan	71	4.8		80.9	33.0	323.4	7
12	55	13 30 14.2	11.7N	86.9W	Near Coast of Nicaragua	83	4.9		35.0	356.8	175.5	6
12	55	14 28 50.0	60.7S	19.4W	Southwestern Atlantic	N	5.4		121.1	310.9	147.3	6
12	54	21 27 18.6	17.6N	100.4W	Guerrero,. Mexico	73	5.1		30.4	14.8	200.8	6
12	57	23 46 13.9	24.0N	122.4E	Taiwan Region	26	5.1		103.9	22.0	330.1	7
13	56	00 15 56.8	6.1S	150.8E	New Britain Region	37	4.9		114.5	41.1	288.2	7

Az and Baz measured CW from North

EVENTS RECORDED AT THE HGLP SEISMIC STATION WPM

MONTH: August 1974

Day	PDE #	Origin Time (UCT) Hr Mn Sec	Geographic Coordinates Latitude	Longitude	Region and Comments	Depth Km	Mb	Ms	Δ°	Az	Baz	Box #
13	55	03 46 20.3	51.5N	178.1W	Andreanof Is. Aleutians	52	5.8		54.7	57.4	310.0	7
13	56	05 53 07.4	16.1S	179.4W	Fiji Islands Region	29	5.3	5.4	101.4	44.5	258.7	7
13	54	07 18 03.2	2.7N	126.2E	Molucca Passage	N	5.2	5.4	121.6	28.1	316.8	7
13	55	12 52 47.3	15.8S	179.5W	Fiji Islands Region	55	5.4		101.3	44.5	259.0	6
13	56	15 03 14.7	5.3S	150.8E	New Britian Region	100	5.5		113.9	40.8	288.8	6
14	54	03 44 04.8	28.1N	142.8E	Bonin Islands Region	61	4.7		91.8	33.0	315.6	6
14	55	05 34 54.4	51.6N	178.1W	Andreanof Is. Aleutians	56	5.7		54.7	57.4	310.1	6
15	58	00 26 57.7	16.6N	145.5E	Mariana Islands	51	5.2		99.9	34.9	307.1	5
15	54	01 33 09.2	6.9N	73.0W	Northern Colombia	157	4.6		42.2	343.0	155.1	5
15	54	08 49 15.6	10.3S	161.4E	Solomon Islands	99	5.1		110.5	43.9	276.8	8
15	56	10 55 37.7	36.6S	99.1W	Southern Pacific Ocean	N	4.7	4.7	83.4	6.6	187.7	8
15	55	15 15 59.6	33.1N	140.8E	South of Honshu, Japan	45	4.3		88.5	32.0	319.7	8
16	56	06 13 37.5	12.5N	141.4E	South of Mariana Island	51	5.2		105.5	33.6	308.1	8
16	57	09 41 31.7	51.5N	177.8W	Andreanof Is. Aleutians	46	5.7	5.8	54.6	57.5	309.9	8
17	58	05 13 08.1	54.9N	143.9E	Sakhalin Island	1	5.4	4.9	69.1	36.2	330.2	9
17	57	08 19 49.1	1.6S	81.1W	Off Coast of Ecuador	50	4.7		48.7	352.3	168.7	9
17	57	16 18 19.4	1.1N	126.1E	Molucca Passage	N	5.2	4.4	123.0	28.5	316.0	9
17	57	21 36 12.6	49.1N	128.4W	Vancouver Island	N	4.7		25.9	80.3	289.6	9
17	61	22 19 06.1	1.1N	126.0E	Molucca Passage	119	4.7		123.1	28.5	316 1	9
17	62	23 50 58.9	39.2N	73.9E	Tadzhik-Sinkiang Border	32	5.0	5.3	93.2	348.7	12 8	9
18	57	10 44 12.8	38.5S	73.4W	Near Coast Central Chile	36	5.9	7.1	86.1	348.9	167.4	9
18	63	17 16 26.0	50.6N	175.1E	Rat Island, Aleutians	N	5.0	4.7	58.8	53.2	312.1	9
18	61	19 23 29.5	43.8N	127.2W	Off Coast of Oregon	N	4.1		26.5	70.3	277.5	9
18	60	19 53 28.0	45.7S	76.1W	Off Coast of S.Chile	30	4.7		92.8	350.8	170.6	9
18	58	23 07 47.8	41.7S	75.2W	Off Coast of S.Chile	21	5,3	4.3	89.0	350.2	169.3	10
19	58	05 14 14.2	15.3S	173.4W	Tonga Islands	13	5.0		96.8	43.5	255.1	10
19	57	12 17 32.5	33.3N	139.5E	South of Honshu, Japan	23	5.3	4.6	88.9	31.3	320.7	10
19	59	15 11 23.8	14.7N	93.5W	Near Coast Chiapas, Mex.	67	4.4		32.1	5.1	187.2	10
19	58	19 54 44.8	12.3N	88.9W	Off Coast Central Amer.	67	5.2		34.3	359.2	178.9	10

Az and Baz measured CW from North

EVENTS RECORDED AT THE HGLP SEISMIC STATION WPM

MONTH: August 1974

Day	PDE #	Origin Time (UCT) Hr Mn Sec	Geographic Coordinates Latitude	Longitude	Region and Comments	Depth Km	Mb	Ms	Δ°	Az	Baz	Box #
20	61	04 25 08.4	51.2N	129.9W	Queen Charlotte Is. Reg.	N	4.3		26.6	83.7	294.6	9
20	58	06 31 47.3	24.0N	122.4E	Taiwan Region	67	4.8		103.9	22.0	330.1	10
20	61	14 10 59.2	11.1N	86.5W	Near Coast of Nicaragua	N	4.4	3.7	35.6	356.4	174.8	10
20	58	18 31 15.7	11.3N	140.7E	West Carolinas Islands	6	5.3	4.4	106.8	33.5	308.0	10
20	57	20 45 01.4	52.2N	175.0E	Rat Island, Aleutians	58	5.6		57.8	53.9	313.6	10
21	59	23 59 02.0	20.0S	71.1W	Off Coast of N.Chile	60	5.1		68.5	346.5	161.3	11
22	57	06 05 52.4	2.8N	99.0E	Northern Sumatra	N	5.0		130.1	7.7	348.8	11
22	60	13 06 26.3	11.3N	103.4W	Off Coast of Mexico	N	4.6	3.7	37.2	15.8	202.8	11
23	55	03 58 49.1	23.8N	121.6E	Taiwan	N	5.0		104.3	21.5	330.7	11
23	57	04 50 34.6	7.5S	127.5E	Banda Sea	136	5.8		129.6	32.6	309.1	11
23	57	12 00 35.7	25.6S	69.0W	Northern Chile	102	5.4		74.4	345.5	160.8	11
23	55	16 52 03.0	4.6S	105.4W	Northern Easter Is. Reg.	N	4.8	5.3	53.0	13.6	199.9	11
23	55	23 55 36.8	19.1N	68.0W	North Atlantic Ocean	N	5.0	4.3	32.8	332.2	140.1	11
24	55	04 16 27.1	22.6S	68.8W	Northern Chile	109	5.4		71.5	345.1	159.8	11
24	58	10 41 11.2	52.4N	163.8W	Fox Islands, Aleutians	41	5.7	5.6	46.5	65.8	305.6	11
24	57	16 43 17.6	30.4N	42.0W	North Atlantic Ridge	N	4.7	4.1	40.0	307.8	96.9	11
24	58	22 18 55.4	52.3N	168.3W	Fox Islands, Aleutians	37	5.3	4.7	49.0	63.2	307.1	11
25	59	01 18 39.9	32.0N	142.3E	South of Honshu, Japan	N	5.9	5.6	88.7	32.7	318.1	11
25	55	03 27 46.3	16.8S	175.8E	Fiji Island Region	N	5.1	5.3	105.2	45.2	261.6	11
25	58	04 52 00.3	23.7S	179.7E	South of Fiji Island	583	4.7		107.4	46.1	253.8	11
25	62	09 55 11.7	31.9N	142.5E	South of Honshu Japan	81	5.2		88.7	32.8	317.9	11
25	59	14 34 46.7	23.5S	179.9W	South of Fiji Island	542	5.3		107.0	46.0	253.7	11
26	58	06 27 40.7	16.0N	91.0W	Mexico-Guatemala Border	N	5.1	4.8	30.7	1.9	182.7	12
27	57	12 56 03.2	39.7N	73.8E	Tadzhik-Sinkiang Bor.Reg.	N	5.8	5.9	93.0	348.6	12.8	12
27	58	15 20 49.8	27.9S	66.7W	Catamarca Prov. Argentina	147	5.5		77.1	344.1	159.3	12
27	61	17 33 58.1	39.4N	73.9E	Tadzhik-Sinkiang Border	N	5.3	5.3	93.0	348.7	12.8	12
28	65	07 43 56.0	49.1N	128.5W	Vancouver Island Region	N	4.7	3.9	26.0	80.3	289.6	12
28	61	08 43 12.1	11.4S	163.8E	Solomon Island	38	5.1	4.7	109.6	44.4	274.2	12
28	61	18 43 25.7	59.5N	144.5W	Gulf of Alaska	4	4.9	4.6	34.3	86.9	312.2	12
28	65	23 06 28.4	54.7S	137.1W	South Pacific Cordillera	N	4.6		108.8	32.4	206.9	12

Az and Baz measured CW from North

EVENTS RECORDED AT THE HGLP SEISMIC STATION WPM

MONTH: August 1974

Day	PDE #	Origin Time (UCT) Hr Mn Sec	Geographic Coordinates Latitude	Longitude	Region and Comments	Depth Km	Mb	Ms	Δ°	Az	Baz	Box #
29	63	02 50 14.9	28.9S	177.5W	Kermadec Islands Reg.	58	5.3		109.1	46.7	248.0	12
29	61	04 32 33.3	19.2S	173.3W	Tonga Islands	N	5.2	4.8	99.6	43.9	252.3	12
29	57	06 40 03.3	50.2N	177.6E	Rat Islands, Aleutians	N	4.9		57.7	54.3	310.6	12
29	56	09 59 55.5A	73.4N	55.1E	Novaya Zemlya	0	6.4	5.0	57.7	331.9	11.3	12
30	58	07 45 20.9	12.8N	87.4W	Near Coast of Cen.Chile	62	4.4		33.9	357.3	176.2	13
30	63	15 00 00.2A	37.150N	116.083W	Southern Nevada	0	5.8		21.8	55.6	253.5	13
30	58	18 14 09.9	30.6N	141.8E	South of Honshu, Japan	46	5.1	4.6	90.1	32.5	317.7	13
30	60	19 17 54.9	5.6S	147.2E	East New Guinea Region	205	4.8		116.5	40.0	291.6	13
30	59	23 29 23.6	30.6N	141.9E	South of Honshu, Japan	24	5.3	5.7	90.1	32.5	317.6	13
31	62	09 38 07.1	44.5N	149.0E	Kuril Island Region	56	4.9		75.5	37.3	320.9	13
31	61	11 36 49.5	18.5S	69.8W	Northern Chile	128	4.8		67.3	345.4	159.7	13
31	62	13 47 41.5	16.8S	167.1E	New Hebrides Is. Region	24	*		111.1	45.8	267.7	13

Az and Baz measured CW from North

EVENTS RECORDED AT THE HGLP SEISMIC STATION WPM

MONTH: September 1974

Day	PDE #	Origin Time (UCT) Hr Mn Sec	Geographic Coordinates Latitude	Longitude	Region and Comments	Depth Km	Mb	Ms	Δ°	Az	Baz	Box #

WPM shut down for the month of September due to equipment failure

Az and Baz measured CW from North

EVENTS RECORDED AT THE HGLP SEISMIC STATION WPM

MONTH: October 1974

Day	PDE #	Origin Time (UCT) Hr Mn Sec	Geographic Coordinates Latitude	Longitude	Region and Comments	Depth Km	Mb	Ms	Δ°	Az	Baz	Box #
02	64	02 54 59.7	5.9S	81.1W	Near Coast of N.Peru	5	5.7	5.6	53.0	352.7	169.4	1
02	63	14 06 29.0	22.7S	175.3W	Tonga Island Region	N	4.9	4.8	103.4	44.82	251.2	1
03	71	14 21 29.1	12.3S	77.8W	Near Coast of Peru	13	6.6	7.6	59.7	350.7	166.7	1
04	69	22 24 32.7	26.3N	66.5E	West Pakistan	N	5.8	5.9	104.1	343.3	22.1	1
04	63	22 35 26.6	52.2N	160.5E	Off Coast of Kamchatka	16	5.3		64.7	45.6	320.2	1
06	69	03 50 25.4	12.5S	77.7W	Near Coast of Peru	19	4.3		59.9	350.6	166.6	1
06	64	17 09 35.4	16.8N	98.8W	Near Coast of Guerrero	51	5.0		30.8	12.4	197.5	1
07	69	04 57 51.3	12.2S	77.9W	Near Coast of Peru	N	5.0	4.7	59.6	350.7	166.7	1
07	64	21 52 40.4	58.3S	27.4W	South Sandwich Islands	N	6.0		161.5	241.7	137.5	1
08	69	09 50 58.1	17.3N	62.0W	Leeward Islands Region	47	6.6	7.5	37.2	328.2	133.0	1
09	68	07 32 02.2	44.7N	150.1E	Kuril Islands Region	49	6.3	6.4	74.9	37.9	320.4	1
10	68	06 48 14.0	41.0N	143.1E	Hokkaido Japan Region	29	5.8	6.2	80.9	33.6	322.4	1
11	64	07 43 27.3	13.3S	112.3W	N. Easter Is. Cordillera	N	5.0	5.6	63.2	17.3	204.9	2
11	66	08 33 52.3	60.7S	153.7E	West of Macquarie Island	N	5.3	6.1	141.7	81.9	225.1	2
11	68	09 12 19.3	67.7N	20.1W	Iceland Region	N	4.8	5.4	40.2	274.8	33.6	2
11	70	17 54 07.7	16.0S	74.2W	Near Coast of Peru	69	4.8		64.0	348.3	163.5	2
12	64	04 47 31.4	40.5N	143.5E	Off East Coast of Honshu	26	5.3	5.3	81.1	33.8	321.8	2
12	64	06 14 51.5	40.5N	143.6E	Off East Coast of Honshu	24	5.5	6.0	81.1	33.8	321.8	2
12	68	18 43 46.9	40.3N	124.7W	Near Coast of N.California	8	4.5		26.1	64.0	268.6	2
13	64	02 34 53.1	0.5N	126.0E	Molucca Passage	41	5.5	5.1	123.6	28.7	315.7	2
13	68	21 29 52.2	34.7N	87.2E	Tibet	N	5.0		98.9	357.7	2.7	2
14	66	07 45 17.2	2.4S	76.4W	Peru-Ecuador Border Reg	162	5.1		50.3	348.3	162.8	2
14	68	14 11 41.1	40.6N	143.7E	Off East Coast of Honshu	15	5.3	5.7	80.9	33.9	321.8	2
16	67	05 45 09.8	52.6N	32.1W	North Atlantic	N	5.8	6.9	36.8	284.5	59.2	2
16	66	09 29 49.0	40.3N	143.7E	Off East Coast of Honshu	24	5.6	5.2	81.2	33.9	321.7	2
16	67	17 30 34.7	6.3S	148.4E	New Britain Region	70	5.7		116.2	40.5	290.1	2

Az and Baz measured CW from North

EVENTS RECORDED AT THE HGLP SEISMIC STATION WPM

MONTH: October 1974

Day	PDE #	Origin Time (UCT) Hr Mn Sec	Geographic Coordinates Latitude	Longitude	Region and Comments	Depth Km	Mb	Ms	Δ°	Az	Baz	Box #
18	70	00 26 42.6	17.6N	62.2W	Leeward Islands	45	5.2	4.4	36.8	328.2	133.0	2
18	70	06 25 28.1	44.7N	110.7W	Yellowstone Nat. Park	5	4.4		14.9	74.6	269.8	2
18	66	09 04 04.3	3.2S	142.0E	Near N. Coast of New Guinea	36	5.4	5.4	117.8	37.5	297.8	2
18	66	11 51 49.0	16.3S	172.4W	Samoa Island Region	N	5.4	5.2	96.9	43.4	253.7	2
18	66	17 17 44.3	55.4S	128.8W	South Pacific Cordillera	N	5.0	5.5	107.0	27.1	202.2	2
19	66	01 56 47.8	2.2N	100.9W	East Central Pacific	N	4.6	4.4	45.5	10.9	196.0	3
19	67	03 56 19.7	30.8N	141.5E	South of Honshu, Japan	27	4.9	4.9	90.1	32.3	318.0	3
19	66	06 45 17.0	0.1S	123.8E	Northern Celebes	70	5.5		125.1	27.5	317.7	3
19	66	15 00 58.4	31.0N	41.5W	North Atlantic Ridge	N	4.5	4.6	39.9	307.2	95.7	3
19	67	18 08 26.5	20.2S	67.3E	Mid Indian Rise	N	4.5		147.5	329.8	43.3	3
21	64	02 14 39.3	54.3S	133.1W	South Pacific Cordillera	N	5.4		107.2	29.7	205.1	3
21	64	04 12 29.4	17.9S	178.6W	Fiji Island Region	602	6.0		102.2	44.7	256.9	3
21	64	12 48 13.6	53.9N	160.5E	Near Coast of Kamchatka	N	5.7	4.7	63.5	46.2	321.6	3
22	70	05 06 16.2	62.1N	26.4W	Iceland Region	N	5.1	5.4	38.1	276.3	42.8	3
22	64	06 08 01.4	15.0N	45.0W	North Atlantic Ridge	N	4.7	4.7	48.7	320.0	115.5	3
22	68	06 50 59.0	0.7S	98.1E	Southern Sumatra	89	4.9		133.6	7.3	349.4	3
22	68	09 16 41.0	0.7S	98.1E	Southern Sumatra	84	5.2		133.6	7.3	349.4	3
22	71	12 06 11.2	62.1N	26.2W	Iceland Region	N	4.9	5.6	38.2	276.4	42.8	3
22	69	12 13 39.1	34.0N	118.4W	Southern California	8	4.1		25.2	51.0	250.0	3
22	66	22 45 42.1	13.5N	120.6E	Mindoro, Philippines	41	5.2	5.1	114.2	22.2	327.6	3
23	64	06 14 54.0	8.4S	154.0E	Dentrecasteaux Island Reg.	48	6.1	7.2	114.1	42.4	283.9	3
23	64	11 46 56.0	1.0S	16.0W	North of Ascension Is.	N	4.9	5.1	79.5	317.9	102.8	3
24	65	07 30 49.5	30.9N	141.5E	South of Honshu Japan	45	5.1	4.8	90.0	32.3	318.0	4
25	66	00 05 34.1	15.8N	93.1W	Near Coast of Chiapas	120	5.5		31.0	4.7	186.6	4
25	64	03 19 07.7	6.3S	152.3E	New Britain Region	18	5.7	5.0	113.7	41.4	286.8	4
29	69	03 14 14.6	6.9S	129.5E	Banda Sea	117	6.5		128.1	33.4	307.4	4
30	72	16 07 33.2	29.9N	130.4E	Ryukyu Island	N	5.3	5.8	95.6	26.3	325.9	4
31	76	08 58 18.9	15.3S	71.0W	Southern Peru	31	5.1	4.8	64.0	345.9	160.0	4
31	68	14 34 10.4	15.1S	70.7W	Southern Peru	83	5.2		63.9	345.7	159.6	4

Az and Baz measured CW from Nort

EVENTS RECORDED AT THE HGLP SEISMIC STATION WPM

MONTH: November 1974

Day	PDE #	Origin Time (UCT) Hr Mn Sec	Geographic Coordinates Latitude	Longitude	Region and Comments	Depth Km	Mb	Ms	Δ°	Az	Baz	Box #
01	69	03 36 19.6	21.6S	174.3W	Tonga Islands	N	4.7	4.9	101.9	44.4	251.3	1
02	66	01 03 36.7	10.3N	40.9W	North Atlantic Ridge	N	4.9	5.0	54.8	320.8	115.3	1
02	69	04 59 56.7	70.8N	54.1E	Novaya Zemlya	0	6.7	5.3	59.8	331.9	13.1	1
02	69	22 19 05.2	15.2S	174.1W	Tonga Islands	97	5.6		97.2	43.6	255 6	1
04	72	17 29 24.4	22.3S	174.8W	Tonga Island Region	N	4.9	4.9	102.8	44.6	251.1	1
05	71	00 02 01.1	15.4S	173.4W	Tonga Islands	N	4.9	4.8	96.9	43.5	255.0	1
05	72	10 38 41.2	39.7S	173.8E	Off W. Coast of N. Island	N	5.3	4.9	121.6	53.3	244.0	1
07	69	13 17 37.3	15.4S	70.5W	Southern Peru	153	5.4		64.2	345.6	159.5	1
08	69	13 38 12.1	15.7S	173.2W	Tonga Islands	N	5.4	5.2	97.0	43.5	254.7	1
08	69	21 23 21.8	42.5N	141.8E	Hokkaido, Japan Region	132	6.0		80.1	33.0	324.1	1
09	71	07 14 23.9	29.1N	43.5W	North Atlantic Ridge	N	4.7	4.2	39.7	309.2	99.5	1
09	69	12 59 49.8	12.5S	77.8W	Near Coast of Peru	6	6.0	7.2	59.9	350.7	166.7	1
09	69	19 10 55.2	6.5S	105.3E	Sunda Strait	51	6.1		137.9	15.2	337.6	1
11	69	05 17 51.0	51.6N	178.1W	Andreanof Islands, Aleutian	68	5.8		54.6	57.4	310.1	1
11	69	05 59 16.1	61.5N	146.4W	Southern Alaska	61	*		35.1	88.2	315.8	2
11	70	19 53 10.6	10.5S	166.6E	Santa Cruz Islands	N	4.9	5.1	107.5	44.3	272.8	2
12	70	00 53 54.2	10.7S	79.1W	Off Coast of Peru	N	5.0	4.5	57.8	351.5	167.8	2
12	69	22 13 25.8	2.3N	121.1E	Celebes Sea	54	5.8		124.2	25.1	322.0	2
13	69	02 36 25.5	42.7N	46.6E	Eastern Caucasus	42	5.1	4.7	82.8	331.3	31.0	2
13	70	05 23 16.7	25.8S	176.3W	South of Fiji Islands	N	4.9	4.4	106.2	45.6	249.6	2
13	69	16 59 16.5	58.0S	148.3E	West of Macquarie Island	N	5.3	5.9	144.0	82.5	230.1	2
14	69	04 48 54.7	58.8N	154.6W	Alaska Peninsula	37	5.5	5.6	39.6	78.2	312.0	2
14	70	13 24 10.4	55.3N	162.5W	Alaska Peninsula	18	4.4		44.7	69.2	309.0	2
14	69	14 26 45.8	38.5N	23.0E	Greece	3	5.1	5.2	76.0	319.1	48.3	2
14	69	15 29 44.8	38.5N	23.1E	Greece	24	5.0	5.1	76.0	319.5	48.3	2
14	70	19 17 35.2	12.8S	77.1W	Near Coast of Peru	N	5.4		60.3	350.2	166.0	2
14	70	21 48 18.2	49.3N	129.2W	Vancouver Island Region	N	4.4		26.4	80.3	290.2	2
15	70	03 01 31.6	58.7N	154.6W	Alaska Peninsula	42	4.8	4.1	39.6	78.1	312.0	2

Az and Baz measured CW from North

EVENTS RECORDED AT THE HGLP SEISMIC STATION WPM

MONTH: November 1974

Day	PDE #	Origin Time (UCT) Hr Mn Sec	Geographic Coordinates Latitude	Longitude	Region and Comments	Depth Km	Mb	Ms	Δ°	Az	Baz	Box #
20	75	04 14 46.9	15.0S	167.1E	New Hebrides Islands	N	6.4	6.9	110.0	45.3	269.1	3
20	75	13 21 41.2	53.6S	28.3W	Southwestern Atlantic	N	6.0	5.6	112.7	319.2	145.5	3
21	68	07 32 49.5	8.0S	155.7E	Solomon Islands	N	5.1	5.2	112.7	42.6	283.0	3
22	69	16 25 49.6	31.2N	115.2W	Baja California	N	4.9		25.1	44.5	241.0	3
23	69	09 44 03.8	23.5N	123.8E	Southwestern Ryukyu	N	5.4	5.1	103.9	23.0	328.7	3
24	68	07 05 37.2	5.6N	82.6W	South of Panama	36	5.0	4.9	41.4	353.0	169.5	3

Az and Baz measured CW from North

EVENTS RECORDED AT THE HGLP SEISMIC STATION WPM

MONTH: December 1974

Day	PDE #	Origin Time (UCT) Hr Mn Sec	Geographic Coordinates Latitude	Longitude	Region and Comments	Depth Km	Mb	Ms	Δ°	Az	Baz	Box #
03	72	03 06 35.2	5.0S	129.8E	Banda Sea	N	6.2	6.5	126.3	32.8	308.3	1
05	72	11 57 31.3	7.7S	74.5W	Peru-Brazil Border Reg.	162	6.0		55.8	347.5	161 9	1
06	72	13 58 38.5	8.3N	82.9W	Panama-Costa Rica Bor.	46	5.4	5.4	38.4	352.7	169.4	1
06	74	17 08 53.8	21.6N	145.7E	Mariana Islands Region	N	5.4		95.7	34.6	309.8	1
07	73	07 34 11.0	51.9N	170.8W	Fox Islands, Aleutians	N	5.5	5.8	50.6	61.6	307.6	1
07	72	14 26 52.3	5.6S	154.3E	Solomon Islands	93	5.4		111 8	41.7	285.7	1
07	72	22 02 40.2	51.7N	174.8E	Near Islands, Aleutians	N	5.0	4.9	58 2	53.6	313.2	1
08	76	00 26 53.6	64.0N	22.8W	Iceland	N	4.3		39.5	276.9	39.5	1
08	76	01 26 34.5	63.7N	22.6W	Iceland Region	28	4.6		39.6	277.4	40.0	1
08	76	01 46 28.7	64.0N	22.8W	Iceland	N	4.4		39.5	276.9	39.5	1
08	76	03 56 13.9	63.9N	22.1W	Iceland Region	34	4.3		39.8	277.6	39.6	1
08	76	06 47 54.4	63.8N	22.5W	Iceland Region	11	4.3		39.7	277.4	39.8	1
08	78	07 05 16.8	64.1N	22.5W	Iceland	N	4.3		39.6	277.0	39.3	1
08	72	11 37 42.0	9.7S	150.4E	East New Guinea Region	5	5.2		117.4	42.1	285.9	1
09	76	09 46 32.1	20.3S	174.3W	Tonga Islands	N	5.4	4.9	101.0	44.2	252.2	1
09	73	10 50 07.9	17.0S	66.9E	Mascarene Island Region	N	5.0		144.5	331.7	41.2	1
09	72	20 49 47.4	11.5N	142.8E	South of Marian Islands	36	5.2		105.5	34.4	306.3	1
09	76	21 24 39.9	60.8S	37.1W	Scotia Sea	N	5.3		115.3	322.9	154.5	1
10	72	01 41 05.9	36.5N	70.5E	Hindu Kush Region	204	5.5		95.2	346.4	16.0	1
12	75	02 49 12.8	10.5S	164.0E	Santa Cruz Island Reg.	N	4.9		108.8	44.2	274.7	1
13	73	07 30 02.3	4.9N	127.4E	Talaud Islands	90	5.4		119.1	28.2	316.7	1
14	75	02 36 38.4	38.3N	20.8E	Greece	N	5.3		74.9	318.1	49.8	1
15	75	02 25 19.0	42.5N	126.6W	Off Coast of Oregon	N	4.2		26.5	67.9	274.4	1
17	77	15 31 16.4	13.2N	88.5W	El Salvador	50	5.0	5.3	33.5	358.7	178.1	1
17	77	15 35 21.2	54.1S	143.4E	West of Macquarie Is.	N	5.1	5.8	146.2	80.4	237.6	1
17	79	21 39 11.1	20.9S	175.2W	Tonga Islands	N	4.8		102.0	44.5	252.4	1
17	77	23 01 52.6	20.5S	175.3W	Tonga Islands	31	5.4	5.2	101.8	44.5	252.8	1
18	80	07 54 40.3	48.4N	103.1N	Mongolia	N	5.0	5.1	84.6	8.7	351.6	1
19	78	16 00 49.0	7.4N	78.7W	Panama	13	5.4	5.8	40.3	348.4	163.2	1

Az and Baz measured CW from North

EVENTS RECORDED AT THE HGLP SEISMIC STATION WPM

MONTH: December 1974

Day	PDE #	Origin Time (UCT) Hr Mn Sec	Geographic Coordinates Latitude	Longitude	Region and Comments	Depth Km	Mb	Ms	Δ°	Az	Baz	Box #
21	75	00 26 53.8	7.3N	78.6W	Panama	N	5.1		40.4	348.4	163.1	1
21	77	08 28 55.9	14.6S	175.2W	Samoa Island Region	N	5.6	6.1	97.5	43.8	256.8	1
22	79	02 18 36.9	26.9S	176.2W	South of Fiji Islands	N	5.1		106.9	45.8	248.7	1
22	77	16 44 15.5	19.0S	69.8W	Northern Chile	63	5.2		67.8	345.5	159.8	1
22	78	18 06 36.2	27.0S	176.3W	Kermadec Islands	N	5.2	5.0	107.0	45.9	248.7	1
23	78	00 33 10.8	5.0S	153.4E	New Ireland Region	76	4.8		112.0	41.3	286.9	1
23	76	01 04 02.7	14.6S	175.7W	Samoa Island Region	N	5.4	5.6	97.9	43.8	257.2	1
23	77	05 22 08.4	43.1N	47.0E	Eastern Caucasus Region	N	4.9	5.0	82.6	331.5	30.5	1
23	75	09 45 42.8	29.4N	81.4E	Nepal	45	5.2		103.8	353.6	8.1	1
23	76	23 42 14.5	5.3N	82.5W	South Panama	N	5.1	5.0	41.7	352.7	169.4	1
24	77	02 10 25.4	14.3N	90.1W	Guatemala	155	5.4		32.3	0.7	180.9	1
24	75	06 55 47.1	2.3S	99.0E	Southern Sumatra	N	5.8	6.8	135.1	8.3	347.8	1
25	76	02 49 13.0	51.7N	174.6E	Near Islands, Aleutians	40	5.7	5.8	58.3	53.5	313.3	1
25	76	07 54 46.0	51.7N	174.5E	Near Islands, Aleutians	37	5.1	4.8	58.4	53.4	313.4	1
25	75	17 13 26.2	7.8N	134.5E	West Caroline Islands	24	5.2	4.7	113.1	31.3	311.5	1
26	75	08 38 02.7	5.0S	153.5E	New Ireland Region	42	4.8	4.9	111.9	41.3	286.8	1
27	80	11 28 57.8	29.3S	177.4W	Kermadec Islands	61	5.0		109.3	46.7	247.6	1
27	82	11 56 18.1	29.4S	177.3W	Kermadec Islands	22	4.9		109.3	46.7	247.5	1
27	82	22 53 44.8	76.6N	106.2W	Queen Elizabeth Islands	N	4.8	4.2	30.7	157.3	352.5	1
27	82	23 21 40.6	76.7N	106.0W	Queen Elizabeth Islands	N	4.3		30.8	157.6	352.6	1
28	77	23 18 38.8	30.9N	116.1W	Baja California	N	4.7		25.9	44.8	241.7	1
29	82	03 50 06.1	64.5N	17.6W	Iceland	N	5.2		41.7	280.6	38.2	1
29	75	18 25 00.7	61.6N	150.5W	Southern Alaska	67	5.6		37.1	84.9	316.2	1
30	76	20 33 23.1	17.5N	62.0W	Leeward Islands	N	4.6	4.3	37.0	328.1	132.8	1

Az and Baz measured CW from North

EVENTS RECORDED AT THE HGLP SEISMIC STATION WPM

MONTH: January

Day	PDE #	Origin Time (UCT) Hr Mn Sec	Geographic Coordinates Latitude	Longitude	Region and Comments	Depth Km	Mb	Ms	Δ°	Az	Baz	Box #
01	01	03 55 12.0	61.9N	149.7W	Southern Alaska	66	5.9		36.7	85.9	316.6	1
01	11	13 20 54.4	19.5N	155.6W	Hawaii	10	5.1	5.3	59.7	46.7	266.7	1
01	03	22 52 36.4	14.1N	91.9W	Guatemala	80	5.0		32.6	2.99	184.2	1
02	07	08 59 00.5	46.9N	151.6E	Kuril Islands	52	5.7		72.5	39.2	321.0	1
02	04	17 14 52.9	15.3S	173.3W	Tonga Islands	N	5.1		96.8	43.5	255.0	1
02	02	19 31 43.9	53.0N	159.4E	Near E. Coast Kamchatka	47	5.5	5.0	64.6	45.3	321.4	1
04	04	04 30 14.7	18.3N	102.6W	Michoacan Mexico	47	4.9		30.4	17.9	205.1	1
05	11	01 32 06.8	19.5N	155.7W	Hawaii	10	5.1	5.3	59,8	46.7	266.8	1
05	04	09 41 19.4	15.6S	173.4W	Tonga Islands	71	5.0		97.7	43.7	255.5	1
06	01	19 09 52.5	29.2N	130.3E	Ryukyu Islands	41	5.6	5.8	96.3	26.3	325.7	1
08	01	01 58 55.1	3.0S	101.8E	Southern Sumatra	95	6.0		135.3	11.1	343.8	1
10	02	10 24 12.8	2.6N	95.4W	Galapagos Island Region	N	5.0	5.1	44.3	5.76	188.4	1
12	03	17 47 23.5	33.5S	178.1W	South of Kermadec	23	5.8	6.0	112.6	48.1	244.8	1
13	01	09 19 10.3	52.2N	171.1W	Fox Islands, Aleutians	42	5.7	5.6	50.6	61.6	308.0	1
14	02	19 48 59.2	5.0S	130.0E	Banda Sea	N	6.3	6.5	126.2	32.9	308.1	1
15	03	11 34 41.3	29.4N	101.7E	Szechwan Prov., China	N	5.7	6.0	103.5	7.93	349.9	1
5	03	19 10 09.1	74.2N	8.5E	Greenland Sea	N	5.1	5.2	47.8	293.2	21.5	1
17	06	09 30 42.3	17.9S	174.6W	Tonga Islands	153	5.8		99.5	44.0	254.1	1
17	07	10 28 09.2	2.9S	126.1E	Ceram Sea	N	5.7	5.5	126.5	29.9	313.6	1
19	16	08 02 02.5	32.5N	78.4E	Kashmir-Tibet Border	N	6.2	6.8	100.4	351.6	10.3	1
19	17	08 09 48.1	32.0N	78.5E	Kashmir-Tibet Border	N	6.0		100.9	351.7	10.3	1
20	05	17 31 10.6	35.0N	141.2E	E.Coast Honshu Japan	28	5.9	5.7	86.7	32.2	320.4	1
23	10	14 19 14.9	33.0N	131.1E	Kyushu Japan	10	5.2	5.8	92.6	26.6	326.8	1
23	22	17 02 29.7	32.9N	115.5W	Southern California	8	4.9	4.5	24.1	47.5	244.3	1
25	10	02 08 41.5	7.2N	77.8W	Panama-Colombia Bor.	36	6.1	6.5	40.7	347.6	161.9	1
28	06	11 53 16.4	56.1N	164.6E	Komandorsky Islands	N	5.2	5.2	60.3	49.6	321.6	1
28	14	13 53 16.4	40.4N	125.4W	Off Coast N.California	10	4.9	5.0	26.6	64.2	269.3	1
31	14	16 14 31.0	15.4N	104.8W	Off Coast Michoacan Mex.	44	5.1	5.2	33.8	18.99	207.2	1

Az and Baz measured CW from North

EVENTS RECORDED AT THE HGLP SEISMIC STATION WPM

MONTH: February

Day	PDE #	Origin Time (UCT) Hr Mn Sec	Geographic Coordinates Latitude	Longitude	Region and Comments	Depth Km	Mb	Ms	Δ°	Az	Baz	Box #
02	12	07 24 53.3	53.1N	173.4E	Near Islands, Aleutians	25	5.9	5.5	58.1	53.5	315.2	1
02	11	08 43 39.1	53.1N	173.5E	Near Islands, Aleutians	10	6.1	7.5	58.1	53.6	315.1	1
03	08	01 03 25.2	15.6N	91.8W	Mexico-Guatemala Bor.	218	5.4		31.1	2.99	184.2	1
03	06	16 45 15.0	4.9S	130.0E	Banda Sea	22	5.6		126.2	32.8	308.2	1
04	07	01 32 52.1	48.2N	114.1W	Montana	8	4.6		16.6	85.8	284.0	1
04	12	11 36 07.5	40.6N	122.6E	Northeastern China	N	6.4	7.4	88.4	21.5	336.1	1
08	09	11 31 00.7	15.4S	173.5W	Tonga Islands	72	5.0		97.0	43.5	255.1	1
09	09	04 45 24.5	6.7S	106.7E	Java	27	5.2	5.6	137.7	16.6	335.6	1
09	11	11 01 19.4	52.8N	174.5E	Near Islands, Aleutians	14	5.4	5.4	57.8	54.0	314.4	1
10	10	19 10 27.0	46.5N	27.5W	North Atlantic Ridge	N	4.8	5.1	41.6	293.9	66.8	1
16	16	16 13 40.3	8.5S	82.1W	Off Coast N. Peru	29	5.2	5.1	55.4	353.8	171.0	1
17	16	03 38 19.8	17.6N	97.7E	Burma	6	5.6	5.9	115.6	5.68	352.1	1
18	17	22 59 46.8	35.2S	15.8W	Tristan Da Cunha Reg.	N	4.9		105.0	316.9	125.5	1
22	16	00 47 21.7	17.4N	100.5W	Guerrero Mexico	40	5.3	5.8	30.6	14.8	200.8	1
22	16	08 36 07.4	51.4N	179.4W	Andreanof Is. Aleutians	48	6.3	6.5	55.5	56.6	310.5	1
22	16	22 04 37.7	24.9S	179.1W	South of Fiji Islands	375	6.2		107.4	46.1	252.1	1
26	12	04 48 54.7	85.0N	98.0E	North of Severnaya Zemlya	N	5.4	5.6	48.4	6.94	359.1	1
27	12	14 23 59.3	6.1S	148.2E	New Britian Region	78	5.9		116.2	40.4	290.4	1
28	18	15 15 00.0A	37.105N	116.056W	Southern Nevada (NTS)	0	5.7		21.86	55.50	253.4	1

Az and Baz measured CW from North

EVENTS RECORDED AT THE HGLP SEISMIC STATION WPM

MONTH: March

Day	PDE #	Origin Time (UCT) Hr Mn Sec	Geographic Coordinates Latitude	Longitude	Region and Comments	Depth Km	Mb	Ms	Δ°	Az	Baz	Box #
01	14	14 53 19.0	8.4S	82.0W	Off coast of N.Peru	N	5.5	5.3	55.3	353.7	170.9	1
02	14	14 23 26.6	85.0N	98.2E	N. of Severnaya Zemlya	N	5.0	5.0	48.4	7.12	359.1	1
05	16	00 22 19.7	2.4S	126.1E	Ceram Sea	N	6.4	6.6	126.1	29.8	313.9	1
05	13	13 48 00.7	9.0N	69.9W	Venezuela	51	5.6		41.2	339.4	149.7	1
07	15	07 04 42.6	27.5N	56.3E	Southern Iran	27	5.8	6.1	99.9	336.9	30.4	1
08	16	05 20 40.9	79.2N	96.1W	Queen Elizabeth Islands	N	4.4	4.7	32.6	171.7	357.7	1
17	24	05 35 15.2	40.5N	26.1E	Turkey	5	5.2	5.9	76.0	320.3	45.1	1
17	29	22 11 01.6	2.5S	138.2E	West New Guinea	N	5.4	6.0	119.6	35.8	301.8	1
18	18	06 54 08.0	2.6S	138.3E	West New Guinea	48	5.2	5.4	119.6	35.8	301.6	1
18	18	17 21 23.4	4.2S	77.0W	Northern Peru	98	6.2		51.9	349.1	164.0	1
18	21	18 44 16.4	35.2N	86.6E	Tibet	N	5.3	5.8	98.4	357.3	3.18	1
20	19	07 30 38.8	51.3N	179.6W	Andreanof Is. Aleutians	57	5.4		55.6	56.4	310.5	1
23	21	07 32 36.5	22.7N	122.8E	Taiwan Region	21	6.2	6.6	104.9	22.4	329.2	1
25	20	02 31 22.2	13.6N	90.7W	Near Coast of Guatemala	N	5.2	5.3	33.1	1.44	182.0	1
25	22	06 41 33.0	28.0S	66.7W	Catamarca Prov. Argen.	178	5.9		77.2	344.1	159.4	1
27	24	05 15 06.2	40.4N	26.1E	Turkey	5	5.7	6.7	76.0	320.3	45.2	1
28	25	02 31 05.7	42.1N	112.55W	Eastern Idaho	5	6.1	6.0	17.1	66.2	262.4	1
29	20	09 36 21.0	13.3N	50.7E	Eastern Gulf of Aden	N	5.4	5.6	110.4	332.0	41.6	1
31	20	05 48 37.8	49.4N	125.6W	Vancouver Is. Region	N	5.3		24.1	82.5	289.6	1

Az and Baz measured CW from North

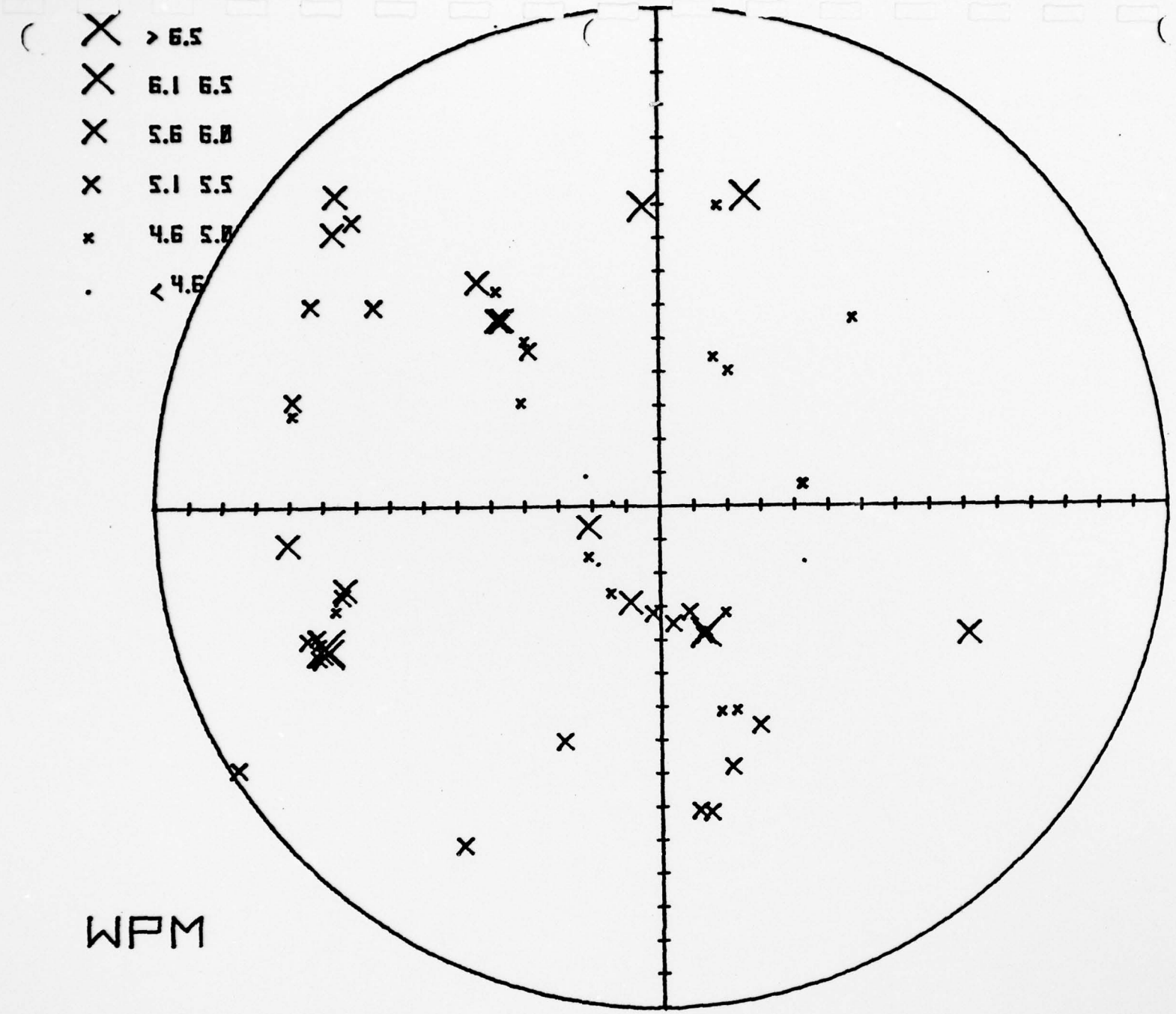
EVENTS RECORDED AT THE HGLP SEISMIC STATION WPM

MONTH: April

Day	PDE #	Origin Time (UCT) Hr Mn Sec	Geographic Coordinates Latitude	Longitude	Region and Comments	Depth Km	Mb	Ms	Δ°	Az	Baz	Box #
04	23	17 41 16.3	21.2S	45.1E	Malagasay Republic	N	5.4	5.6	135.4	315.9	71.0	1
05	20	09 34 36.6	10.0N	69.8W	Venezuela	N	5.6	6.1	40.3	338.9	149.0	1
05	20	20 38 30.1	10.1N	75.7W	Near N.Coast Colombia	52	5.5		38.4	344.6	157.7	1
06	20	09 55 18.9	52.2N	160.2E	Off E.Coast Kamchatka	N	5.6	6.2	64.8	45.5	320.3	1
12	23	15 33 08.6	14.8S	72.7W	Peru	81	5.9		63.1	347.1	161.7	1
13	23	01 34 36.2	5.7N	125.4E	Mindanao, Philippines	225	5.7		119.3	26.9	319.2	1
15	23	09 47 43.6	9.3N	61.5W	Near Coast Venezuela	47	5.4	4.9	44.3	332.4	138.4	1
16	22	01 27 18.7	71.5N	10.4W	Jan Mayen Is. Region	13	6.1	6.5	43.2	279.2	27.3	1
16	25	14 07 59.5	22.8S	175.3W	Tonga Island Region	38	5.3	5.3	103.4	44.8	251.1	1
16	22	21 33 25.1	48.4N	154.9E	Kuril Islands	32	5.8	5.6	69.9	41.4	320.2	1
17	25	01 15 50.6	22.8S	175.2W	Tonga Island Region	N	5.0	5.1	103.4	44.8	251.1	1
18	25	12 34 09.8	12.5S	78.0W	Off Coast of Peru	N	5.3	4.9	59.9	350.8	166.9	1
19	29	06 23 02.5	55.4S	124.6W	Easter Is. Cordillera	N	5.1	4.3	106.0	24.3	199.9	1
19	26	20 15 43.5	14.4N	56.4E	Arabian Sea	N	5.1		111.9	335.5	35.8	1
20	25	11 40 39.9	36.4S	98.8W	Southern Pacific Ocean	N	6.0	6.2	83.2	6.39	187.5	1
20	24	17 35 50.4	33.2N	131.3E	Kyushu, Japan	7	5.7	6.1	92.3	26.8	326.7	1
21	24	03 49 17.9	3.2S	147.1E	Bismarck Sea	N	5.2	4.9	114.7	39.2	293.4	1
21	23	06 14 32.2	45.3N	28.0W	North Atlantic Ridge	N	5.0	5.1	41.8	294.9	68.6	1
21	22	19 14 56.3	45.3N	28.0W	North Atlantic Ridge	N	4.8		41.8	294.9	68.6	1
21	23	23 34 19.8	30.3S	177.9W	Kermadec Islands	44	5.0		110.3	47.1	247.2	1
28	28	00 17 49.7	32.0N	114.8W	W.Ariz.-Mexico Bor.Reg.	10	4.8		24.3	45.4	341.7	1
28	28	11 06 43.5	35.8N	79.9E	Kashmir-Tibet Bor.Reg	N	5.8	6.3	97.3	352.7	8.63	1
29	29	08 41 53.7	13.6N	120.8E	Mindoro, Philippine	53	5.2		113.8	22.3	327.6	1
29	28	08 49 25.8	13.8N	120.9E	Mindoro, Philippine	50	5.0		113.8	22.4	327.4	1
30	30	04 28 56.9	36.2N	30.8E	Turkey	56	5.6		81.6	323.1	44.9	1
30	28	07 08 00.1	51.4N	179.7E	Rat Islands, Aleutians	48	5.2	4.9	55.9	56.1	310.9	1

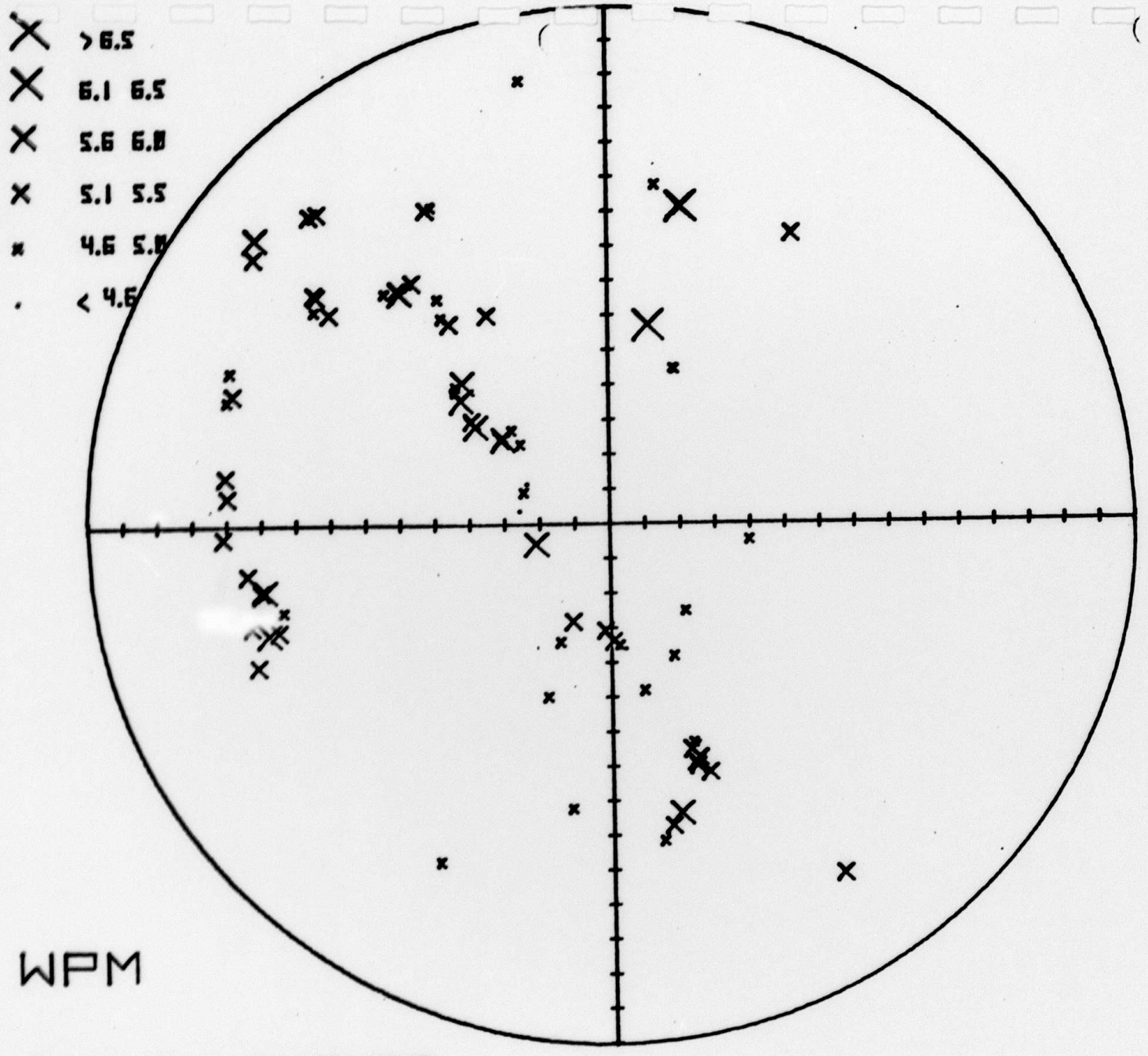
Az and Baz measured CW from North

The following pages are plots of events recorded at the White Pine Observatory on a monthly basis. Each plot is an azimuthal equidistant projection centered on White Pine. Each tic mark represents a 10^{o} distance increment with the outer circle at 150^{o}. The size of the "X" plotted is dependent on the reported mb magnitude of the National Earthquake Information Service. When several events were recorded from the same locality, all subsequent events were displaced slightly to make them visible.



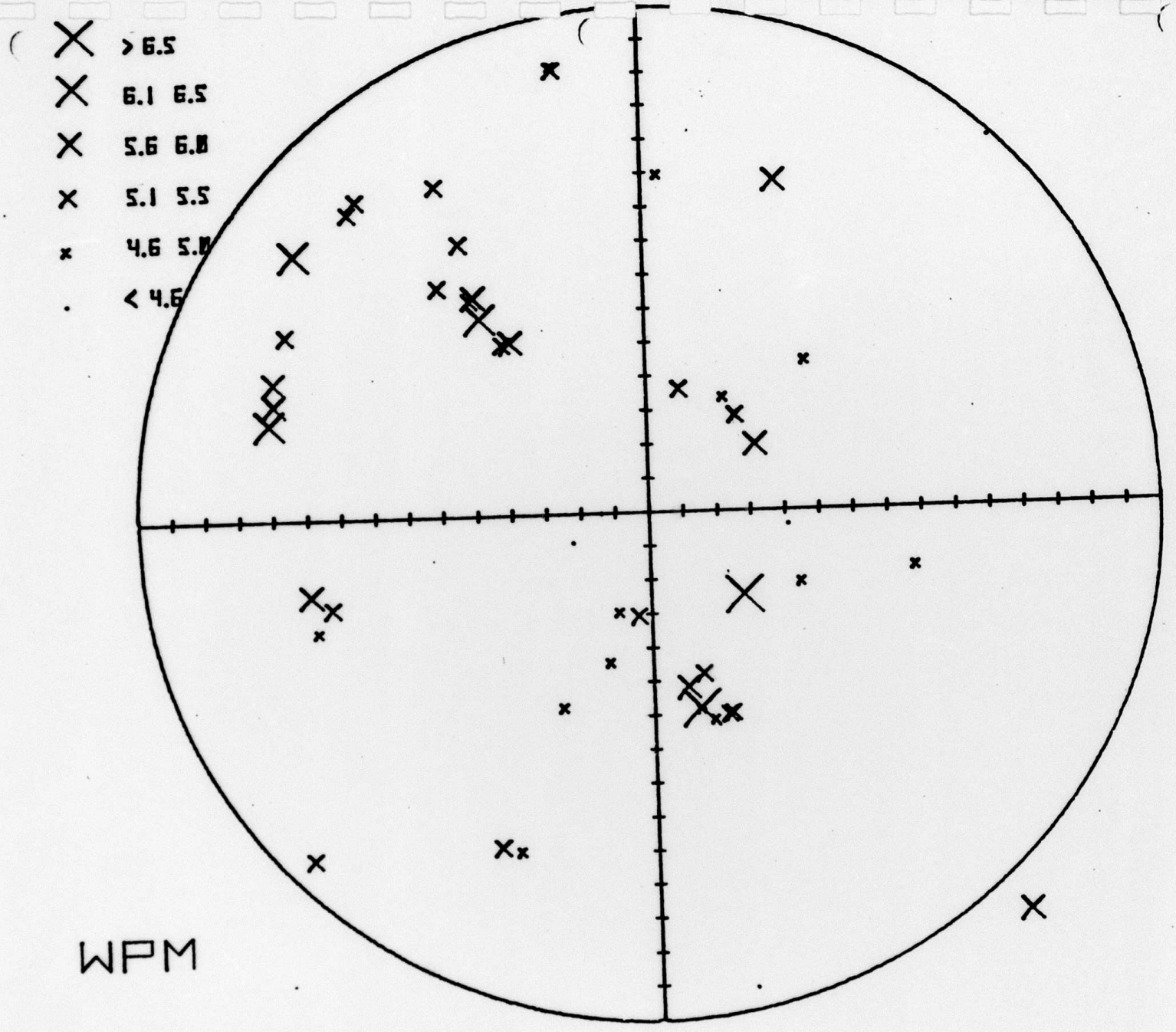
WPM

JULY EVENTS



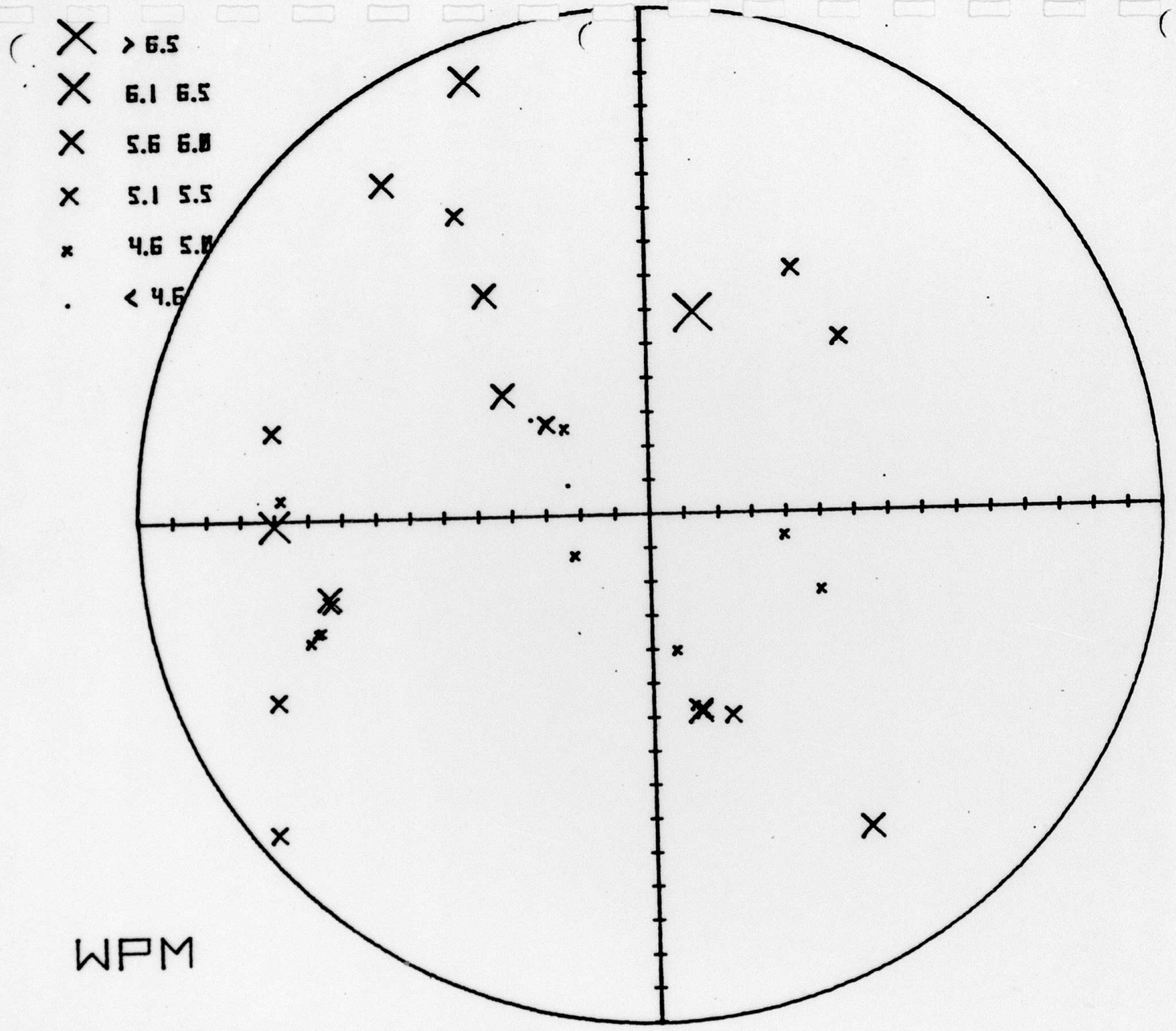
WPM

AUGUST EVENTS



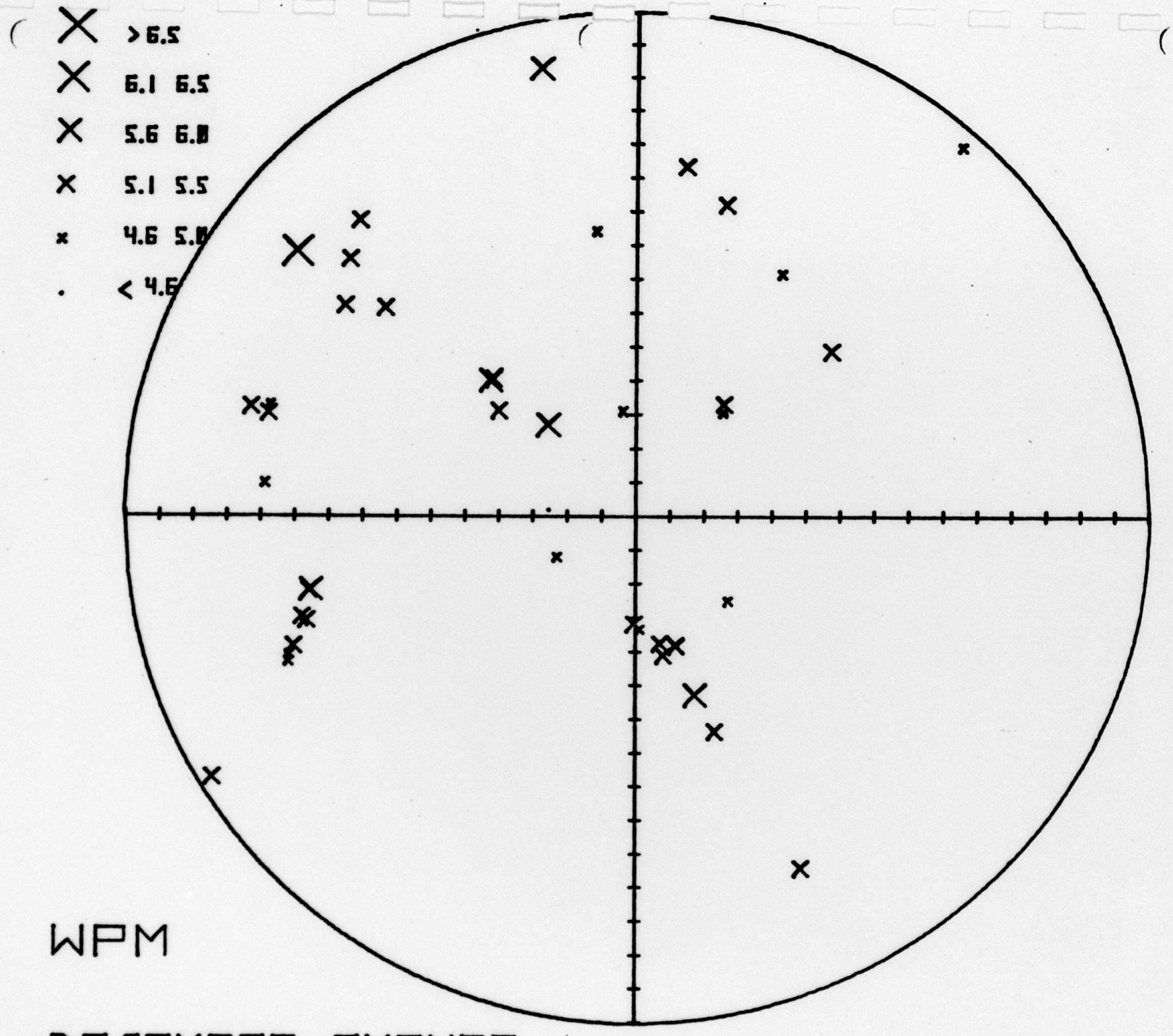
WPM

OCTOBER EVENTS



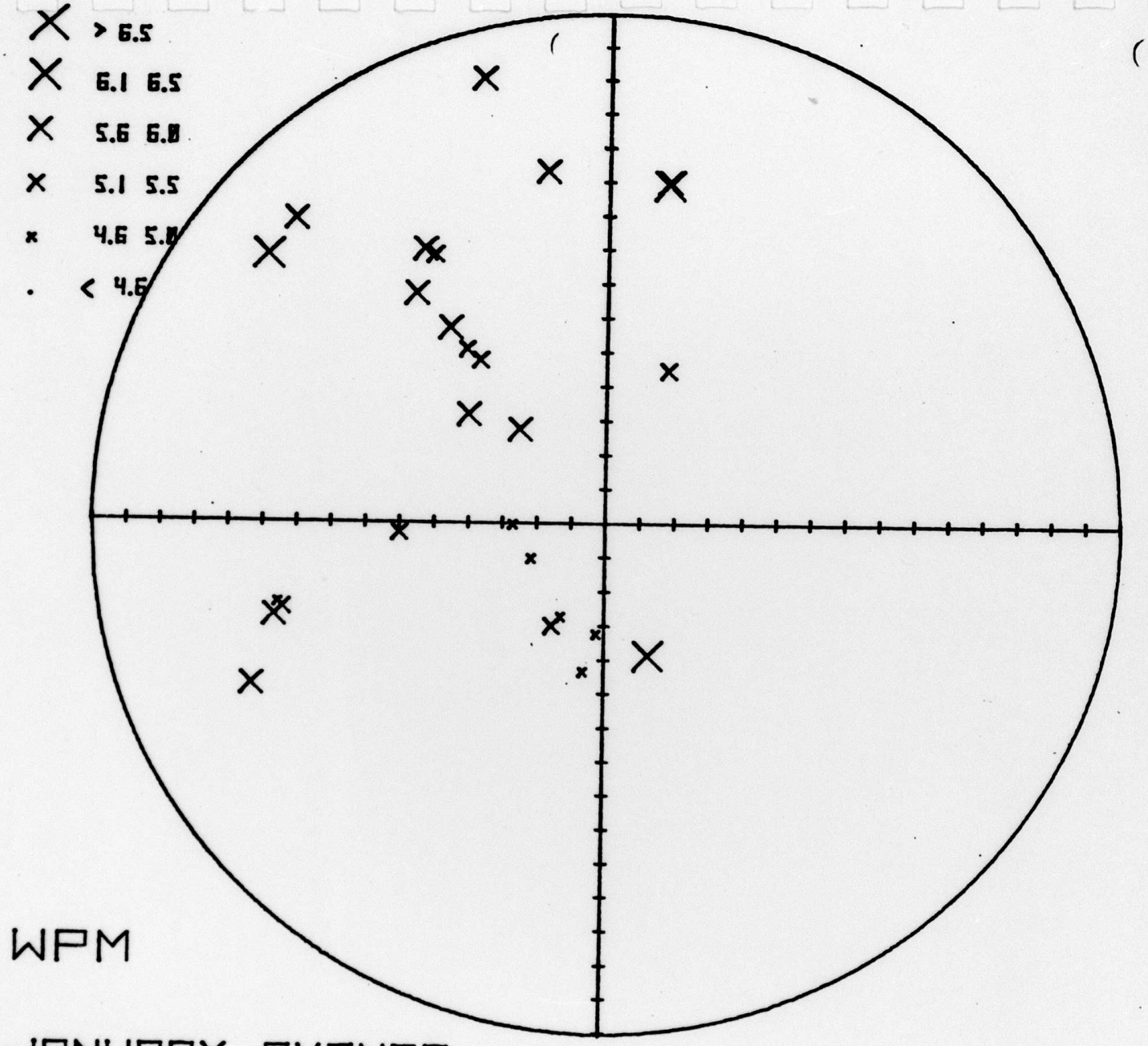
WPM

NOVEMBER EVENTS



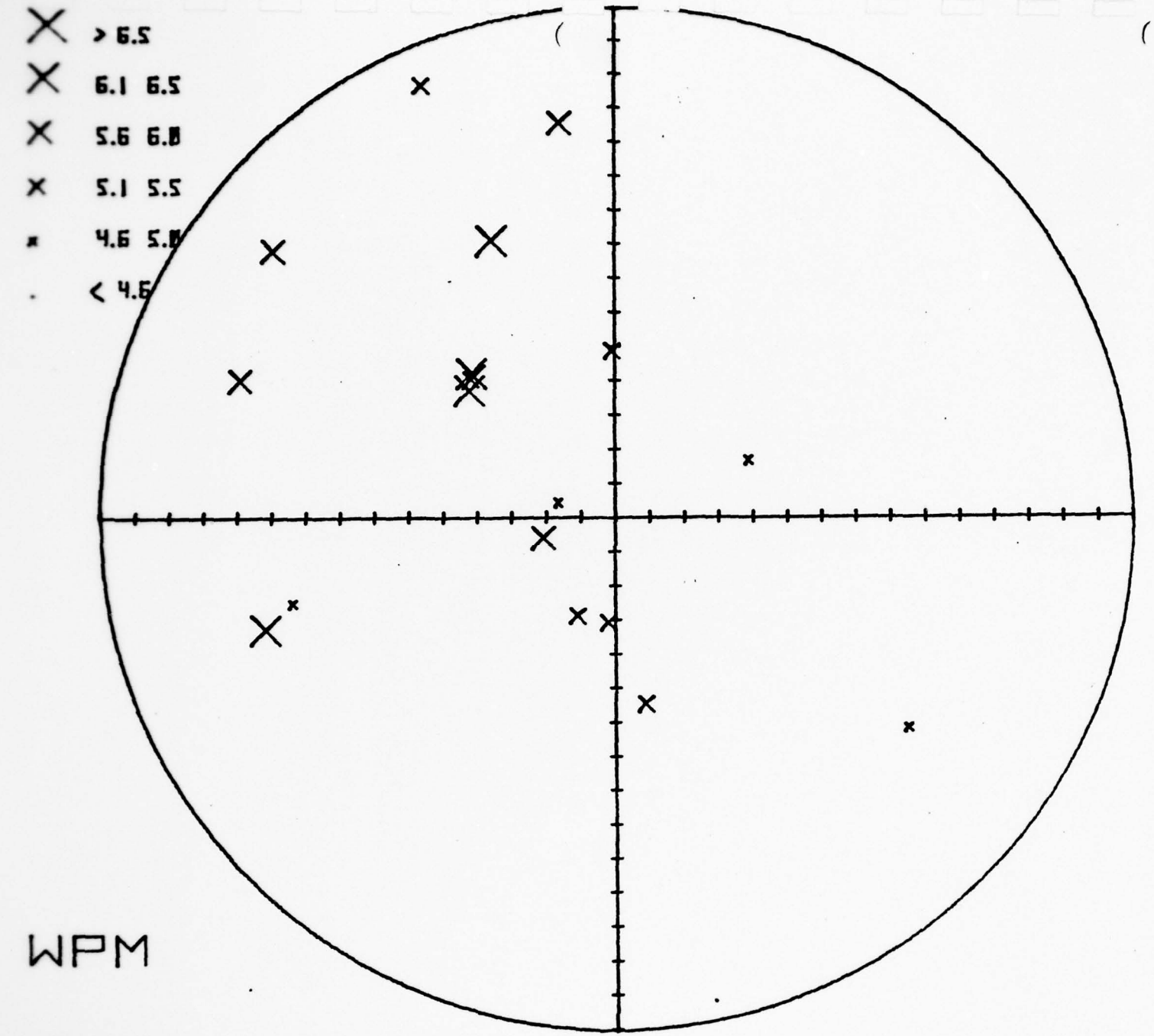
WPM

DECEMBER EVENTS



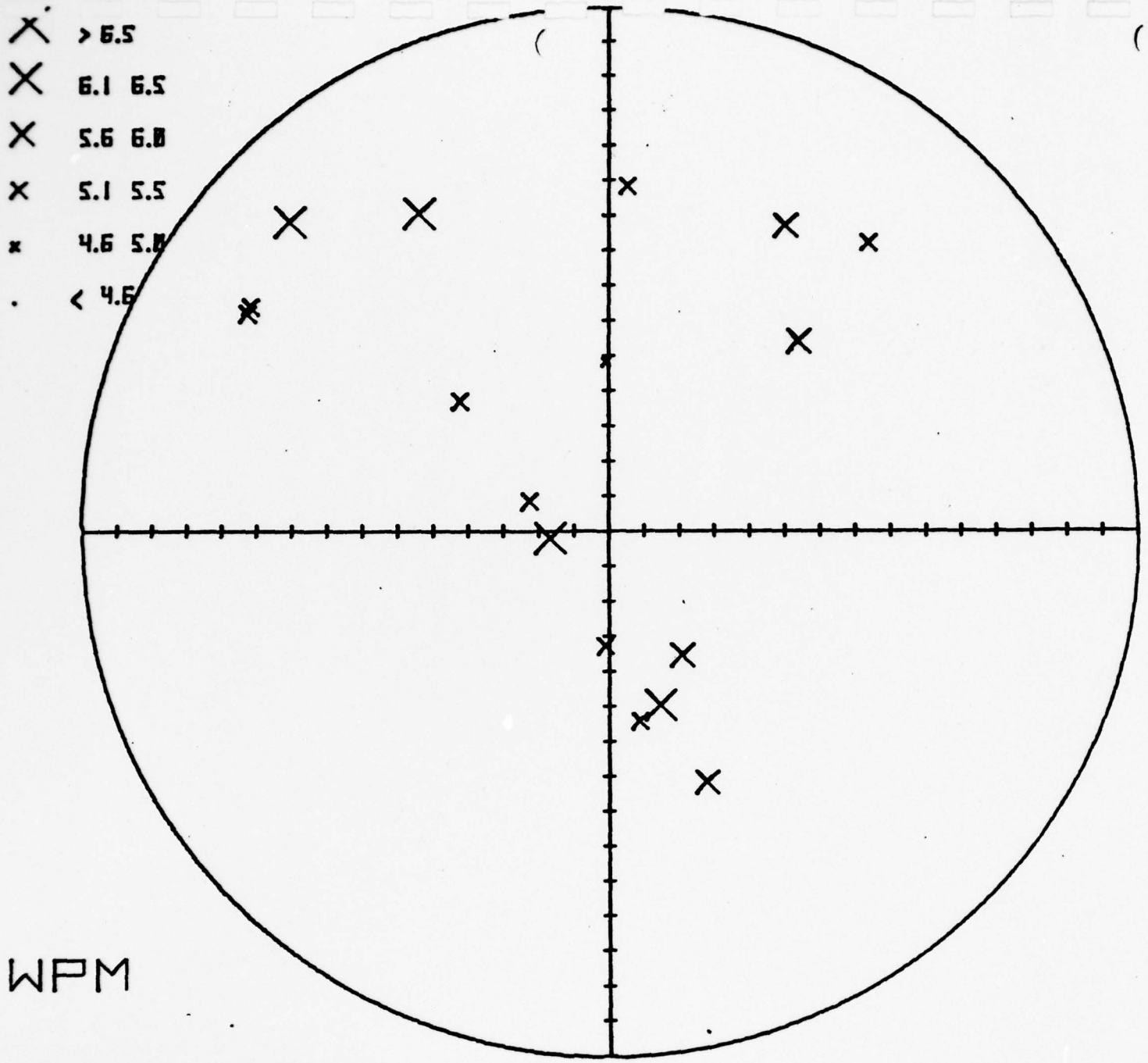
WPM

JANUARY EVENTS



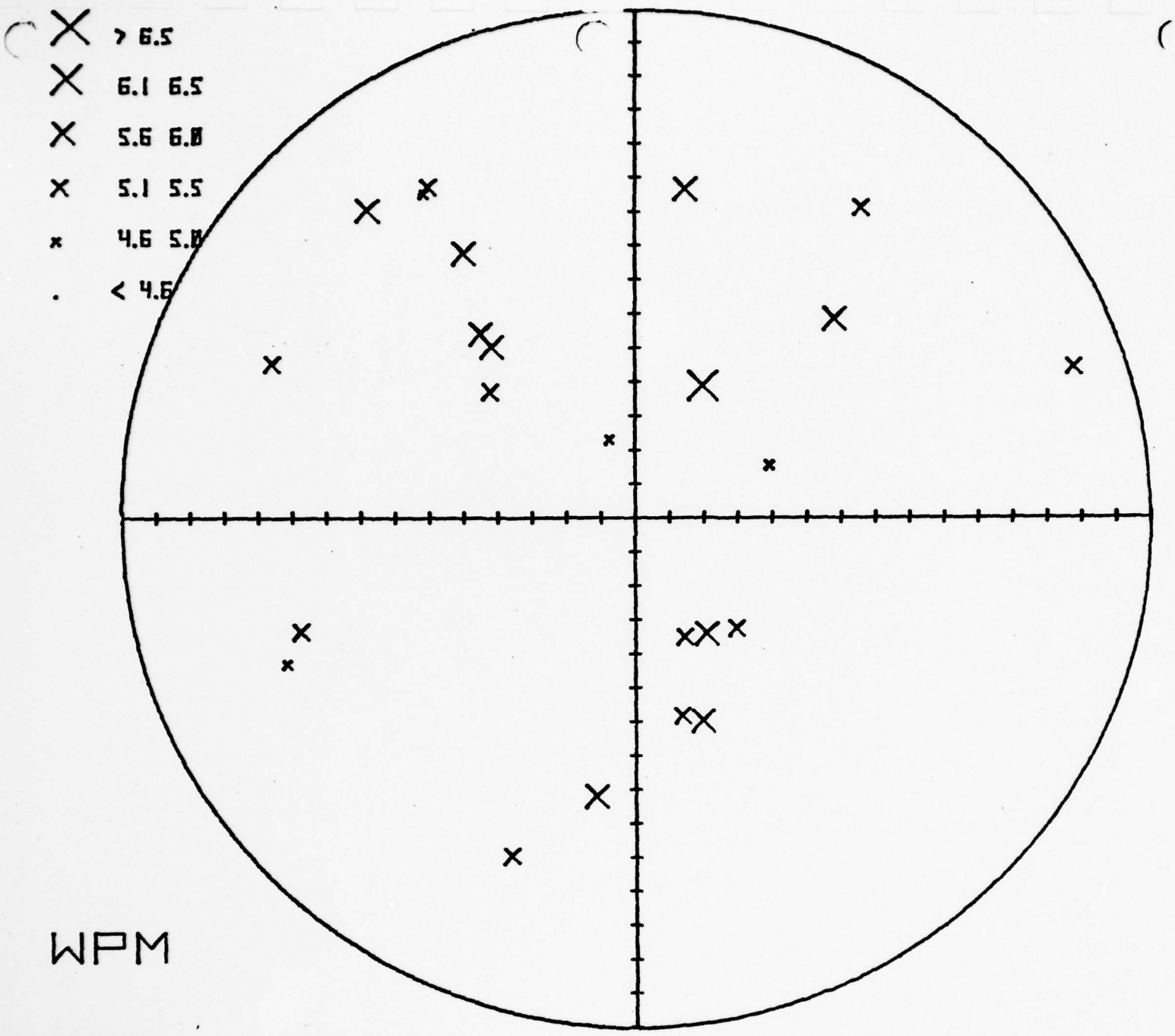
WPM

FEBRUARY EVENTS



WPM

MARCH EVENTS



WPM

APRIL EVENTS

UNCLASSIFIED

SECURITY CLASSIFICATION OF THIS PAGE (When Data Entered)

REPORT DOCUMENTATION PAGE	READ INSTRUCTIONS BEFORE COMPLETING FORM
1. REPORT NUMBER: AFOSR-TR-78-1010	2. GOVT ACCESSION NO. / 3. RECIPIENT'S CATALOG NUMBER
4. TITLE (and Subtitle): HIGH GAIN LONG PERIOD SEISMOGRAPH STATION	5. TYPE OF REPORT & PERIOD COVERED: Final rept. 1 Apr 73 - 15 Mar 78
	6. PERFORMING ORG. REPORT NUMBER
7. AUTHOR(s): James T. Wilson	8. CONTRACT OR GRANT NUMBER(s): F44620-73-C-0060 ARPA Order-32
9. PERFORMING ORGANIZATION NAME AND ADDRESS: Institute of Science and Technology, University of Michigan, Ann Arbor, MI 48105	10. PROGRAM ELEMENT, PROJECT, TASK AREA & WORK UNIT NUMBERS: AO 3291-1 62701E 7F10
11. CONTROLLING OFFICE NAME AND ADDRESS: ARPA/NMR, 1400 Wilson Boulevard, Arlington, Va 22209	12. REPORT DATE: 1978
	13. NUMBER OF PAGES: 104
14. MONITORING AGENCY NAME & ADDRESS (if different from Controlling Office): AFOSR/NP, Bolling AFB, Bldg.#410, Wash., D.C. 20332	15. SECURITY CLASS. (of this report): Unclassified
	15a. DECLASSIFICATION/DOWNGRADING SCHEDULE

16. DISTRIBUTION STATEMENT (of this Report)

Approved for public release, distribution unlimited

17. DISTRIBUTION STATEMENT (of the abstract entered in Block 20, if different from Report)

18. SUPPLEMENTARY NOTES

19. KEY WORDS (Continue on reverse side if necessary and identify by block number)

20. ABSTRACT (Continue on reverse side if necessary and identify by block number)

This final report on Contract No. F44620-73-C-0060, April 1, 1973 - March 15, 1978, describes the work carried out under the terms of the contract. A High Gain Long Period (HGLP) seismograph station was installed in the White Pine Copper Mine in Ontonagan County, Michigan. The station went through a series of stages starting with a long period vertical recording through a phototube amplifier on a strip chart and ending as an essentially standard HGLP station. Because of the difficulties of servicing and recording without

DD FORM 1 JAN 73 1473 EDITION OF 1 NOV 65 IS OBSOLETE

UNCLASSIFIED

SECURITY CLASSIFICATION OF THIS PAGE (When Data Entered)

telemetry, the station was closed at the end of 1976. Much useful information regarding the engineering and installation of HGLP stations in mines was obtained. The station produced many months of useful long period data. Concurrently with the station installation two extensive research efforts in long period seismology were carried on. One developed a Rayleigh wave velocity model for ocean basins and the other applied long period P wave spectra to the determination of seismic moments.